Synthesis and characterization of innovative catalysts for the selective oxidation of 5-hydroxymethylfurfural

Danilo Bonincontro

N°d'ordre NNT : 2019LYSE1014

THESE de DOCTORAT DE L'UNIVERSITE DE LYON
opérée au sein de
l'Université Claude Bernard Lyon 1

Ecole Doctorale n° 206
Ecole Doctorale de Chimie de Lyon

Spécialité de doctorat : Chimie
Discipline : Chimie industrielle durable

Soutenue publiquement le 30/01/2019, par :
Danilo BONINCONTRO

Synthesis and characterization of innovative catalysts for the selective oxidation of 5-hydroxymethylfurfural

---

Devant le jury composé de :

Dr. Francesco DI RENZO	CNRS – ICG Montpellier	Rapporteur
Dr. Carlo LUCARELLI	Università dell'Insubria	Rapporteur
Prof. Bruno ANDRIOLETTI	UCBL – Lyon1	President
Prof. Laura PRATI	Università di Milano	Examinatrice
Dr. Elsje Alessandra QUADRELLI	CNRS – C2P2 Lyon	Directrice de thèse
Prof. Stefania ALBONETTI	Università di Bologna	Co-Directrice de thèse

Alma Mater Studiorum – Università di Bologna
in cotutela con Università UCBL-Lyon 1

DOTTORATO DI RICERCA IN

CHIMICA

Ciclo XXXI

Settore Concorsuale: 03/C2

Settore Scientifico Disciplinare: CHIM/04

SYNTHESIS AND CHARACTERIZATION OF INNOVATIVE CATALYSTS FOR THE SELECTIVE OXIDATION OF 5-HYDROXYMETHYLFURFURAL

Presentata da: Danilo Bonincontro

Coordinatore Dottorato

Prof. Aldo Roda

Supervisori

Prof.ssa Stefania Albonetti

Dr.ssa Elsje Alessandra Quadrelli

Esame finale anno 2019

Abstract

The depletion of fossil-derived resources and the need to decrease the emission of green-house gases led scientists to look for sustainable materials to replace the already existing fossil-derived ones. For instance, 2,5-furandicarboxylic acid (FDCA) has been pointed out as the bioderived counterpart of terephthalic acid for the synthesis of polyesters. In fact, FDCA could be obtained by means of selective oxidation of 5-hydroxymethylfurfural (HMF), a bio-derived platform molecule produced by glucose hydrolysis. This reaction is known to be catalyzed by supported metal nanoparticle systems in presence of inorganic bases under batch conditions.

This work deals with the development of catalytic systems able to perform the base-free HMF oxidation, since the possibility to circumvent base addition leads more sustainable processes. In particular, two different sets of catalytic systems have been studied: mono- and bimetallic Au and Pd nanoparticles on nano-sized NiO, and mono- and bimetallic Pt/Sn systems on titania, prepared via cluster precursor decomposition.

Another topic that will be discussed in this thesis focuses on the development of catalytically active polymeric membranes obtained via electrospinning and their application as catalytic system for HMF oxidation either under basic and neutral aqueous conditions. In details, polyacrylonitrile and nylon have been tested as electrospun polymeric matrixes for the embedding of Au-based nanoparticles and Pt clusers.

Abstract

Riassunto

Il progressivo esaurimento delle materie prime di origine fossile e la necessità di ridurre le emissioni di gas serra hanno spinto la comunità scientifica verso la ricerca di materiali la cui produzione non dipenda da risorse non rinnovabili e che al tempo stesso possano essere già introdotti sul mercato al fine di sostituire i prodotti già esistenti, per la cui produzione vengono utilizzate materie prime non rinnovabili. Ad esempio, l'acido furandicarbossilico (FDCA), ottenuto dalla valorizzazione di biomasse lignocellulosiche, è stato indicato come potenziale sostituto dell'acido tereftalico per la produzione di poliesteri. Infatti, FDCA può essere ottenuto dall'ossidazione selettiva delle funzionalità legate all'anello furanico della 5-idrossimetilfurfurale (HMF), la quale si ottiene per disidratazione acido catalizzata degli esosi contenuti nelle biomasse lignocellulosiche.

Tale reazione viene condotta a livello industriale mediante le tecnologie già sviluppate per la produzione di acido tereftalico. Tuttavia, le severe condizioni operative, l'uso di solventi corrosivi e catalizzatori omogenei rendono questo processo non più compatibile con le moderne concezioni di sostenibilità industriale. Per tale motivo, sono stati sviluppati catalizzatori eterogenei a base di nanoparticelle metalliche supportate, le quali possono garantire elevate rese di FDCA in fase acquosa in condizioni *batch* e ad elevati pH di reazione. Tali condizioni operative tuttavia possono promuovere la formazione di sottoprodotti indesiderati e, in particolare, l'aggiunta di grandi quantità di basi inorganiche per raggiungere le condizioni di pH ottimali, porta ad un abbassamento generale dell'efficienza atomica della reazione. Dunque, questo lavoro di tesi ha affrontato due principali problematiche: (1) lo sviluppo di catalizzatori per l'ossidazione di HMF a FDCA in assenza di basi inorganiche (Capitolo 3 e 4) e (2) sviluppo di membrane polimeriche catalitiche il cui obiettivo è la futura implementazione in sistemi reattivi per la produzione in continuo di FDCA da HMF (Capitolo 5).

Per quanto riguarda l'ossidazione di HMF in condizioni neutre, un primo studio ha riguardato la possibilità di utilizzare ossido di nichel nanometrico (nNiO) come supporto per nanoparticelle. In particolare, è stata testata l'attività catalitica di sistemi nanoparticellari di Au, Pd e AuPd (rapporto molare Au:Pd 6:4) e fra questi, i sistemi a base di Au hanno mostrato buone rese del prodotto desiderato. In particolare, l'uso del sistema bimetallico AuPd ha mostrato le prestazioni catalitiche migliori, indice del fatto che l'iterazione sinergica dei due metalli porta a un'attività catalitica più marcata rispetto a quanto non avvenga per i sistemi monometallici.

Tale sistema a più elevata attività ha mostrato anche una buona riusabilità, e il calo di attività registrato al termine del quarto uso è stato attribuito al parziale ricoprimento della fase attiva ad opera del supporto.

Successivamente si è studiata la possibilità di utilizzare nanoparticelle di Pt supportate su TiO_2 ottenute per decomposizione controllata di cluster carbonilici. In tale studio è stata evidenziata maggiore attività di tali sistemi rispetto a quelli ottenuti per impregnazione diretta dei sali metallici, e in particolare si è rilevato come la presenza di Sn nel cluster carbonilico di partenza vada ad impartire al sistema catalitico una maggiore attività ed una migliore stabilità catalitica. Tali caratteristiche sono state attribuite al fatto che in determinati rapporti Pt/Sn si ottengono fasi bimetalliche nanometriche aventi più elevata stabilità termica ed attività catalitica.

Dunque, è stato valutato l'uso di membrane polimeriche ottenute mediante elettrofilatura decorate con nanoparticelle metalliche quali sistemi catalitici per l'ossidazione di HMF. In particolare, tre differenti metodi di introduzione della fase attiva soso stati testati: (1) introduzione di nanoparticlle di Au supportate su TiO_2 in membrane a base di poliacrilonitrile (PAN); (2) elettrofilatura diretta di sospensioni di cluster carbonilici di Pt/TiO_2/PAN e (3) elettrofilatura di nanoparticelle AuPd con TiO_2 e nylon. Tale studio ha mostrato che per quanto tutte le membrane sintetizzate siano attive nella reazione di ossidazione di HMF, le loro performances sono inferiori rispetto ai catalizzatori in polvere in cui la fase attiva (Au, Pt o AuPd) è direttamente impregnata. Tale ridotta attività è stata associata alla ridotta quantità di siti attivi esposti nelle membrane.

Tuttavia, risultati promettenti in termini di attività catalitica e stabilità sono stati ottenuti con la membrana a base di nylon, suggerendone un potenziale uso come membrana catalitica da implementare in apparati catalitici in continuo progettati specificatamente per la produzione di FDCA da HMF.

Résumé

L'épuisement progressif des matières premières d'origine fossile et la nécessité de réduire les émissions de gaz à effets de serre ont conduit la communauté scientifique à rechercher de nouveaux matériaux dont la production ne dépendra pas de ressources non renouvelables. Dans un autre temps ces matériaux pourront déjà être introduits sur le marché afin de substituer des produits déjà existant qui proviennent de matières premières fossiles. Par exemple, l'acide 2,5-furandicarboxylique (FDCA) obtenu par valorisation de la biomasse lignocellulosique est un potentiel substituant de l'acide téréphtalique actuellement utilisé pour la production de polyesters. En effet, le FDCA peut être obtenu par oxydation sélective des fonctions chimiques liées au cycle furane du 5-hydroxyméthylfurfural (HMF) préalablement synthétisé par déshydratation par catalyse acide des hexoses de la biomasse lignocellulosique.

Cette réaction est réalisée à l'échelle industrielle en exploitant les mêmes procédés utilisés pour la production d'acide téréphtalique. Cependant, les conditions dures de synthèses, l'utilisation de solvants corrosifs et de catalyseurs homogènes ne répondent plus aux exigences de la chimie verte industrielle. Pour remédier à cela, des catalyseurs hétérogènes à bases de nanoparticules métalliques supportées ont été développés. Ces catalyseurs appliqués en procédé *batch* dans des conditions aqueuses à pH optimisés élevés permettent la conversion de HMF en FDCA avec des hauts rendements. Néanmoins, ces conditions opératoires peuvent conduire à la formation de sous-produits indésirables, en particulier l'ajout d'une grande quantité de base inorganique conduit à la diminution du rendement atomique de la réaction. Ainsi, ce travail de thèse peut être défini par deux problématiques principales : (1) Le développement de catalyseurs pour l'oxydation de HMF en FDCA sans utiliser de bases inorganiques (Parties 3 et 4) et (2) Développement de membranes catalytiques de polymères pour la future adaptation du procédé d'oxydation en réacteur à flux continu (Partie 5).

Pour ce qui concerne l'oxydation de HMF dans des conditions neutres, une première étude s'est intéressée à la possibilité d'utiliser de l'oxyde de nickel nanométrique (nNiO) comme support pour des nanoparticules métalliques. Plus particulièrement, l'activité catalytique des nanoparticules de Au, Pd et de l'alliage AuPd (ratio molaire 6:4) a été étudiée et les premiers résultats indiquent que les systèmes catalytiques à base de Au permettent l'oxydation de HMF avec un bon rendement relatif au FDCA. En particulier, le système bimétallique AuPd a conduit au meilleur rendement en

FDCA, de fait que l'interaction synergique des deux métaux renforce l'activité catalytique par rapport à l'utilisation d'un système catalytique monométallique.

En plus, d'offrir une bonne activité catalytique ce système présente aussi une bonne réutilisabilité, le déclin de l'activité observé après la quatrième utilisation est essentiellement causé par le recouvrement de la phase métallique active par le support.

Ensuite, la possibilité d'utiliser des nanoparticules de Pt supportées sur du TiO2 obtenues par décomposition contrôlée de clusters carbonyliques. Les essais ont permis de déterminer que ces systèmes offrent une meilleure activité catalytique que les systèmes obtenus par imprégnation manuelle des sels métalliques, en particulier la présence initiale de Sn dans les clusters carbonyliques confère au système une meilleur activité et stabilité catalytique. Ceci peut s'expliquer par le fait que pour certains rapports Pt/Sn, des phases bimétalliques et nanométriques peuvent être obtenues, garantissant ainsi une meilleur activité et stabilité catalytique.

Ainsi, des membranes de polymère obtenues par électrospinning, contenant les nanoparticules métalliques étudiées précédemment, ont été appliquées comme système catalytique pour l'oxydation du HMF. Trois différentes méthodes d'introduction de la phase active ont été testées : (1) Introduction de nanoparticules de Au supportée sur du TiO2 dans des membranes à base de polyacrylonitryle (PAN); (2) Electrospinning direct des suspensions de clusters carbonyliques de Pt/TiO2/PAN et (3) Electrospinning de nanoparticules AuPd avec du TiO2 et du nylon. Ces tests ont permis de montrer que toutes les membranes synthétisées possèdent une activité catalytique pour l'oxydation du HMF, leurs performances sont moindres par rapport aux catalyseurs en poudre dans lesquels la phase active (Au, Pt ou AuPd) est imprégnée directement sur le support. Ce constat peut s'expliquer par le fait que le nombre de sites actifs exposés dans les membranes est moindre que ceux des catalyseurs inorganiques.

Toutefois, des résultats prometteurs en termes d'activité catalytique ont été obtenus pour la membrane à base de nylon. Ainsi, une application potentielle de ces membranes dans des dispositifs catalytiques de réacteurs à flux continu pourrait donc être imaginée pour la production de FDCA à partir de HMF.

Aim of the work and rationale

The aims of the research works shown in this thesis can be divided in two groups:

1. Development of catalytic systems for the base-free HMF conversion to FDCA
2. Design and preparation of catalytically active polymeric membranes obtained via electrospinning and their use as catalyst for the HMF oxidation to FDCA

As far as the first group is concerned, two different strategies have been tested: the first focuses on the effect that synthetic protocol and thermal treatments have on the definition of Pt/Sn-based catalytic systems (Chapter 3: Pt and Pt/Sn clusters as precursors for the synthesis of catalysts), while the second is aimed in understanding how nanosized NiO (nNiO) as support affects Au-based nanoparticles performances (Chapter 4: Au based nanoparticles supported on nanosized NiO)
In the second part of the work (Chapter 5: Catalysts grafted onto electrospun polymeric membranes), the possibility to use composite membranes decorated with active metal nanoparticles as catalysts has been investigated. In this frame, three synthetic ways to introduce the metal within the polymeric network have been evaluated: as nanoparticles supported onto TiO_2 (Paragraph 5.2: PAN electrospun fibers as matrix for Au-containing supported nanoparticles), as carbonyl clusters (Paragraph 5.3 Pt inorganic cluster as catalyst precursor for composite PAN-TiO_2 membranes) and as unsupported nanoparticles (Paragraph 5.4 Unsupported Au-nanoparticles embedded in electrospun nylon membrane).

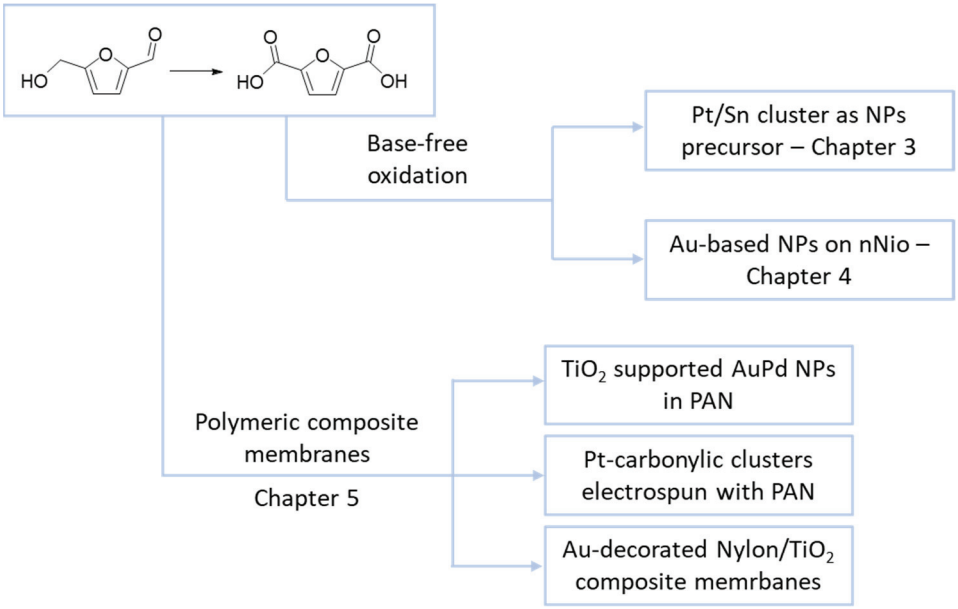

Aim of the work and rationale

Chapter 1. Introduction

1.1 Lignocellulose biomass as raw material for chemical industry

The depletion of fossil resources and the concentration increase of greenhouse gases in the atmosphere have forced the scientific community to look for alternative renewable raw materials to produce chemicals and energy able to fulfill the needs of a growing humanity, in both terms of needs and numbers. In this frame, lignocellulosic biomass has attracted significant interest due to its availability, abundance and virtual carbon neutral nature.[1] In addition to these positive features, versatility of such bio-derived feedstocks could be considered of primary importance, since bio-chemicals, bio-polymers and bio-fuels can be obtained via suitable valorization of lignocellulosic materials.[1-4]

The processes developed for lignocellulose conversion could be ascribed to two families: thermochemical and hydrolytic.[5] Among the first group, pyrolysis and gasification represent the most important examples: in the first case the raw material is converted to a mixture of charcoal and pyrolysis oil, while in the second treatment syn gas is obtained, which can be further converted into platform chemicals or fuels via well-established processes, such as the Fisher-Tropsch. As far as the hydrolytic processes are concerned, they are based on the separation of lignocellulose in its constituent biopolymers: a phenolic-based polymer (lignin) and two polysaccharides (cellulose and hemicellulose).[6] Typically, the polysaccharides are separated from lignin and hydrolyzed to their C_6 and C_5 sugars, which can be converted into the so called platform molecules, key intermediates that could be further upgraded into the final targeted chemical.[7]

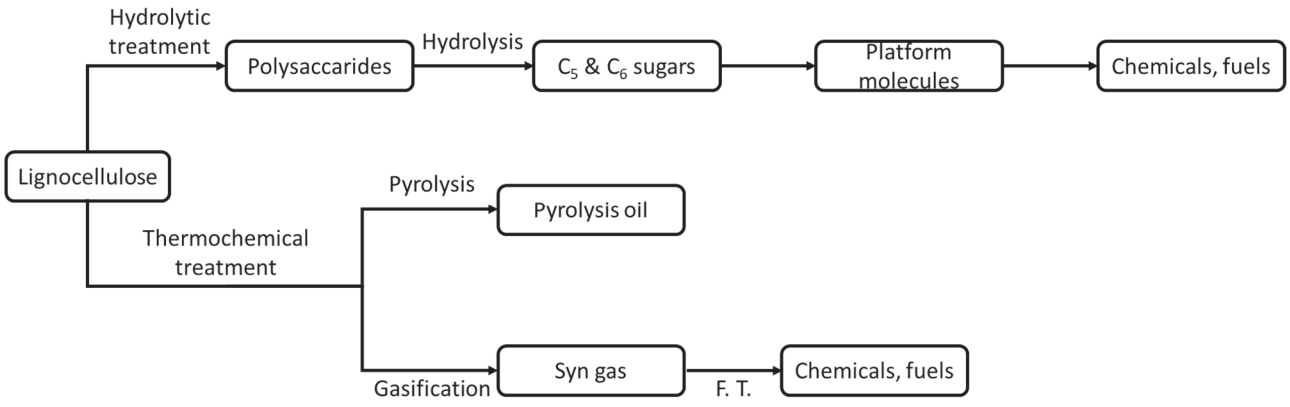

Figure 1-1 Lignocelluose conversion paths, adapted and modified from[8]

Among all the sugar-derived platform molecules,[9] 5-hydroxymethylfurfral (HMF) could be considered as one of the most representative example, since it can be converted to chemicals whose applications range from polymer science to fine chemical production.[10] Next two paragraphs will review synthetic approaches and industrial applications of this platform molecule.

1.2 HMF synthesis

HMF is a natural molecule which could be found in foods and beverages, whose global market is currently growing and expected to reach 123k million USD in 2022.[11] It is currently obtained via acid-catalyzed dehydration of C_6 sugars, such as fructose and glucose and superior results in terms of HMF yield are generally obtained using the previous feedstock. This has been ascribed to the higher stability of the glucose pyranoside ring structure,[12] and two mechanisms have been described for the conversion of fructose to HMF, depending on whether fructose is involved in its cyclic configuration or not. In the so-called cyclic pathway mechanisms, D-fructofuranose is dehydrated to form a carbenium ion which undergo three subsequent dehydration steps to form HMF.[13] On the other hand, linear D-fructose is isomerized into a 1,2-enediolglucose which is converted into the final product (Figure 1-3).[14]

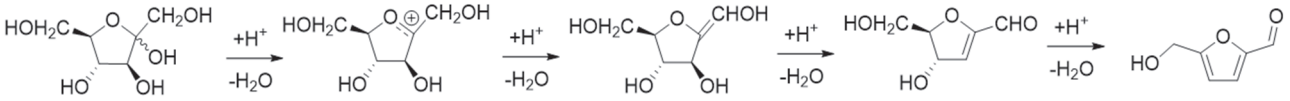

Figure 1-2 Cyclic pathway for fructose dehydration to HMF, adapted from[13]

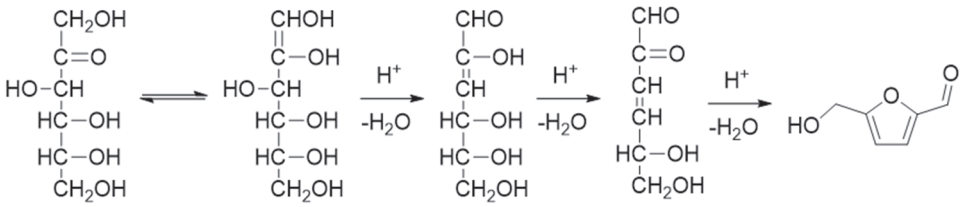

Figure 1-3 Linear mechanism for fructose dehydration to HMF, adapted from[14]

Regardless from the mechanism involved in sugar conversion, it is evident how the catalytic system must possess acid feature to promote all the dehydration steps involved in the reaction path. Homogeneous acids (both mineral and organic) have been proven to be suitable catalyst for the production of HMF under aqueous conditions.[13, 15-16] However, in these conditions, HMF yield is limited by its further conversion to levulinic acid and byproducts (humin) formation, which are strongly favored by the pH conditions and the presence of water. Thus, biphasic systems have been developed to continuously remove HMF from the aqueous medium, thus preventing its

degradation. As an example, methylisobutylketone (MIBK) was successfully used as organic phase to extract HMF from the acidic aqueous solution where the glucose conversion of HMF takes place.[17] Similar approach was proven to be viable for microwave setups, as demonstrated by Sweygers et al..[18]

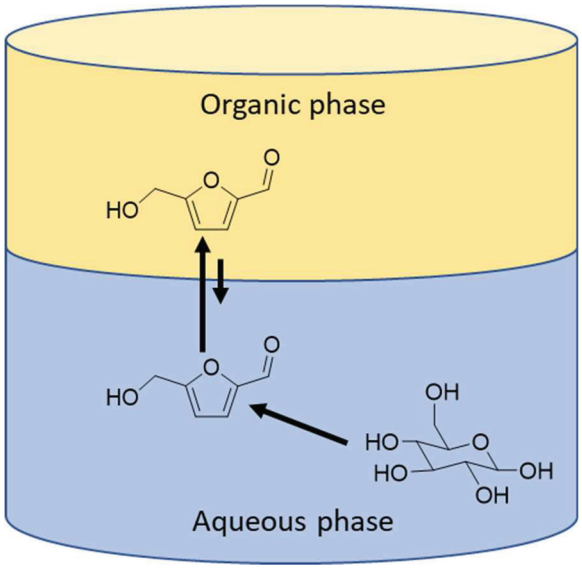

Figure 1-4 Schematic representation of biphasic reactor for HMF production, adapted from[17]

Alternatively, homogeneous acid catalysts have been successfully tested in HMF production from sugars, such as zeolites. However, their use is limited because of deactivation phenomena they undergo during reaction in aqueous environment (such as dealumination and framework collapse).[19] Thus, efforts have been devoted to the development of more stable catalysts such a phsphates,[20-22] modified polymeric resins[23-25] and W-based catalysts.[26]

1.3 HMF use as platform molecule

HMF, due to its versatility, has a prominent role in the production of bio-derived chemical and fuels, since a broad range of molecules could be obtained from its upgrade.[10, 27-28]

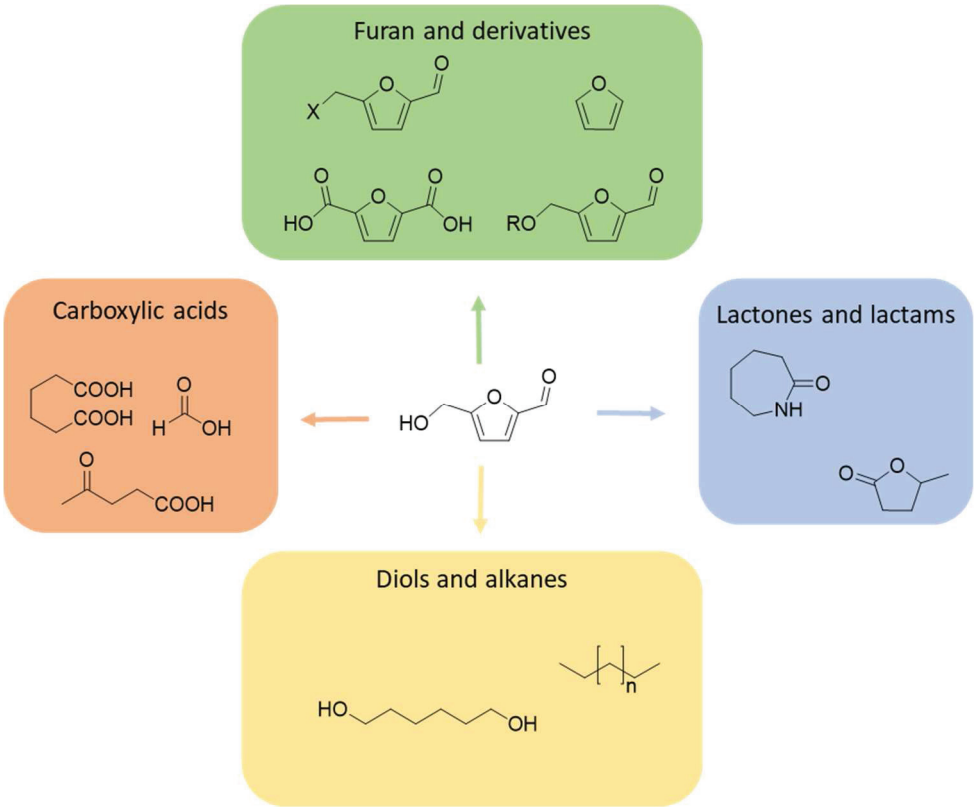

Figure 1-5 Chemical families obtained from HMF upgrade and most representative examples, adapted from[11]

Among all the valorization paths reported, the production of furandicarboxylic acid (FDCA) from HMF attracted big deal of interest, since FDCA has been proven to be suitable as monomer in the production of polyesters, such as PEF.[29-30] This bio-derived material has been proven to possess higher mechanical properties than its oil-derived counterpart PET, indicating that PEF could replace PET in different application, such as soft drinks bottling.[31]

Polymer	Structure	Density (g/cc)	T_g (°C)	Gas barrier properties		
				O_2	CO_2	H_2O
PEF	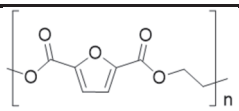	1.43	88	0.891	10.154	X2
PET	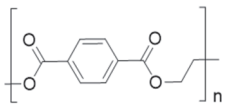	1.33	76	0.095	4.449	1

Figure 1-6 PEF and PET physical properties, adapted from[32]

Thus, HMF oxidation into FDCA has been widely studied, and it is known to occur via subsequent oxidation of the moieties bonded to the furan ring.

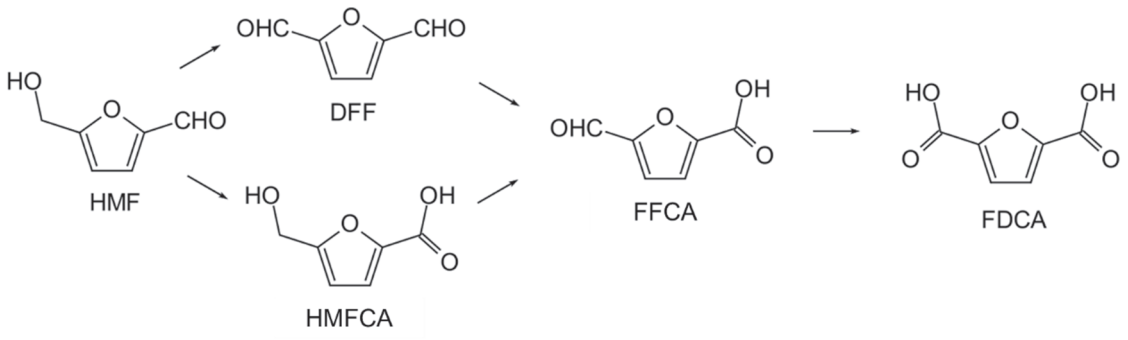

Figure 1-7 HMF oxidation path to FDCA (DFF: diformylfuran; HMFCA: hydroxymethylfurancarboxylic acid; FFCA: formylfurancarboxylic acid)

From an industrial point of view, HMF oxidation is carried out using the technologies and the catalytic systems already developed for p-Xylene oxidation to terephthalic acid. In these setups, the reaction is carried out under harsh operative conditions, using acetic acid as solvent and Co-based homogeneous catalysts.[33] All those features represent severe concerns in terms of process sustainability, and efforts have been devoted to develop heterogeneous catalytic systems able to perform HMF oxidation under aqueous conditions. In this frame, the high potential of metal nanoparticles has been highlighted, being Au, Pd and Pt the most used.[32, 34] Then, a general approach is based on the use of air or oxygen as oxidant, water as solvent and soluble inorganic base as promotors. The role of the base is thought to be crucial in the reaction mechanism: Davis at al. proved that the OH^- group directly participates in the reaction mechanism, and in such high pH conditions, HMFCA formation is strongly favored respect to DFF formation.[35] The presence of an inorganic base enhances the rates of all the reactive steps involved in the conversion of HMF to FDCA[36]. Nevertheless, the use of soluble inorganic bases lowers the overall atom efficiency of the reaction and can lead to HMF degradation by formation of insoluble oligomers (humins). Thus, further research focused on the development of catalytic systems that are able to operate in absence of inorganic bases. Some research groups circumvent the use of inorganic base by supporting the metal nanoparticles onto intrinsically basic supports, such as hydrotalcite.[37] In this case the reaction pathway seems to be the same as the previously described one, i.e. HMFCA production favored over DFF. On the other hand, when non-basic supports (such as carbon and functionalized carbon nanotubes)[38-40] have been used, DFF has been detected in the reaction mixture, indicating that the reaction pathway involved is different from the one that takes place in presence of base. In addition, it must be noted that, in absence of base, higher temperatures are usually required to perform the oxidation than the one required in basic condition.

1.4 Bibliography

1. Sheldon, R. A., Green and sustainable manufacture of chemicals from biomass: state of the art. *Green Chemistry* **2014,** *16* (3), 950-963.

2. Gallezot, P., Conversion of biomass to selected chemical products. *Chemical Society Reviews* **2012,** *41* (4), 1538-1558.

3. Gallezot, P., Catalytic routes from renewables to fine chemicals. *Catalysis Today* **2007,** *121* (1), 76-91.

4. Dhyani, V.; Bhaskar, T., A comprehensive review on the pyrolysis of lignocellulosic biomass. *Renewable Energy* **2018,** *129*, 695-716.

5. Lange, J.-P., Lignocellulose conversion: an introduction to chemistry, process and economics. *Biofuels, Bioproducts and Biorefining* **2007,** *1* (1), 39-48.

6. Bajpai, P., Structure of Lignocellulosic Biomass. In *Pretreatment of Lignocellulosic Biomass for Biofuel Production*, Springer Singapore: Singapore, 2016; pp 7-12.

7. Farmer, T. J.; Mascal, M., Platform Molecules. In *Introduction to Chemicals from Biomass*, John Wiley & Sons, Ltd: 2015; pp 89-155.

8. Sheldon, R. A., The Road to Biorenewables: Carbohydrates to Commodity Chemicals. *ACS Sustainable Chemistry & Engineering* **2018,** *6* (4), 4464-4480.

9. Bozell, J. J.; Petersen, G. R., Technology development for the production of biobased products from biorefinery carbohydrates-the US Department of Energy's "Top 10" revisited. *Green Chemistry* **2010,** *12* (4), 539-554.

10. Rosatella, A. A.; Simeonov, S. P.; Frade, R. F. M.; Afonso, C. A. M., 5-Hydroxymethylfurfural (HMF) as a building block platform: Biological properties, synthesis and synthetic applications. *Green Chemistry* **2011,** *13* (4), 754-793.

11. Mika, L. T.; Cséfalvay, E.; Németh, Á., Catalytic Conversion of Carbohydrates to Initial Platform Chemicals: Chemistry and Sustainability. *Chemical Reviews* **2018,** *118* (2), 505-613.

12. Hu, L.; Zhao, G.; Hao, W.; Tang, X.; Sun, Y.; Lin, L.; Liu, S., Catalytic conversion of biomass-derived carbohydrates into fuels and chemicals via furanic aldehydes. *RSC Advances* **2012,** *2* (30), 11184-11206.

13. Antal, M. J.; Mok, W. S. L.; Richards, G. N., Mechanism of formation of 5-(hydroxymethyl)-2-furaldehyde from d-fructose and sucrose. *Carbohydrate Research* **1990,** *199* (1), 91-109.

14. Moreau, C.; Durand, R.; Razigade, S.; Duhamet, J.; Faugeras, P.; Rivalier, P.; Ros, P.; Avignon, G., Dehydration of fructose to 5-hydroxymethylfurfural over H-mordenites. *Applied Catalysis A: General* **1996,** *145* (1), 211-224.

15. Bicker, M.; Hirth, J.; Vogel, H., Dehydration of fructose to 5-hydroxymethylfurfural in sub- and supercritical acetone. *Green Chemistry* **2003,** *5* (2), 280-284.

16. Asghari, F. S.; Yoshida, H., Acid-catalyzed production of 5-hydroxymethyl furfural from D-fructose in subcritical water. *Industrial and Engineering Chemistry Research* **2006,** *45* (7), 2163-2173.

17. Pagán-Torres, Y. J.; Wang, T.; Gallo, J. M. R.; Shanks, B. H.; Dumesic, J. A., Production of 5-Hydroxymethylfurfural from Glucose Using a Combination of Lewis and Brønsted Acid Catalysts in Water in a Biphasic Reactor with an Alkylphenol Solvent. *ACS Catalysis* **2012,** *2* (6), 930-934.

18. Sweygers, N.; Harrer, J.; Dewil, R.; Appels, L., A microwave-assisted process for the in-situ production of 5-hydroxymethylfurfural and furfural from lignocellulosic polysaccharides in a biphasic reaction system. *Journal of Cleaner Production* **2018,** *187*, 1014-1024.

19. Kang, S.; Fu, J.; Zhang, G., From lignocellulosic biomass to levulinic acid: A review on acid-catalyzed hydrolysis. *Renewable and Sustainable Energy Reviews* **2018,** *94*, 340-362.

20. Xu, S.; Pan, D.; Li, W.; Shen, P.; Wu, Y.; Song, X.; Zhu, Y.; Xu, N.; Gao, L.; Xiao, G., Direct conversion of biomass-derived carbohydrates to 5-hydroxymethylfurfural using an efficient and inexpensive manganese phosphate catalyst. *Fuel Processing Technology* **2018,** *181*, 199-206.

21. Asghari, F. S.; Yoshida, H., Dehydration of fructose to 5-hydroxymethylfurfural in sub-critical water over heterogeneous zirconium phosphate catalysts. *Carbohydrate Research* **2006,** *341* (14), 2379-2387.

22. Benvenuti, F.; Carlini, C.; Patrono, P.; Raspolli Galletti, A. M.; Sbrana, G.; Massucci, M. A.; Galli, P., Heterogeneous zirconium and titanium catalysts for the selective synthesis of 5-hydroxymethyl-2-furaldehyde from carbohydrates. *Applied Catalysis A: General* **2000,** *193* (1), 147-153.

23. Tacacima, J.; Derenzo, S.; Poco, J. G. R., Synthesis of HMF from fructose using Purolite®strong acid catalyst: Comparison between BTR and PBR reactor type for kinetics data acquisition. *Molecular Catalysis* **2018,** *458*, 180-188.

24. Lansalot-Matras, C.; Moreau, C., Dehydration of fructose into 5-hydroxymethylfurfural in the presence of ionic liquids. *Catalysis Communications* **2003,** *4* (10), 517-520.

25. Qi, X.; Watanabe, M.; Aida, T. M.; Smith, R. L., Efficient Catalytic Conversion of Fructose into 5-Hydroxymethylfurfural in Ionic Liquids at Room Temperature. *ChemSusChem* **2009,** *2* (10), 944-946.

26. Yue, C.; Li, G.; Pidko, E. A.; Wiesfeld, J. J.; Rigutto, M.; Hensen, E. J. M., Dehydration of Glucose to 5-Hydroxymethylfurfural Using Nb-doped Tungstite. *ChemSusChem* **2016,** *9* (17), 2421-2429.

27. Delidovich, I.; Hausoul, P. J. C.; Deng, L.; Pfützenreuter, R.; Rose, M.; Palkovits, R., Alternative Monomers Based on Lignocellulose and Their Use for Polymer Production. *Chemical Reviews* **2016,** *116* (3), 1540-1599.

28. van Putten, R.-J.; van der Waal, J. C.; de Jong, E.; Rasrendra, C. B.; Heeres, H. J.; de Vries, J. G., Hydroxymethylfurfural, A Versatile Platform Chemical Made from Renewable Resources. *Chemical Reviews* **2013,** *113* (3), 1499-1597.

29. Gandini, A.; Silvestre, A. J. D.; Neto, C. P.; Sousa, A. F.; Gomes, M., The furan counterpart of poly(ethylene terephthalate): An alternative material based on renewable resources. *Journal of Polymer Science Part A: Polymer Chemistry* **2009,** *47* (1), 295-298.

30. Moreau, C.; Belgacem, M. N.; Gandini, A., Recent Catalytic Advances in the Chemistry of Substituted Furans from Carbohydrates and in the Ensuing Polymers. *Topics in Catalysis* **2004,** *27* (1), 11-30.

31. Nakajima, H.; Dijkstra, P.; Loos, K., The Recent Developments in Biobased Polymers toward General and Engineering Applications: Polymers that are Upgraded from Biodegradable Polymers, Analogous to Petroleum-Derived Polymers, and Newly Developed. *Polymers* **2017,** *9* (10), 523.

32. Huang, Y.-T.; Wong, J.-J.; Huang, C.-J.; Li, C.-L.; Jang, G.-W. B., 2,5-Furandicarboxylic Acid Synthesis and Use. In *Chemicals and Fuels from Bio-Based Building Blocks*, Wiley-VCH Verlag GmbH & Co. KGaA: 2016; pp 191-216.

33. Partenheimer, W.; Grushin, Vladimir V., Synthesis of 2,5-Diformylfuran and Furan-2,5-Dicarboxylic Acid by Catalytic Air-Oxidation of 5-Hydroxymethylfurfural. Unexpectedly Selective Aerobic Oxidation of Benzyl Alcohol to Benzaldehyde with Metal=Bromide Catalysts. *Advanced Synthesis & Catalysis* **2001,** *343* (1), 102-111.

34. Zhang, Z.; Huber, G. W., Catalytic oxidation of carbohydrates into organic acids and furan chemicals. *Chemical Society Reviews* **2018,** *47* (4), 1351-1390.

35. Davis, S. E.; Zope, B. N.; Davis, R. J., On the mechanism of selective oxidation of 5-hydroxymethylfurfural to 2,5-furandicarboxylic acid over supported Pt and Au catalysts. *Green Chemistry* **2012,** *14* (1), 143-147.

36. Ardemani, L.; Cibin, G.; Dent, A. J.; Isaacs, M. A.; Kyriakou, G.; Lee, A. F.; Parlett, C. M. A.; Parry, S. A.; Wilson, K., Solid base catalysed 5-HMF oxidation to 2,5-FDCA over Au/hydrotalcites: fact or fiction? *Chemical Science* **2015,** *6* (8), 4940-4945.

37. Gupta, N. K.; Nishimura, S.; Takagaki, A.; Ebitani, K., Hydrotalcite-supported gold-nanoparticle-catalyzed highly efficient base-free aqueous oxidation of 5-hydroxymethylfurfural into 2,5-furandicarboxylic acid under atmospheric oxygen pressure. *Green Chemistry* **2011,** *13* (4), 824-827.

38. Wan, X.; Zhou, C.; Chen, J.; Deng, W.; Zhang, Q.; Yang, Y.; Wang, Y., Base-Free Aerobic Oxidation of 5-Hydroxymethyl-furfural to 2,5-Furandicarboxylic Acid in Water Catalyzed by Functionalized Carbon Nanotube-Supported Au–Pd Alloy Nanoparticles. *ACS Catalysis* **2014,** *4* (7), 2175-2185.

39. Zhou, C.; Deng, W.; Wan, X.; Zhang, Q.; Yang, Y.; Wang, Y., Functionalized Carbon Nanotubes for Biomass Conversion: The Base-Free Aerobic Oxidation of 5-Hydroxymethylfurfural to 2,5-Furandicarboxylic Acid over Platinum Supported on a Carbon Nanotube Catalyst. *ChemCatChem* **2015,** *7* (18), 2853-2863.

40. Yi, G.; Teong, S. P.; Zhang, Y., Base-free conversion of 5-hydroxymethylfurfural to 2,5-furandicarboxylic acid over a Ru/C catalyst. *Green Chemistry* **2016,** *18* (4), 979-983.

Chapter 2. Experimental

In this chapter the catalyst characterization techniques and experimental setup for catalytic tests are described. Due to their variety, catalyst synthesis descriptions are excluded from this chapter, and they will be reported in the single chapter they are referred to.

2.1 Catalyst characterization

DLS

Measurement of nanoparticles hydrodynamic diameter was performed with the DLS techniques, using a Zetasizer Nanoseries (Malvern Instruments). From this measurement average nanoparticle diameter size, curve of their distributions and polydispersivity quantitative information have been obtained. Samples have been prepared by diluting 10 drops of the metal suspension in 10mL of water.

XRD

XRD analyses were performed on the dried nanoparticles metal suspension to evaluate the crystallite size before and after impregnation. XRD measurements were carried out at room temperature with a Philips X'Pert diffractometer, using as source a Cu anode (Kα, λ = 1,5718 nm).

TGA

Thermogravimetric analyses have been carried out using a Q500 instrument by TA instruments. The analyses have been performed constant air flow (100mL/min) and the weight variation has been evaluated within the range between 30 to 800°C (temperature ramp 10°C/min).

HRTEM

HRTEM analyses were performed using a TEM/STEM FEI TECNAI F20, which uses a high-angle annular dark field (HAADF) imaging mode at 200kV and with an EDS PV9761N SUTW energy dispersive X-ray spectrometer (EDX) for X-ray microanalysis. The analyses of suspension were performed by diluting them in water and then the obtained suspensions were dispersed on a holey carbon film. As far as the electrospun membrane characterization is concerned, fibers were electrospun directly on a W sample holder for few seconds.

BET

Catalyst surface areas were measured by N_2 physisorption (Sorpty 1750 CE instruments) and a single-point BET analysis method was used. Samples were pre-treated under vacuum conditions below the respective glass transition temperature until full removal of adsorbed species from sample surface.

ATR

ATR analyses were performed with the aim to evaluate the chemical structure of polymer fibers. These analyses were obtained by a Bruker Alpha FTIR instrument equipped with a diamond crystal.

2.2 Catalytic test

The catalytic tests were performed in a lab scale autoclave reactor (100 mL capacity), equipped with a mechanical stirrer (0–600 rpm) and measurement tools for temperature and pressure. The aqueous solution of HMF and catalyst were loaded in the reactor. HMF was purchased from AVABiochem and used without any purification.

The autoclave was purged 3 times with O_2 (2 bar) and then pressurized at 10 bar. The temperature was increased to the set point and the reaction mixture was stirred for the whole experiment. Initial time (time zero) for the reaction was considered when the set point temperature was reached (after 10 min). At the end of the reaction, the reactor was cooled to room temperature and the solution was filtered. Then, 1mL of the reaction mixture was diluted 5 times and, the resulting solution was then analysed with an Agilent Infinity 1260 liquid chromatograph equipped with an Aminex HPX-87H 300 mm × 7.8 mm column using a 0.005 M H_2SO_4 solution as mobile phase. The compound identification and quantification were achieved by calibration using reference commercial samples.

Chapter 3. Pt and Pt/Sn clusters as precursors for the synthesis of catalysts

3.1 Introduction

Among all the parameters that affect the catalytic performances of supported metal nanoparticles, dimension could be considered as one of the most important, thus nanoparticle size control is considered of primary importance when a nanoparticle synthetic strategy is designed. At the same time, in the synthesis of polymetallic nanosystems, the chemical composition of the nanoparticles in the catalyst final form must be considered. In this frame, due to their chemical and structural definite composition, metal clusters have been considered as promising precursor for the synthesis of metal nanoparticles based catalysts.[1]

Pt based catalysts have been found to be active in HMF oxidation by Verdeguer et al..[2] In their study, Pt catalyst was coupled with a co-catalyst (Pb containing species) and the addition of an inorganic base to the reaction medium was found to be crucial to obtain high yield of FDCA. Further studies proved that by changing the catalyst synthesis and choosing the suitable support, co-catalyst could be avoided,[3-6] and more recent approach suggested that HMF oxidation could be carried out without any addition of base, using small Pt nanoparticles as active phase.[7-8]

In view of the above, the synthesis mono- and bimetallic Pt/Sn on TiO2 systems obtained from cluster decomposition has been performed, and these systems have been tested in the base free HMF oxidation.

The homometallic Pt cluster ($[Pt_{12}(CO)_{24}]^{2-}$) has been synthesized by reductive carbonylation of Na_2PtCl_6. Such homometallic cluster has been also used as precursor of the two bimetallic materials having a specific Pt/Sn molar ratio of 1 and 2 ($[Pt_6(CO)_6(SnCl_2)_2(SnCl_3)_4]^{4+}$ and $[Pt_6(CO)_8(SnCl_2)(SnCl_3)_2(PPh_3)_2]^{2+}$, respectively). All the three mentioned clusters have been supported on titania via wetness impregnation (metal loading 2and 4% w/w) and the resulting material has been dried (120°C) and underwent thermic treatment at 450°C

Another set of catalysts has been prepared by incipient wetness impregnation on titania of metal salt solution using the same metal loading and Pt/Sn ratio as the cluster derived materials (i.e. monometallic Pt, bimetallic=Pt/Sn 1 and Pt/Sn=2).

The so-synthesized materials have been used as catalyst in the aqueous phase base-free oxidation of HMF into FDCA.

The material synthesis steps, as well as the catalyst properties before and after reaction, have been analyzed by means of BET, HRTEM, and FTIR techniques.

3.2 Catalyst synthesis

3.2.1 Supported cluster catalyst synthesis

The supported cluster catalysts synthesis has been performed according the procedure designed by Bortoluzzi et al.[9]

Homometallic cluster ($[PPh_4]_2[Pt_{12}(CO)_{24}]$) synthesis

The homometallic cluster ($[PPh_4]_2[Pt_{12}(CO)_{24}]$, named as Pt_{12}) has been synthesized as follows: 2.00g of Na_2PtCl_6 $6H_2O$, 2.00g of anhydrous CH_3COONa were dissolved in 20mL of CH_3OH. The resulting solution was left stirring at room temperature in CO atmosphere for 24 hours. Then, a NaOH saturated methanol solution was slowly added until the formation of $Na_2[Pt_{12}(CO)_{24}]$ occurred. Then, the cation exchange has been performed adding an alcoholic solution of $[PPh_4]Br$, leading to the formation of a precipitate ($[PPh_4]_2[Pt_{12}(CO)_{24}]$). The so obtained solid has been filtered, washed with isopropilic alcohol, and then extracted with acetone. The IR analysis performed over the cluster collected in acetone showed bands at 2047 (s), 1897 (sh), 1881 (sh), 1865 (m), 1833 (sh) cm^{-1}, which are assigned to the desired cluster.

Bimetallic clusters synthesis

The Pt_{12} cluster obtained through the aforementioned protocol, has been used as starting material for the synthesis of the bimetallic cluster $[PPh_4]_4[Pt_6(CO)_6(SnCl_2)_2(SnCl_3)_4]$ (Pt/Sn molar ratio 1, named as Pt_1Sn_1): 1.08g of Pt_{12} has been dissolved in 20mL of acetone in nitrogen atmosphere. To this solution, 0.79g of $SnCl_2$ $2H_2O$ and 0.87g of $[PPh_4]Cl$ were added, and left stirring for 2h. Solvent has been evaporated and the resulting solid has been washed with isopropanol first, and then with acetone. The desired product, Pt_1Sn_1, was then extracted with acetonitrile and the registered IR spectrum showed only one peak at 2038 (s) cm^{-1}, confirming the presence of pure Pt_1Sn_1.

To obtain the $[PPh_4]_2[Pt_6(CO)_8(SnCl_2)(SnCl_3)_2(PPh_3)_2]$ cluster (Pt/Sn molar ratio 2, named as Pt_2Sn_1), 0.52g of Pt_1Sn_1 were dissolved in acetonitrile (20mL) in CO atmosphere and 0.07 of PPh_3 were added after 5 minutes of stirring. The solution was left stirring for 2h and isopropanol was added until the precipitate formation of the solid., which was washed with isopropanol and vacuum dried. The dried

solid was extracted in acetonitrile and the IR analysis proved its purity (2042 (s), 1881 (w), 1829 (m) cm^{-1} characteristic bands).

Cluster impregnation and thermal treatment

The prepared clusters have been supported on titania (2% total metal loading, i.e. Pt and Sn, respect to titania, as confirmed by XRF analyses) by wetness impregnation: the cluster containing solutions were slowly added to the titania in air free condition and left stirring for 2h. At the end of this process, the resulting material has been dried in an oven (120°C for 2h). The dried powder has been then pressed in wafers and then crushed and sieved to obtain pellets having suitable dimension (20-40mesh). Such pellets have been thermally treated up to 450°C (2°C/min) in controlled atmosphere (air or H_2).

The samples prepared via cluster impregnation on TiO_2 are listed in Table 3-1:

Sample	**Precursor**	**Nominal Pt/Sn molar ratio**	**Esperimental Pt/Sn molar ratio**	**Metal (Pt+Sn) loading (w/w %)**	**Thermal treatment**
2-Pt-H_2	Pt_{12}	-	-	2	Drying (2h,120°C) H_2 (2h, 450°C)
2- Pt_2Sn_1-H_2	Pt_2Sn_1	2	1.95	2	Drying (2h,120°C) H_2 (2h, 450°C)
2- Pt_1Sn_1	Pt_1Sn_1	1	1.01	2	Drying (2h,120°C)
2- Pt_1Sn_1-H_2	Pt_1Sn_1	1	1.00	2	Drying (2h,120°C) H_2 (2h, 450°C)
2- Pt_1Sn_1-O_2	Pt_1Sn_1	1	1.03	2	Drying (2h,120°C) air (2h, 450°C)

Table 3-1 Code, metal loading and thermal treatment of the cluster derived materials

Pt and Pt/Sn clusters as precursors for the synthesis of catalysts

3.2.2 Metal salt impregnated catalyst

The metal salt impregnated catalysts have been synthesized by incipient wetness impregnation of titania with containing Pt and Sn metal precursor solution (H_2PtCl_6 and Sn_2Cl, respectively). The concentration of metal ions has been calculated in order to obtain materials having the same Pt/Sn ratio and metal loading as the supported cluster materials.

The impregnated solids underwent the same thermal treatments as reported for the supported cluster materials.

In Table 3-2, the list of metal salt impregnated catalyst is reported.

Sample	Precursor	Nominal Pt/Sn molar ratio	Metal (Pt+Sn) loading (w/w %)	Thermal treatment
2-Pt-s-H_2	H_2PtCl_6	-	2	Drying (2h,120°C) H_2 (2h, 450°C)
2-Pt_2Sn_1-s-H_2	H_2PtCl_6 $SnCl_2$	2	2	Drying (2h,120°C) H_2 (2h, 450°C)
2-Pt_1Sn_1-s-H_2	H_2PtCl_6 $SnCl_2$	1	2	Drying (2h,120°C) H_2 (2h, 450°C)
2-Sn-s-H_2	$SnCl_2$	0	2	Drying (2h,120°C) H_2 (2h, 450°C)

Table 3-2 Code, metal loading and thermal treatment of the metal salt impregnated catalysts

3.3 Cluster derived catalyst characterization

3.3.1 IR study of cluster modification during impregnation procedure and thermal treatments

With the aim to understand how cluster structure is affected by the impregnation procedure, FTIR technique has been used. In detail, the CO bands of the different clusters have been used as probe for the individuation of changes in cluster structure in the three crucial phases of its impregnation procedure, namely, in solution before impregnation, during impregnation (i.e. when it is present in suspension with titania) and as impregnated powder.

The spectrum recorded for the Pt_{12} cluster solution (black line in Figure 3-1) shows the carbonyl signals of the $[PPh_4]_2[Pt_{12}(CO)_{24}]$ cluster (2047cm^{-1} for the terminal carbonyls, 1897, 1881, 1865 and 1833cm^{-1} for the bridged ones), plus a contribution at 2030cm^{-1} probably due to the formation of $[Pt_9(CO)_{18}]^{2-}$ specie. After the titania addition, the spectrum recorded (red line in Figure 3-1) showed no significant change in the signal pattern, which occurs after solvent removal (green line in Figure 3-1): the bands shift to higher wavelength could indicate the formation of $[Pt_{18}(CO)_{30}]^{2-}$ specie, thus a cluster oxidation induced by solvent removal could be hypothesized.

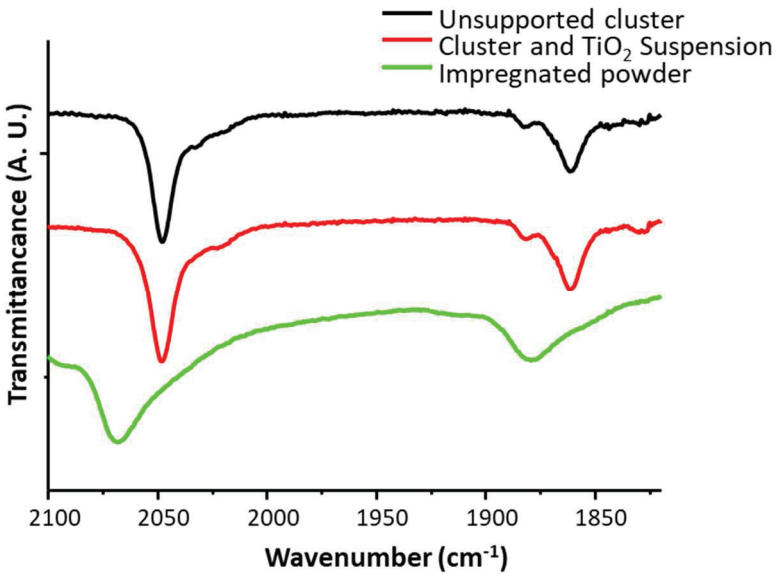

Figure 3-1 FTIR spectra recorded during the Pt_{12} impregnation protocol. From top to bottom: unsupported cluster, cluster and TiO_2 suspension, impregnated powder

As far as the Pt_1Sn_1 cluster impregnation procedure is concerned, the IR performed on its solution clearly shows one peak at 2037cm^{-1}, assignable to the terminal CO species of the cluster (black line, Figure 3-2). The addition of the titania to the solution led to the formation of another specie (peak at 2010cm^{-1}, red line in Figure 3-2) whose structure has not been clarified. The same peaks were found in the impregnated spectrum (green line, Figure 3-2), indicating that in this case no oxidation of the Pt species occurs during solvent removal.

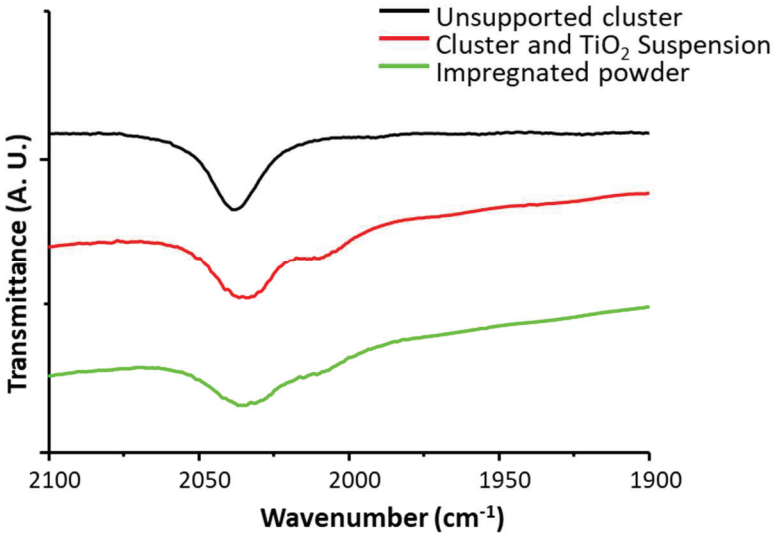

Figure 3-2 FTIR spectra recorded during the Pt_1Sn_1 impregnation protocol. From top to bottom: unsupported cluster, cluster and TiO_2 suspension, impregnated powder

The carbonyl cluster Pt_2Sn_1 dissolved in acetonitrile (black line in Figure 3-3) showed four signals: two attributable to terminal carbonyls (2043 and 2028 cm^{-1}) and two attributable to bridged species (1882 and 1831 cm^{-1}). The presence of a shoulder at 2012cm^{-1} could indicate the formation of another specie (probably, $[Pt_6(CO)_6(SnCl_2)_2(SnCl_3)_2(PPh_3)_2]^{2-}$). The following impregnation steps do not lead to significant changes in carbonyls signals, indicating that the Pt_2Sn_1 does not undergo any structural modification during the impregnation procedure.

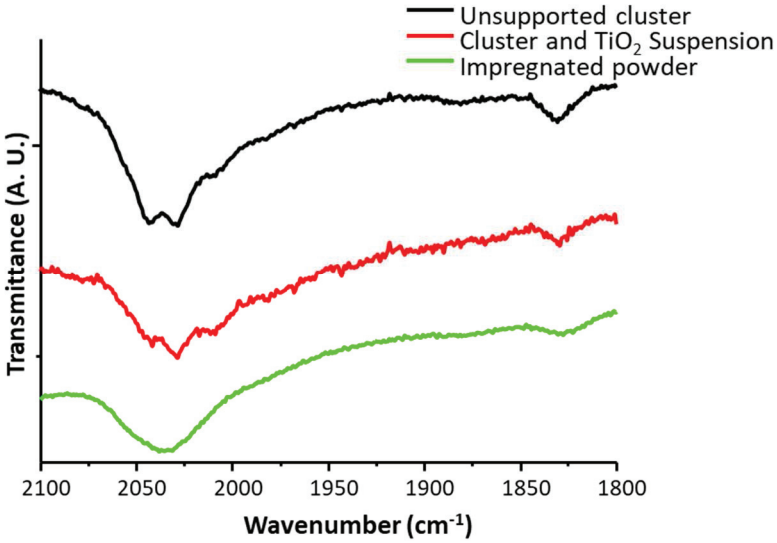

Figure 3-3 FTIR spectra recorded during the Pt_2Sn_1 impregnation protocol. From top to bottom: unsupported cluster, cluster and TiO_2 suspension, impregnated powder

In view of the above, it could be said that the three Pt-based clusters do not suffer any strong structural modification during the impregnation procedure, especially if compared to other cluster systems.

After this study, a similar analysis has been performed on supported Pt_1Sn_1 materials with the aim to understand how the subsequent thermal treatments affect cluster structure. As could be seen from Figure 3-4, cluster decomposition seems to begin after the drying procedure, since the peak pattern differs from the one recorded for the supported Pt_1Sn_1 cluster (black line in Figure 3-4). Then, irrespective of the atmosphere used, the thermal treatment at 450°C leads to the complete decomposition of the cluster since no carbonyl peaks were detected in both 2-Pt_1Sn_1-H_2 and 2-Pt_1Sn_1-O_2 samples (Figure 3-4 red and blue lines, respectively).

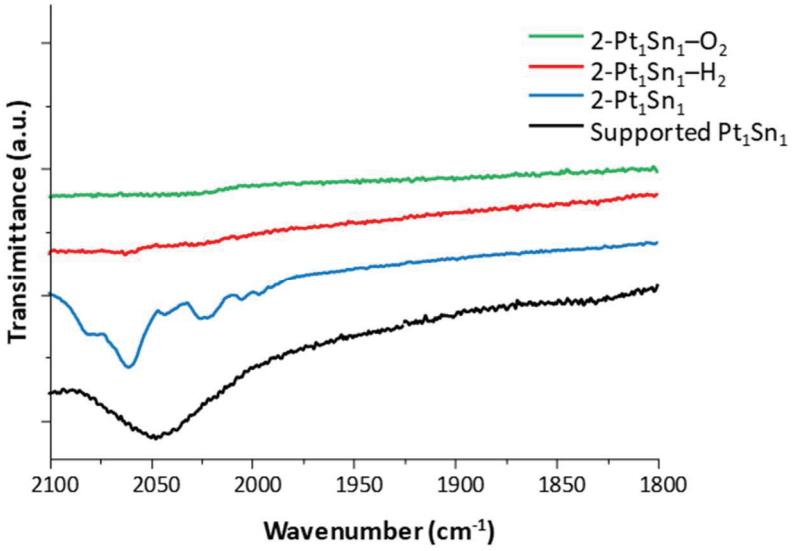

Figure 3-4 FTIR characterization of different 2-Pt_1Sn_1 materials. From bottom to top: supported Pt_1Sn_1, 2-Pt_1Sn_1 (dried sample), 2-Pt_1Sn_1-H_2 (450°C treatment in H_2), 2-Pt_1Sn_1-O_2 (450°C treatment in O_2)

3.3.2 Thermal treatments effect on catalyst feature

To understand how the high temperature treatments (450°C) and related atmosphere (H_2 and air) affect the material final features, Pt_1Sn_1 derived materials (i.e. 2-Pt_1Sn_1-H_2, 2-Pt_1Sn_1-O_2) have been characterized by means of HRTEM and EDX.

STEM technique was used to obtain information on the morphology and size distribution of the metallic species obtained after the treatment at 450°C in both H_2 atmosphere (2-Pt_1Sn_1-H_2, Figure 3-5 right) and air (2-Pt_1Sn_1-O_2, Figure 3-5 left).

This analysis showed that after thermal treatment, small metal nanoparticles are obtained, being their average diameter not strongly influenced by the atmosphere used, as shown in Table 3-3.

Sample	Average nanoparticle diameter (nm)	Standard deviation
2-Pt_1Sn_1-H_2	2.4	1.8
2-Pt_1Sn_1-O_2	2.6	1.6

Table 3-3 Nanoparticle average size and distribution standard deviation of the Pt_1Sn_1 derived materials: 2-Pt_1Sn_1-H_2 (treated at 450°C in H_2 atmosphere) and 2-Pt_1Sn_1-O_2 (treated at 450°C in air)

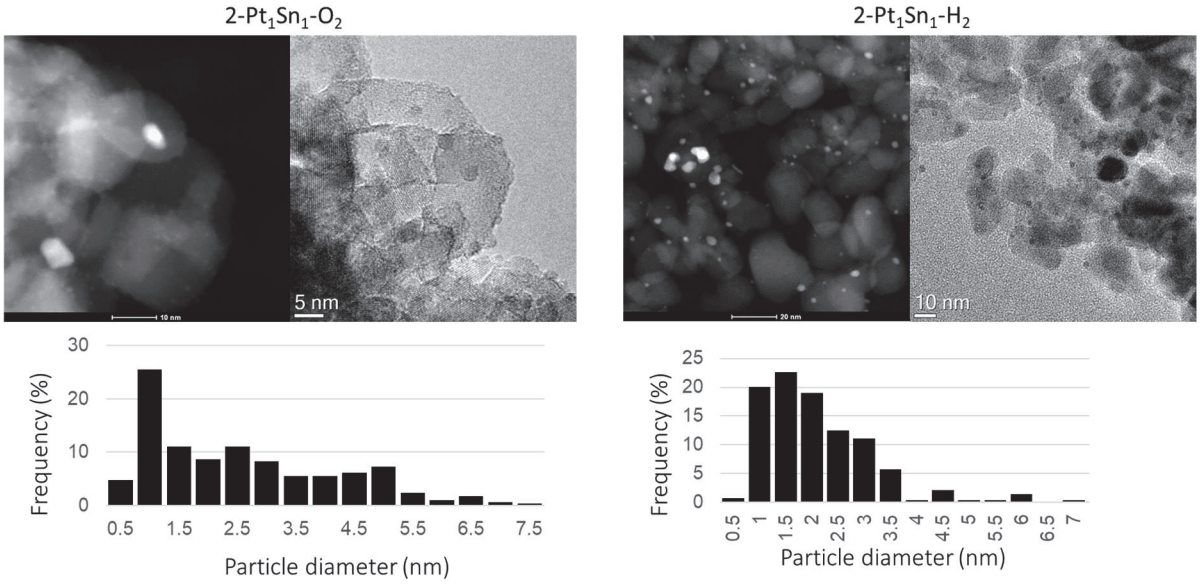

Figure 3-5 STEM, TEM and nanoparticle diameters of the Pt_1Sn_1 derived materials: air treated 2-Pt_1Sn_1-O_2 and H_2 treated 2-Pt_1Sn_1-H_2 (left and right, respectively)

On the other hand, EDX analyses evidenced that the distribution of the two metals over support surface is strongly affected by the atmosphere used in the 450°C treatment. In fact, in the air-treated sample Sn seems to be evenly spread on the TiO_2 surface and Pt is mainly present as NPs, while in the H_2-treated sample, high concentration of the two metals are detected in the same points of the support surface (Figure 3-6). This feature suggests that reducing atmosphere prevent the outmigration of Sn from the cluster structure and Pt/Sn NPs could be obtained in such reducing conditions.

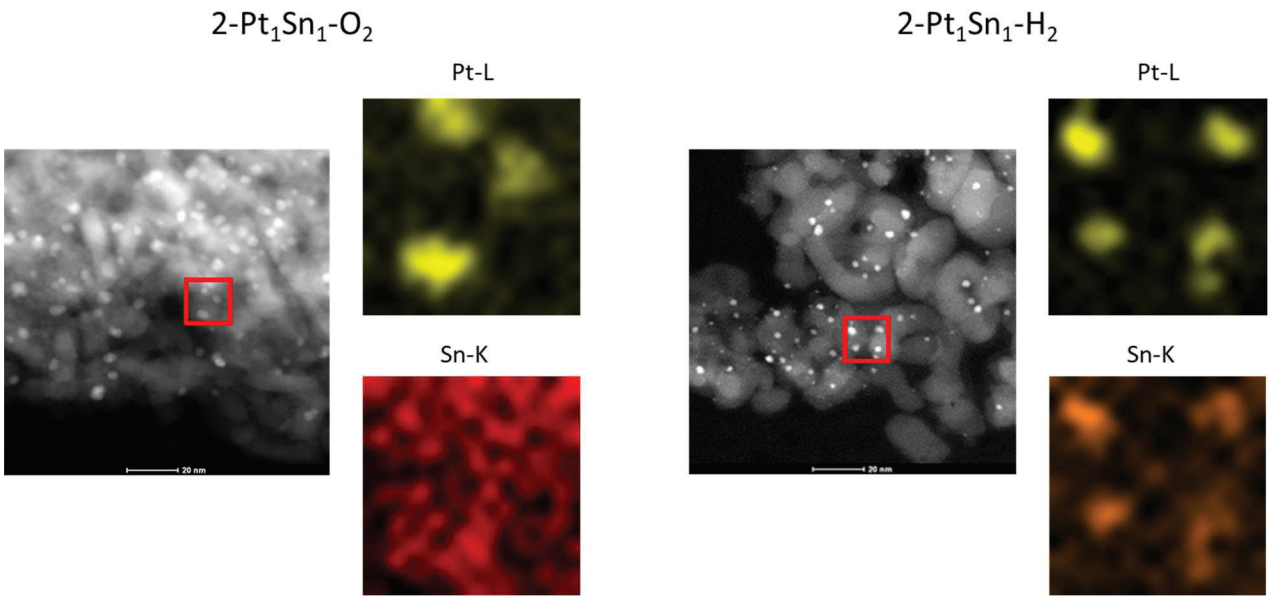

Figure 3-6 EDX maps for Pt and Sn of the indicated region of the air treated 2-Pt_1Sn_1-O_2 and H_2 treated 2-Pt_1Sn_1-H_2 (left and right, respectively)

3.3.3 Effect of Pt/Sn ratio on active phase properties

STEM and EDX analyses were carried out to verify the effect of Pt/Sn ratio on the dispersion of active phase over the support after high temperature (450°C) treatment in H_2. The average nanoparticle size for 2-Pt-H_2, 2-Pt_2Sn_1-H_2 (Figure 3-7 left and right, respectively) and 2-Pt_1Sn_1-H_2 (Figure 3-5, right) samples are given in Table 3-4, and a strong effect of Sn content on the definition of the metal NPs size in the three samples was found.

Sample	Sn weight content (% w/w)	Average nanoparticle diameter (nm)	Standard deviation
2-Pt-H_2	-	2.0	1.0
2-Pt_2Sn_1-H_2	0.5	1.2	0.4
2-Pt_1Sn_1-H_2	0.8	2.4	1.8

Table 3-4 Average nanoparticle diameter according Sn content

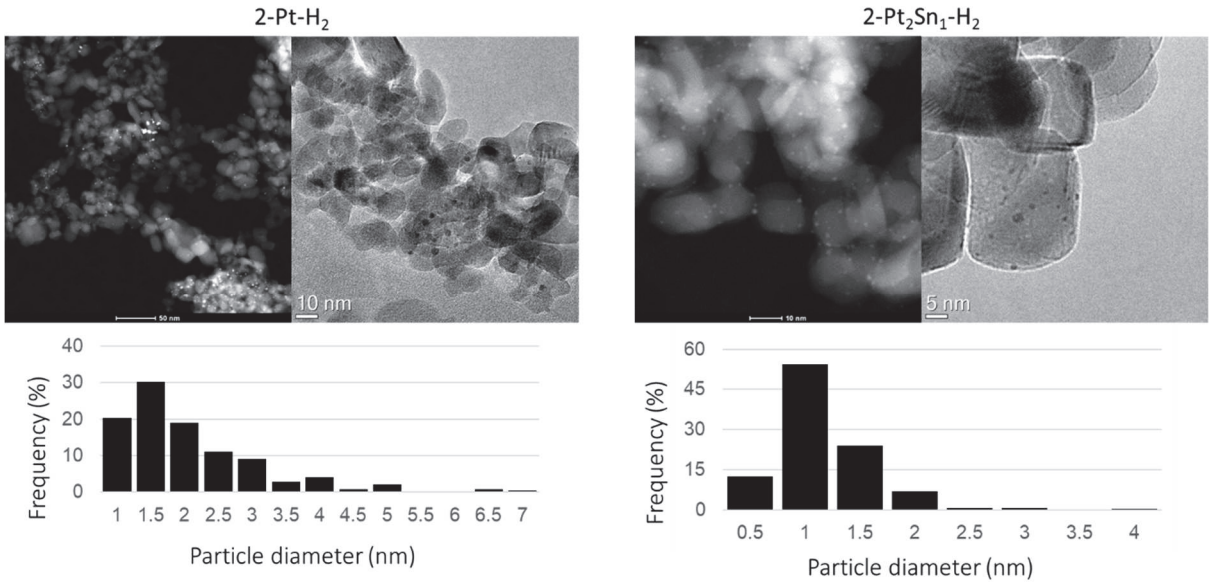

Figure 3-7 STEM, TEM and nanoparticle diameters of the Pt_{12} derived material (2-Pt-H_2, treated in H_2 at 450°C, left) and the Pt_2Sn_1 one (2-Pt_2Sn_1-H_2, treated in H_2 at 450°C, right)

In addition to this, the metal disposition images obtained via EDX mapping for the 2-Pt_2Sn_1-H_2 sample showed that Sn is dispersed over the support surface, while Pt is mainly present as NP (Figure 3-8). This feature is in contrast with the Sn disposition reported for the 2-Pt_1Sn_1-H_2, since in the latter, Pt/Sn aggregates were found (Figure 3-6). This different metal dispersion could explain the different size of the two Sn-containing samples, since it seems reasonable to expect that the monometallic NPs (found in 2-Pt_2Sn_1-H_2) would have smaller size respect to bimetallic aggregates detected in the 2-Pt_1Sn_1-H_2 sample. On the other hand, considering the bigger size of the Pt NPs in the monometallic 2-Pt-H_2 respect to the 2-Pt_2Sn_1-H_2 ones, it could be postulated that Sn acts as NP dimension stabilizer, leading to smaller Pt NPs.

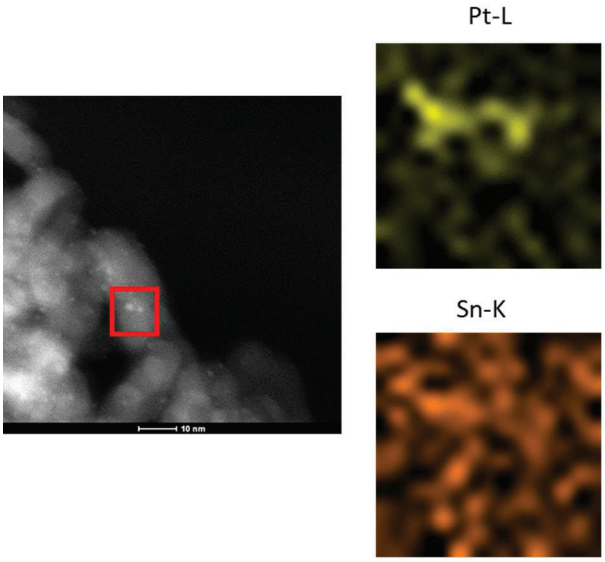

Figure 3-8 STEM image of the H_2 treated 2-Pt_2Sn_1-H_2 sample and EDX maps for Pt and Sn of the indicated region

3.4 Characterization of the salt derived catalysts

STEM analyses have been performed on the salt impregnated 2-Pt-s-H_2 and 2-Pt_1Sn_1-H_2 samples with the aim to understand if the different synthetic protocol has an effect on the features of the synthesized materials.

The 2-Pt-s-H_2 sample TEM analysis showed a poor Pt dispersion over the support surface. As could be seen in Figure 3-9, Pt is present as aggregates, whose size ranges from few nm to 200nm, indicating that the protocol used to synthesize such material did not lead to good Pt aggregates size control, which has been obtained via cluster decomposition protocol, as shown in the previous paragraph.

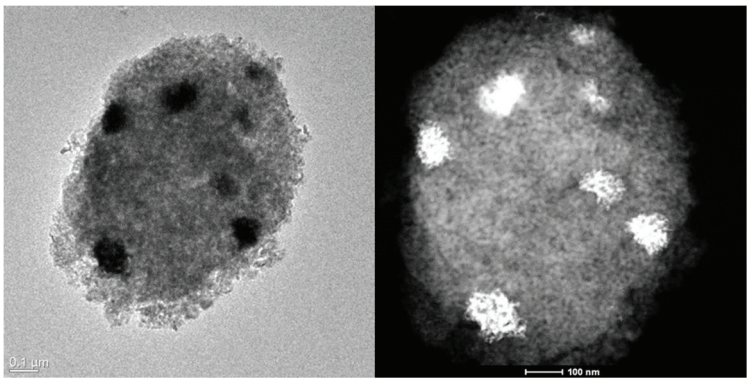

Figure 3-9 STEM characterization of 2-Pt-s-H_2 sample, obtained via direct impregnation of the Pt salt precursor

On the other hand, the STEM analysis of the 2-Pt_1Sn_1-s-H_2 sample showed that the co-impregnation of the two metals led to an improved NPs dispersion, indicating that Sn plays as NPs size stabilizing

agent (Figure 3-10). However, some metal aggregates, having high dimension (ca. 60nm, see Figure 3-11), have been detected.

The EDX analysis performed on this sample showed that, in contrast to 2-Pt_1Sn_1-H_2 sample, Sn does not tend to aggregate close to Pt nanoparticles (Figure 3-12). Thus, it is clear that the metal salt impregnation protocol cannot ensure the same particle size control and surface metal distribution obtained via metal cluster decomposition.

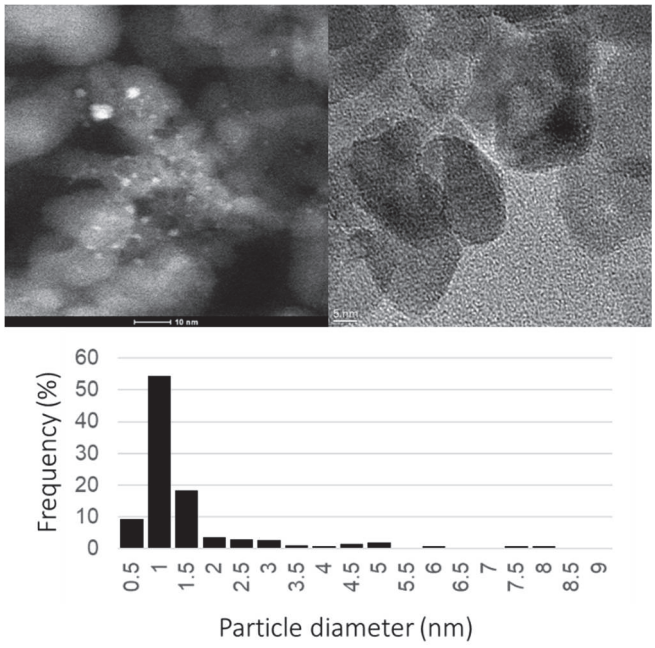

Figure 3-10 TEM (top), STEM characterization and nanoparticle dimension distribution (bottom) 2-Pt_1Sn_1-s-H_2 sample

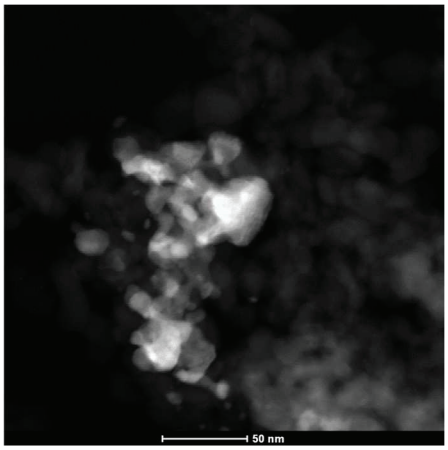

Figure 3-11 Metal aggregates on the 2-Pt_1Sn_1-s-H_2 samples

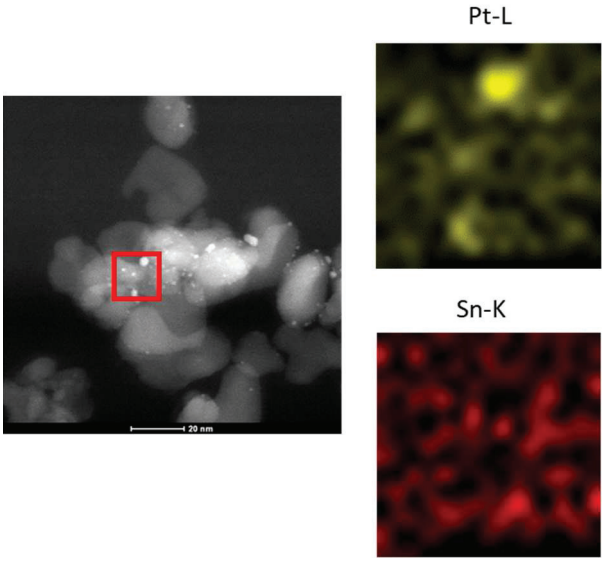

Figure 3-12 STEM image of the H_2 treated 2-Pt_1Sn_1-s-H_2 sample and EDX maps for Pt and Sn of the indicated region

Considering these analyses, it is clear that the metal salt impregnation protocol cannot ensure the same particle size control and surface metal distribution obtained via metal cluster decomposition.

3.5 Catalytic tests

3.5.1 Preliminary screening

The first screening conducted over the monometallic 2-Pt-s-H_2 and 2-Sn-s-H_2, obtained via metal salt impregnation, is showed in Figure 3-13. Such preliminary test revealed that among the two metals, just Pt is active toward HMF oxidation in base-free condition. In detail, Pt is able to convert HMF in both HMFCA and DFF, being the latter more abundant than the previous (1 and 18%, respectively).

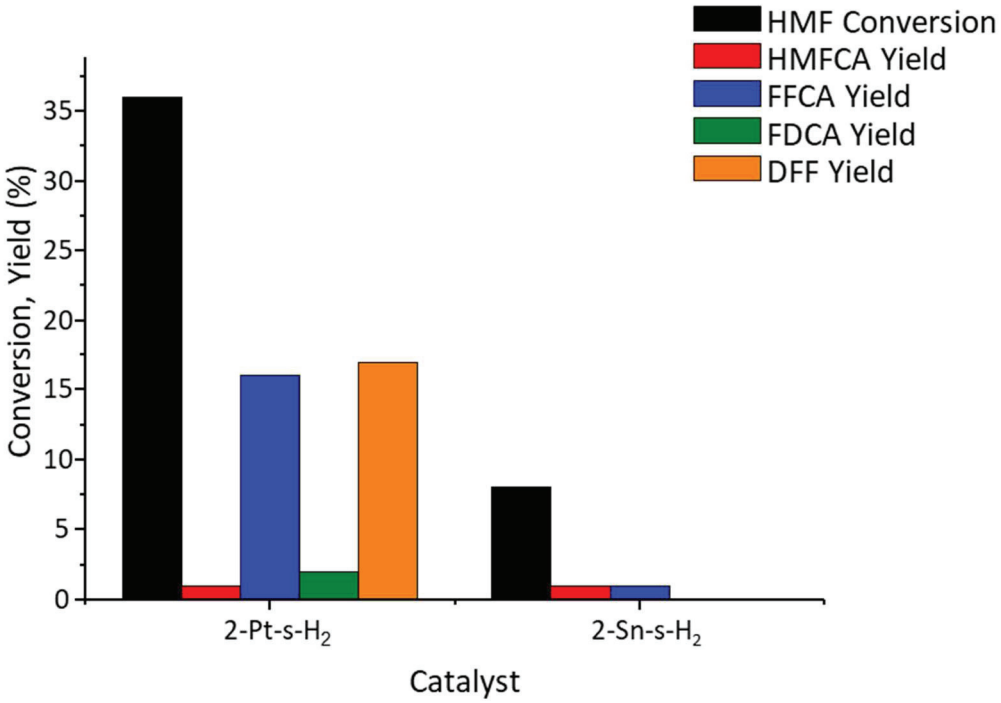

Figure 3-13 Catalytic performances of Pt and Sn impregnated materials. Operative conditions: temperature 110°C, O_2 pressure 10bar, 25mL water, HMF 0.0310g, molar ratio HMF/total metal=50.

This result is in good accordance with the literature, since, in base-free condition, DFF formation is known to be favored over HMFCA. Both products of consecutive oxidation, i.e. FFCA and FDCA were detected (16 and 2% of yield, respectively).

Superior results in terms of HMF conversion and target product (FDCA) yield were obtained by employing the materials prepared via cluster impregnation (Figure 3-14), indicating that such synthetic strategy has a positive effect in determining the catalytic properties of the material.

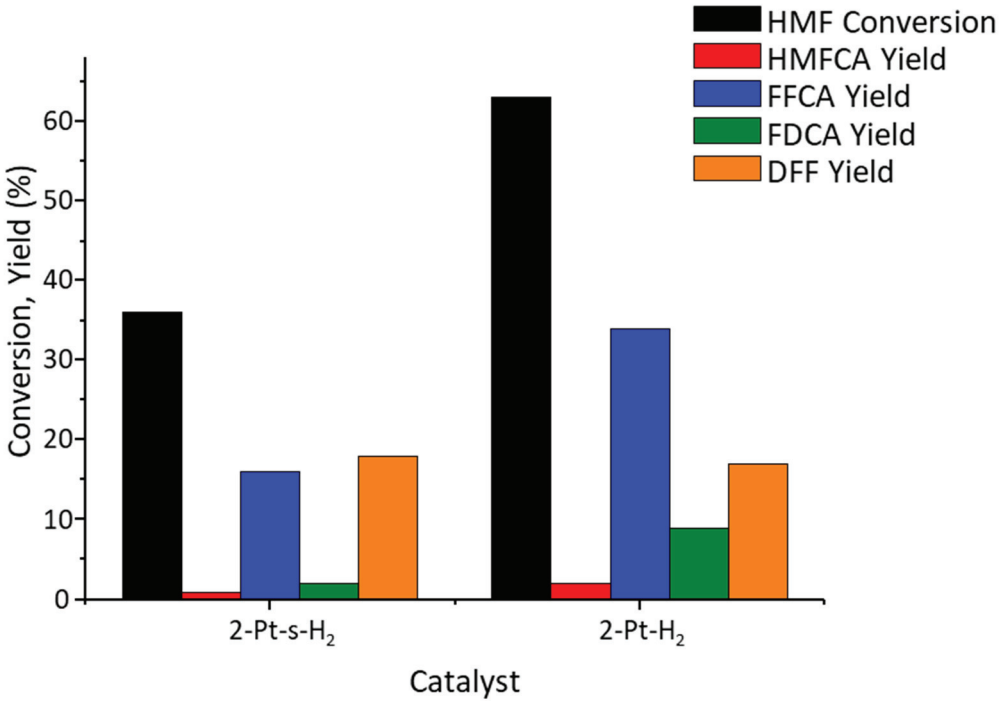

Figure 3-14 Catalytic performances of Pt-monometallic catalysts. Operative conditions: temperature 110°C, O_2 pressure 10bar, 25mL water, HMF 0.0310g, molar ratio HMF/total metal=50.

This feature could be ascribed to the improved dispersion and smaller Pt NPs of the cluster derived material (2-Pt-H_2) respect to its metal salt impregnated counterpart (2-Pt-s-H_2).

3.5.2 Sn content effect on the catalytic activity

The effect of the Sn presence on the catalytic performances have been studied for cluster impregnated catalysts by keeping constant the HMF/metal molar ratio constant (i.e. equal to 50). These results showed that the addition of Sn to the system modifies catalytic material properties, as could be seen in Figure 3-15.

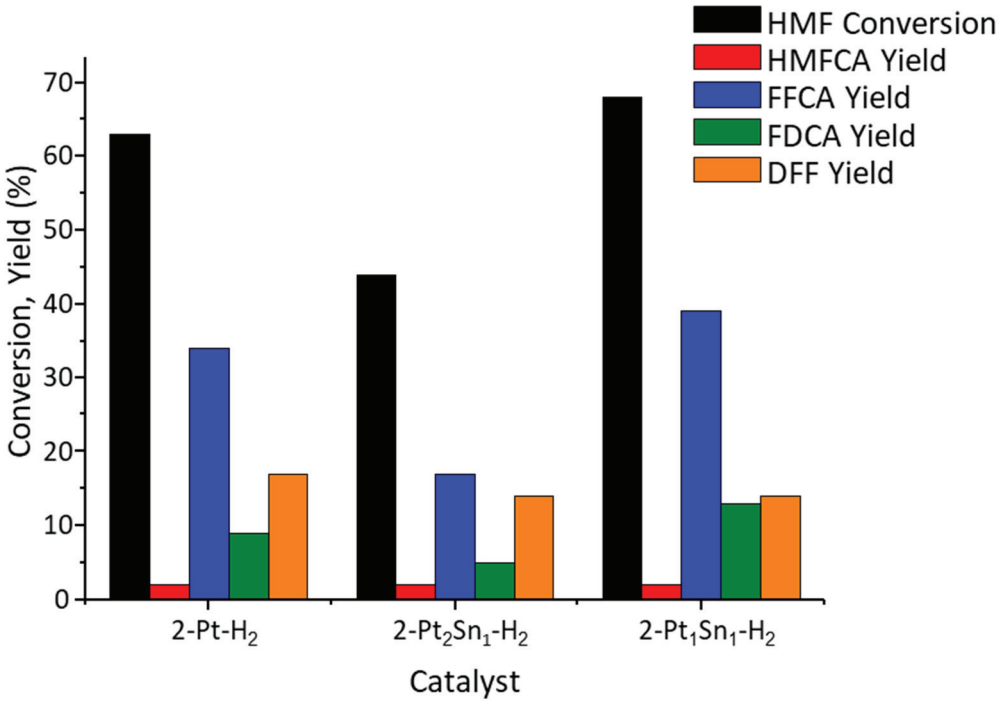

Figure 3-15 Catalytic performances of cluster impregnated catalysts. Operative conditions: temperature 110°C, O_2 pressure 10bar, 25mL water, HMF 0.0310g, molar ratio HMF/total metal=50.

In detail, a Sn/Pt molar ratio equivalent to 0.5 (as in 2-Pt_2Sn_1-H_2) seems to be detrimental for both HMF conversion and FDCA yield, while the equimolar catalyst provides higher FDCA yield if compared to the monometallic 2-Pt-H_2 catalyst (13 and 9% for 2-Pt_1Sn_1-H_2 and 2-Pt-H_2, respectively). This result is of particular interest if considered that Pt, which has been proven to be the active metal, is more diluted in sample 2-Pt_1Sn_1-H_2 than in the other two, thus the best results in term of FDCA yield were obtained with catalyst having the lowest active metal content (Table 3-5).

Catalyst	Pt content (w/w%)	FDCA yield (%)	FDCA/Pt molar ratio
2-Pt-H_2	2	9	4.5
2-Pt_2Sn_1-H_2	1.5	5	3.5
2-Pt_1Sn_1-H_2	1.2	13	13

Table 3-5 Comparison of FDCA yield according according the Pt weight content in the samples prepared via cluster decomposition

The same analysis performed over the metal salt impregnated catalyst showed a similar behavior: best results were obtained with the equimolar loading of the two metals and the Pt/Sn molar ratio equal to 2 led to the poorest catalytic performances (Figure 3-16).

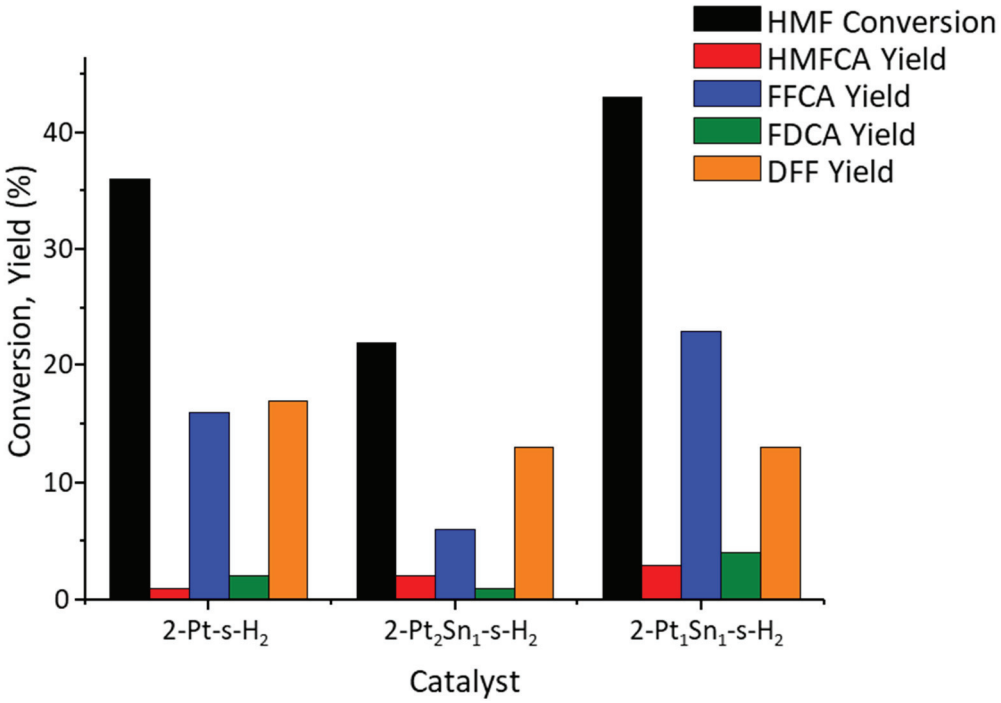

Figure 3-16 Catalytic performances of metal salt impregnated catalysts. Operative conditions: temperature 110°C, O_2 pressure 10bar, 25mL water, HMF 0.0310g, molar ratio HMF/total metal=50.

In addition to this, comparing the results of this catalyst set with those obtained with the cluster impregnated catalysts, it is important to notice that none of them showed better properties than the respective counterpart (in terms of Pt/Sn loading) of the other series. This confirmed, once again, the higher potential of cluster impregnated catalysts than the metal salt impregnated ones.

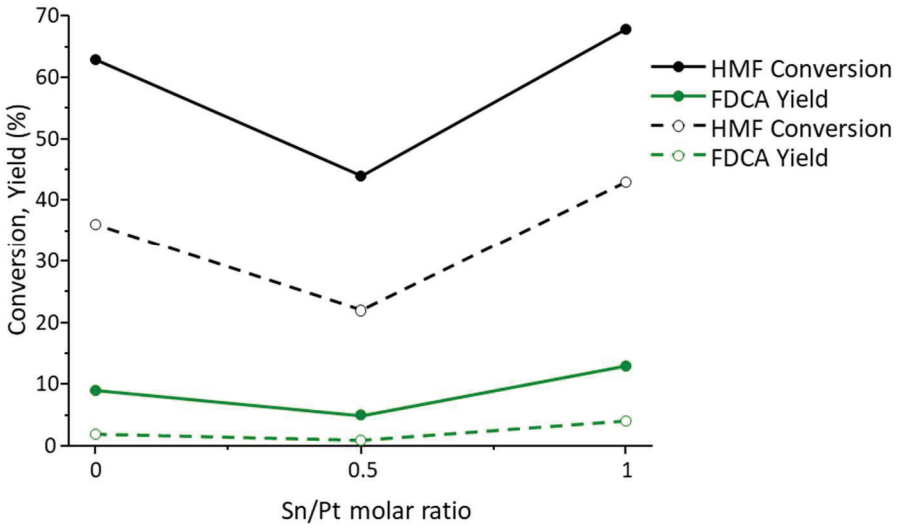

Figure 3-17 HMF Conversion and FDCA yield according the catalyst Sn/Pt molar ratio (solid line cluster impregnated catalysts, dashed line metal salt impregnated catalysts). Operative conditions: temperature 110°C, O_2 pressure 10bar, 25mL water, HMF 0.0310g, molar ratio HMF/total metal=50.

3.5.3 Effect of thermal treatment

To study the effect of the thermal treatment on the material catalytic behavior, performances of the various catalyst prepared via Pt_1Sn_1 impregnation were compared.

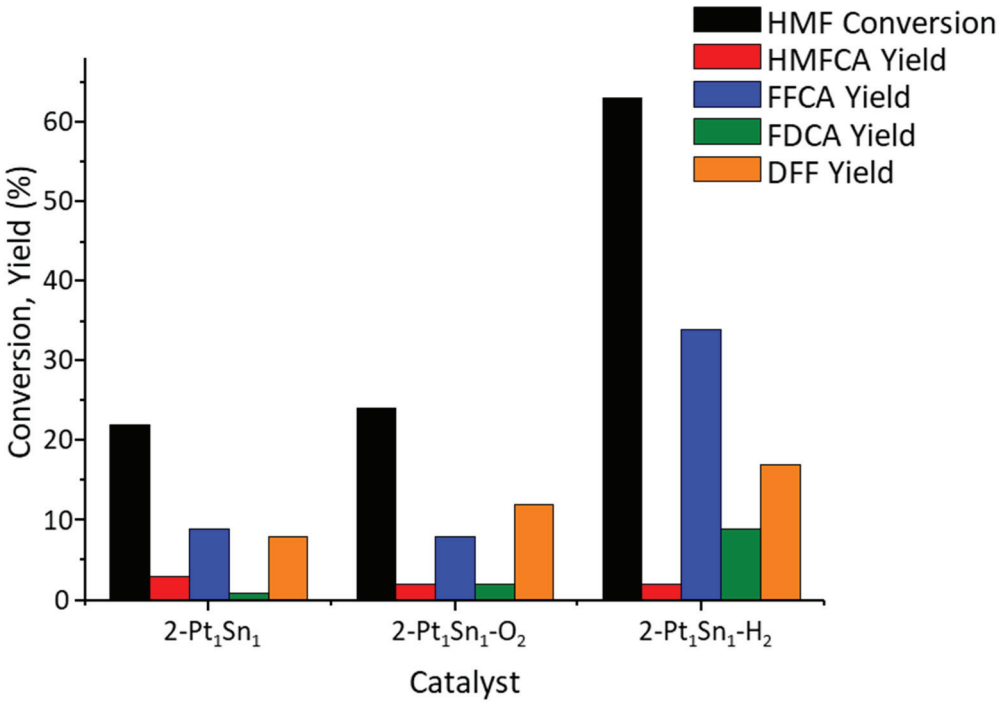

Figure 3-18 Effect of the thermal treatment on the catalysts prepared via Pt_1Sn_1 impregnation. Operative conditions: temperature 110°C, O_2 pressure 10bar, 25mL water, HMF 0.0310g, molar ratio HMF/total metal=50.

The results showed that thermal treatment plays a key role in determining the catalytic performances of the catalyst. Indeed, reducing atmosphere leads to higher catalytic performances if compared to those obtained by using dried and air treated catalysts, indicating that not only the appropriate Pt/Sn ratio is required to have good catalytic properties, but also suitable Pt oxidation state and/or Pt/Sn aggregation play a key role in determining catalyst activity.

3.6 Catalyst stability

Catalyst stability has been studied by reusing the spent catalysts 2-Pt-H_2 and 2-Pt_1Sn_1-H_2 in the same operative conditions. Such tests demonstrated that 2-Pt-H_2 catalyst suffers from deactivation, since HMF conversion dramatically dropped from 63 to 24% after just one use (Figure 3-19).

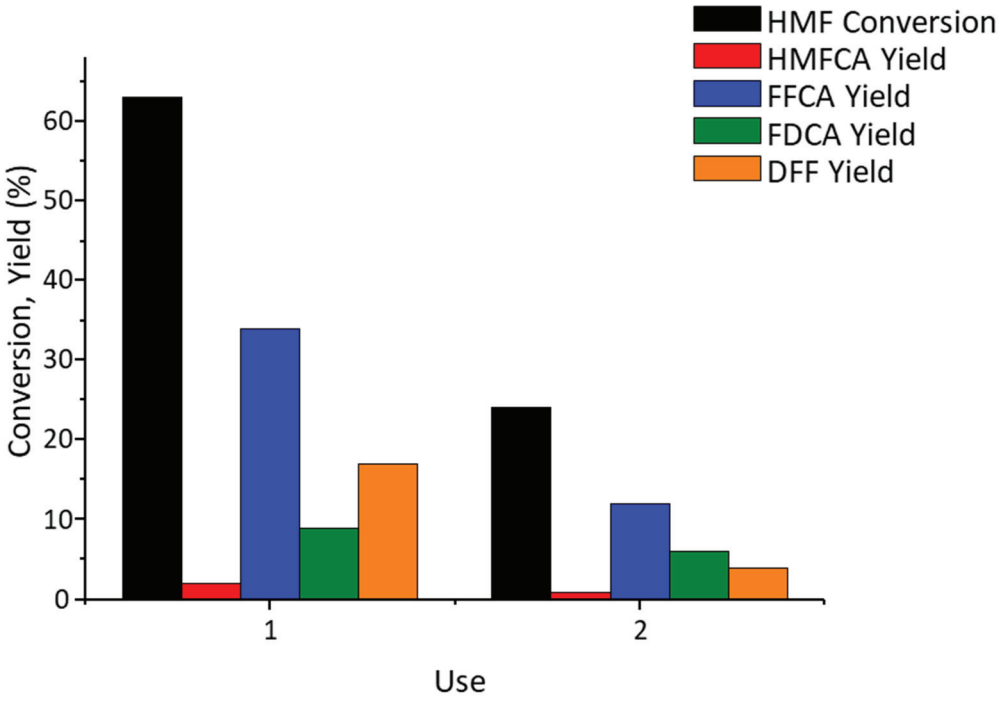

Figure 3-19 2-Pt-H_2 reuse tests. Operative conditions: temperature 110°C, O_2 pressure 10bar, 25mL water, HMF 0.0310g, molar ratio HMF/total metal=50.

On the other hand, the 2-Pt_1Sn_1-H_2 showed higher stability, since the catalyst second use guaranteed the same HMF conversion and products yield respect to first use, while in the third use lower conversion (49%) and lower FDCA yield (11%) were reported (Figure 3-20).

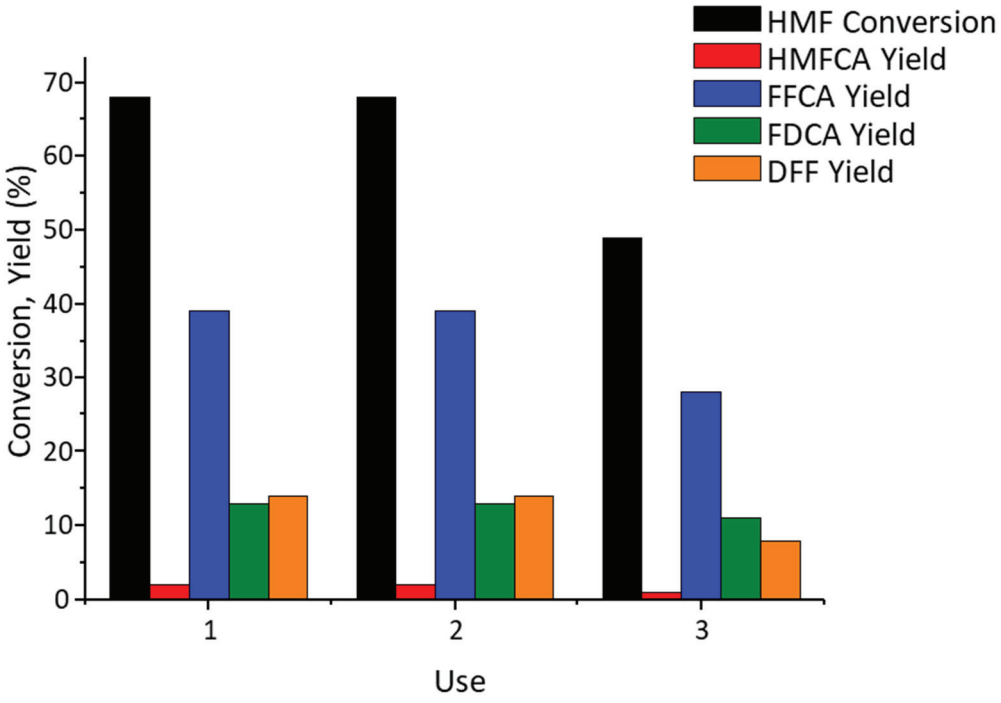

Figure 3-20 2-Pt_1Sn_1-H_2 reuse tests. Operative conditions: temperature 110°C, O_2 pressure 10bar, 25mL water, HMF 0.0310g, molar ratio HMF/total metal=50.

In order to understand the reasons of the different deactivation trends of the two materials, TEM analyses have been performed over the two used catalysts.

In detail, comparing the nanoparticle dimension before and after the reaction, it has been noticed that nanoparticles in 2-Pt-H_2 catalyst suffers from sintering during the reaction, since average diameter increases from to 2.0 to 5.5nm. In addition, some nanoparticle having diameter higher than 10nm were detected (Figure 3-21).

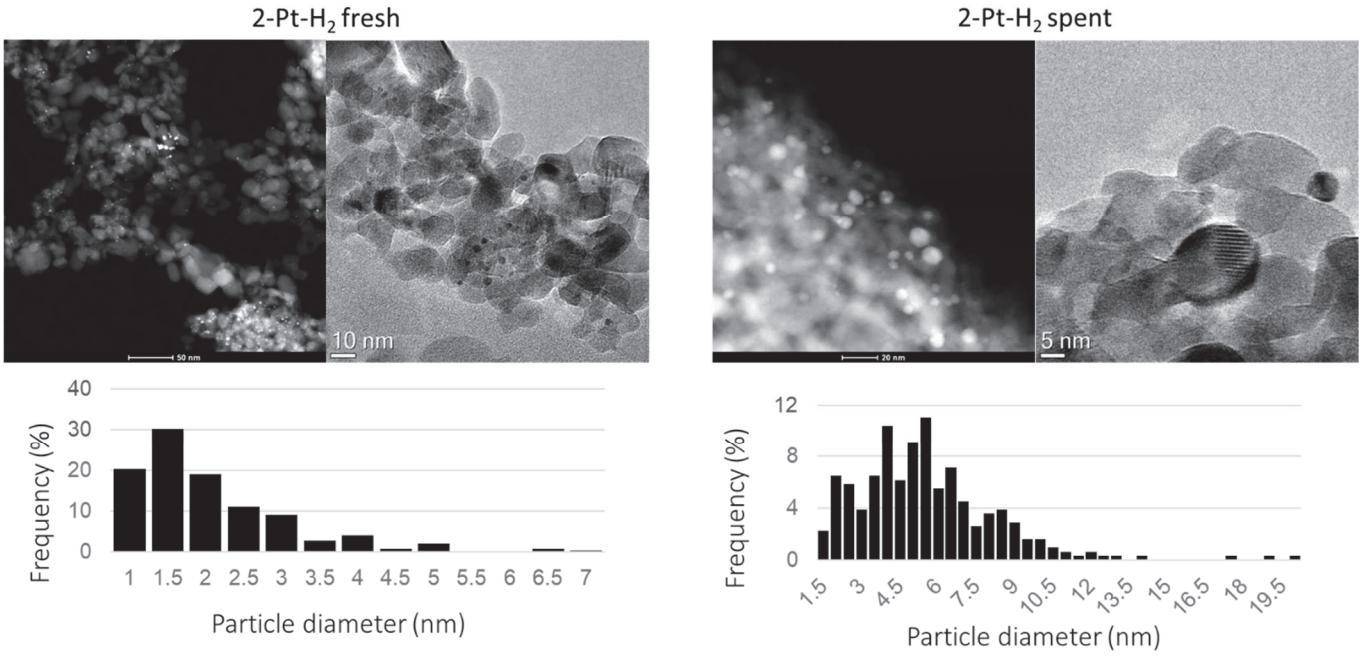

Figure 3-21 Comparison of STEM images (top) and size distribution (bottom) between fresh (left) and used 2-Pt-H_2 (right)

On the other hand, the 2-Pt_1Sn_1-H_2 seemed to not undergo sintering, since average diameter does not change significantly (Figure 3-22).

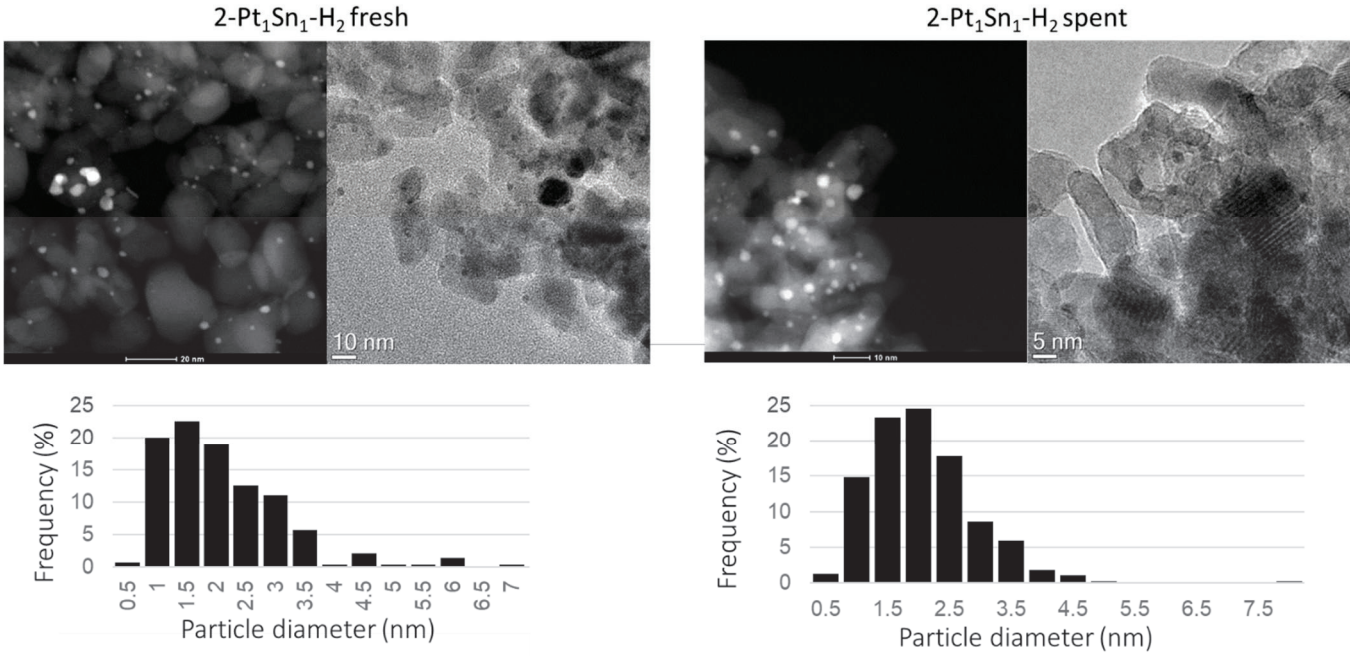

Figure 3-22 Comparison of STEM images (top) and size distribution (bottom) between fresh (left) and used 2-Pt_1Sn_1-H_2 (right)

At the same time, it seems that the Pt/Sn aggregates do not undergo any change in composition, since the EDX maps on the used catalyst showed that the two metals are still close even after the reaction, as detected in the fresh sample (Figure 3-23).

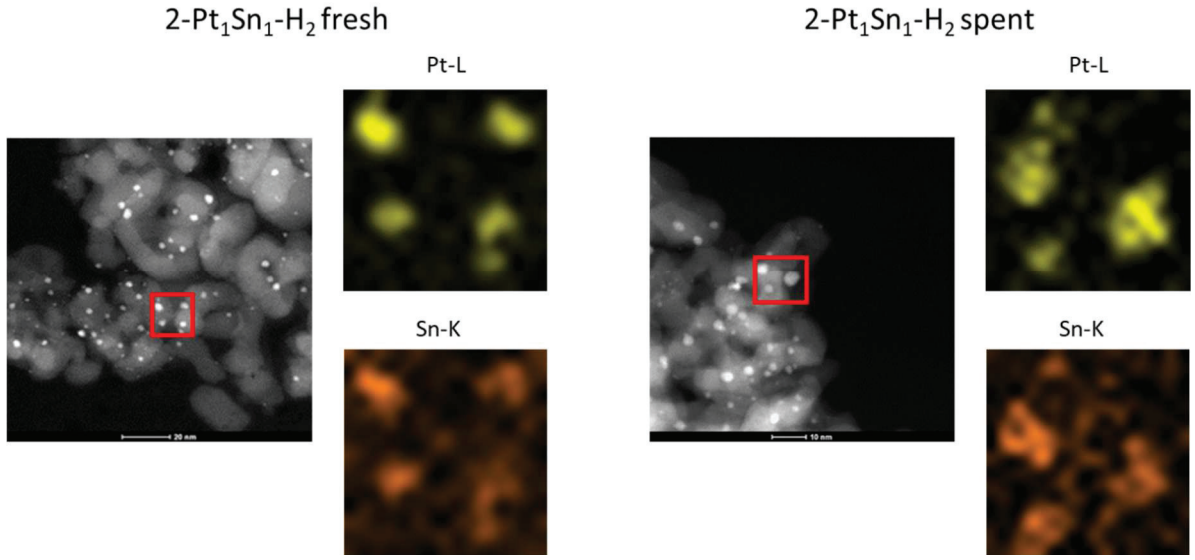

Figure 3-23 STEM image of the used 2-Pt_1Sn_1- H_2 sample and EDX maps for Pt and Sn of the indicated region

In light of all these considerations, it has been hypothesized that Sn enhances nanoparticles structural stability, which is responsible for the higher 2-Pt_1Sn_1-H_2 stability.

3.6.1 Conclusion

This work shows the crucial role played by the synthetic strategy in the definition of the catalyst surface features and the resulting catalytic properties of Pt-containing materials used in HMF base free oxidation. In fact, the use of carbonylic clusters as precursors for the synthesis of Pt nanoparticles led to the formation of nanoparticles having small dimension and relatively narrow distribution, whose catalytic performances were superior if compared to the ones showed by their counterparts prepared via metal salt impregnation. The role of Sn, which is inactive, seems to be twofold, since, in specific Pt/Sn ratio, it acts as both catalytic promoter and nanoparticle stabilizer.

3.7 Bibliography

1. Yermakov, Y. I.; Kuznetsov, B. N., Supported metallic catalysts prepared by decomposition of surface ornagometallic complexes. *Journal of Molecular Catalysis* **1980,** *9* (1), 13-40.

2. Verdeguer, P.; Merat, N.; Gaset, A., Oxydation catalytique du HMF en acide 2,5-furane dicarboxylique. *Journal of Molecular Catalysis* **1993,** *85* (3), 327-344.

3. Davis, S. E.; Houk, L. R.; Tamargo, E. C.; Datye, A. K.; Davis, R. J., Oxidation of 5-hydroxymethylfurfural over supported Pt, Pd and Au catalysts. *Catalysis Today* **2011,** *160* (1), 55-60.

4. Sahu, R.; Dhepe, P. L., Synthesis of 2,5-furandicarboxylic acid by the aerobic oxidation of 5-hydroxymethyl furfural over supported metal catalysts. *Reaction Kinetics, Mechanisms and Catalysis* **2014,** *112* (1), 173-187.

5. Yi, G.; Teong, S. P.; Li, X.; Zhang, Y., Purification of Biomass-Derived 5-Hydroxymethylfurfural and Its Catalytic Conversion to 2,5-Furandicarboxylic Acid. *ChemSusChem* **2014,** *7* (8), 2131-2135.

6. Ait Rass, H.; Essayem, N.; Besson, M., Selective Aerobic Oxidation of 5-HMF into 2,5-Furandicarboxylic Acid with Pt Catalysts Supported on TiO2- and ZrO2-Based Supports. *ChemSusChem* **2015,** *8* (7), 1206-1217.

7. Siankevich, S.; Savoglidis, G.; Fei, Z.; Laurenczy, G.; Alexander, D. T. L.; Yan, N.; Dyson, P. J., A novel platinum nanocatalyst for the oxidation of 5-Hydroxymethylfurfural into 2,5-Furandicarboxylic acid under mild conditions. *Journal of Catalysis* **2014,** *315* (Supplement C), 67-74.

8. Zhou, C.; Deng, W.; Wan, X.; Zhang, Q.; Yang, Y.; Wang, Y., Functionalized Carbon Nanotubes for Biomass Conversion: The Base-Free Aerobic Oxidation of 5-Hydroxymethylfurfural to 2,5-Furandicarboxylic Acid over Platinum Supported on a Carbon Nanotube Catalyst. *ChemCatChem* **2015,** *7* (18), 2853-2863.

9. Bortoluzzi, M.; Ceriotti, A.; Ciabatti, I.; Della Pergola, R.; Femoni, C.; Carmela Iapalucci, M.; Storione, A.; Zacchini, S., Platinum carbonyl clusters stabilized by Sn(ii)-based fragments: syntheses and structures of [Pt6(CO)6(SnCl2)2(SnCl3)4]4-, [Pt9(CO)8(SnCl2)3(SnCl3)2(Cl2SnOCOSnCl2)]4- and [Pt10(CO)14{Cl2Sn(OH)SnCl2}2]2. *Dalton Transactions* **2016,** *45* (12), 5001-5013.

Chapter 4. Au based nanoparticles supported on nanosized NiO

4.1 Introduction

The effectiveness of Au NP in HMF oxidation is well known.[1] Generally, good yield of FDCA can be obtained in a batch reactor using water as solvent and molecular oxygen as oxidant in strongly basic conditions, obtained via addition of inorganic bases (such as NaOH) to the reaction mixtures. Moreover, it has been proven that higher FDCA yield and selectivity can be achieved using bimetallic catalysts such as Au/Cu-TiO_2 (with an Au:Cu ratio equal to 3:1)[2] and Au/Pd-TiO_2 (with a Au:Pd ratio equal to 6:1)[3], since the preparation of alloyed bimetallic particles significantly modified the electronic properties of the original metal (i.e. gold) and specific metal molar ratio led to substantial synergistic effect which improved the catalyst activity.

Other studies highlighted that Au-based nanoparticle activity is modified by changing supports (such as cerium oxide or active carbon),[4-5] indicating that catalyst activity could be enhanced by suitable interaction between the active phase (i.e. the NPs) and the support itself.

However, the main drawback of using gold-based catalysts is the necessity of working at very high pH. Indeed, Au-supported materials are very efficient in HMF oxidation using an aqueous medium, but they require the presence of high amount of sodium hydroxide or other homogeneous bases. Such feature is considered the main drawback in terms of sustainability, and some research group focused their attention on the possibility to use basic support to circumvent the addition of inorganic additives.[6-7]

Recently, Villa and co-workers demonstrated the possibility to oxidize benzyl alcohol and other well-known aromatic and aliphatic alcohols under base free conditions using metal supported nickel oxide catalysts[8]. They demonstrated that the use of nanometric NiO (nNiO) greatly improved catalyst performance, mainly because of a cooperative effect between Au and NiO.

Therefore, in the present study, Au, Pd and Au/Pd nanoparticles (Au:Pd metal molar ratio equal to 6:4) were deposited on nNiO and their catalytic behaviour was tested in the liquid-phase oxidation of HMF in base-free conditions, demonstrating the possibility to obtain high yield FDCA without the addition of any inorganic base.

4.2 Catalyst synthesis

Catalyst has been prepared as reported in literature:[8] nanosized NiO (nNiO) has been obtained via urea route, while the metallic nanoparticles (Au, Pd, AuPd) via reduction of their respective salt precursor. The nanoparticle deposition was performed by adding the dried nNiO to the metal nanoparticle suspensions.

In Table 4-1, the list of the prepared catalysts is reported.

Sample	Au (%)	Pd (%)
nNiO	-	-
Au-nNiO	1	-
Pd-nNiO	-	1
AuPd-nNiO	0.73	0.27

Table 4-1 List of the prepared catalysts and some of their chemical-physical properties.

4.3 Catalyst characterization

On the synthesized materials HRTEM analyses have been performed in order to measure the nanoparticle size of the different samples.

The results of the analysis are reported in table:

Sample	NP average size (nm)	BET surface area (m^2/g)
Au-nNiO	5.9	190
Pd-nNiO	3.1	180
AuPd-nNiO	3.6	186

Table 4-2 Average nanoparticle diameter (measured by TEM analysis) and metal oxidation distribution in the nNiO samples.

The analysis for the Pd-nNiO sample revealed that via the synthetic protocol reported, good dispersion of the metallic nanoparticle was obtained (Figure 4-1 HRTEM analysis of the Pd-nNiO sample)

Au based nanoparticles supported on nanosized NiO

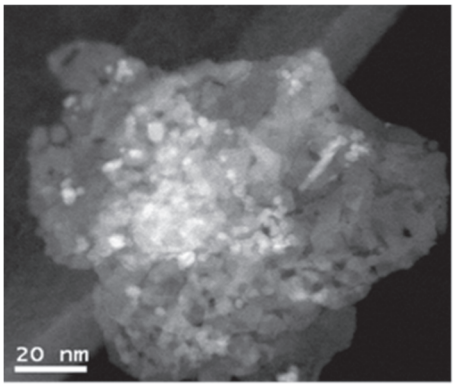

Figure 4-1 HRTEM analysis of the Pd-nNiO sample

As far as the bimetallic sample (Au/Pd-nNiO) is concerned, the HRTEM analysis revealed that the two metals are alloyed in the NPs, and the calculated Au/Pd ratio corresponds to the nominal one (6/4 Au/Pd molar ratio).

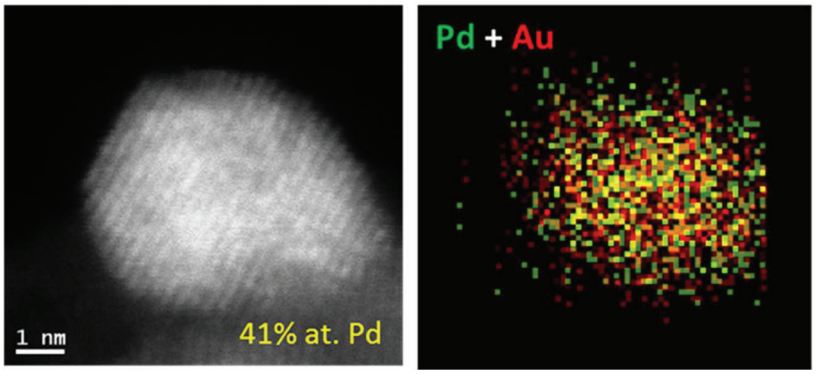

Figure 4-2 HRTEM analysis of AuPd-nNiO sample

4.4 Catalytic test

4.4.1 Catalyst screening

Firstly, the reaction performed in the presence of the bare nNiO demonstrated the inability of the support to catalyse the reaction (Figure 4-3).

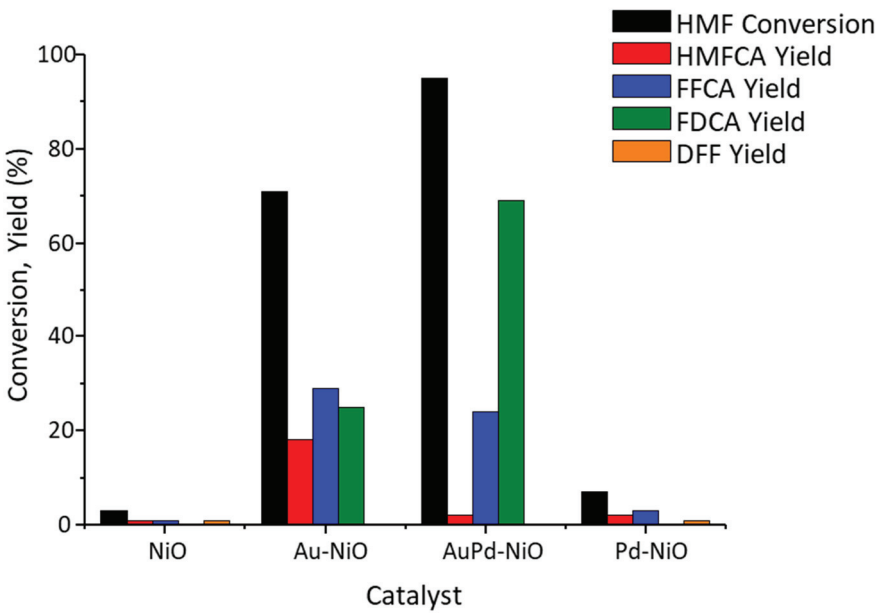

Figure 4-3 HMF conversion and products yield for the prepared Au, Pd and AuPd catalysts supported on NiO. Reaction conditions: 90°C, 6h, 10 bar O2, HMF:metal loading = 100. Legend: ■ HMF, ■ HMFCA, ■ DFF, ■ FFCA, ■ FDCA.

On the contrary, the results obtained using Au-nNiO sample demonstrate that, even without the addition of any base, the 71% of HMF is converted after 6h of reaction. Both HMFCA and FFCA can be found at the end of the process and FDCA was produced with 25% of yield.

The preparation of a bimetallic Au/Pd system led to an increase in the activity (95% of HMF conversion and 69% FDCA yield), confirming once again that the alloyed bimetallic structure enhances the catalytic performance as already reported with titania[3] and active carbon[5] supported materials. However, since these reactions have been carried out without the base, an important role is played by the support. The use of nNiO changes the electronic properties of the metal and favours HMF conversion even without the base addition. Surprisingly, the results obtained using Au-nNiO and Au/Pd-nNiO samples indicated the presence of high amount of FFCA intermediate after 6 h of reaction. This is quite unusual; indeed, analogues Au and Au/Pd catalysts supported on TiO_2 and AC, that resulted very active in HMF oxidation in the presence of a base, formed HMFCA as main intermediate while FFCA was quickly converted to FDCA. The conversion of OH group in HMFCA was, in fact, considered to be the rate limiting step of the reaction and FFCA was generally rapidly converted once formed. On the contrary, in the studied base-free HMF oxidation using nNiO supported systems, a significant change in the reaction rate seems to be present, with a strong decline in the rate of transformation of FFCA to FDCA.

Monometallic palladium supported sample did not show any relevant catalytic activity but the presence of small amount of DFF beside HMFCA at the end of the reaction, demonstrated the possibility to follow, in the reported conditions, both the reaction pathways. The use of an increased reaction time (15h) led to very similar results; moreover, the introduction of NaOH (HMF/NaOH molar ratio 2) confirmed the inability of Pd-nNiO to convert HMF also at high pH. Indeed, these conditions just promoted the formation of by-products due to HMF decomposition (77% HMF conversion was reached but 54% of carbon loss was observed).

4.4.2 Mechanism study

In order to gain further insight on the reaction mechanism, the catalytic performance of Au-nNiO and Au/Pd-nNiO samples were studied carrying out different tests as a function of reaction time.

Figure 4-4 shows HMF conversion and product selectivity for Au-nNiO catalyst.

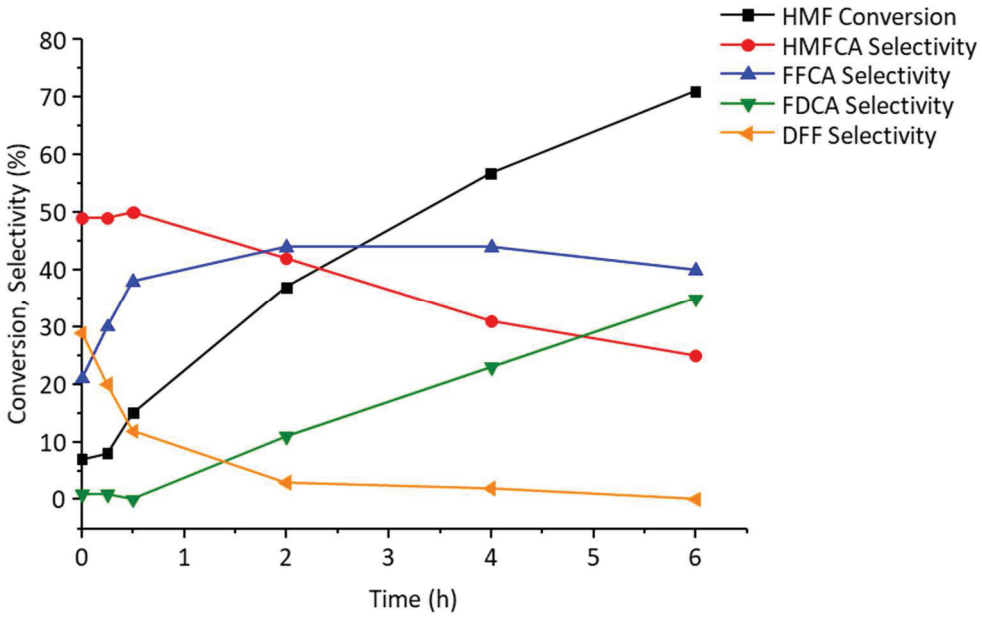

Figure 4-4 HMF Conversion and product selectivity as a function of time* using Au-nNiO. Reaction conditions: 90°C, 10 bar O2, HMF:metal loading = 100. Legend: ■ HMF, ● HMFCA, ♦ DFF, ▲ FFCA, x FDCA.

The reported data show the Au-nNiO sample is able to convert HMF in base-free conditions even during the heating of the reactor, obtaining 7% of HMF conversion when 90°C are reached (t=0); by further increasing the reaction time up to 6 h, the HMF conversion reached 71%.

HMFCA and DFF were the main products detected at the initial stage of the reaction, meaning that both reaction pathways can occur. DFF was present with high selectivity at t=0, then it reacted faster than HMFCA leading to the formation of FFCA. On the other hand, HMFCA started to be converted

* in these tests, t=0 is considered as the time at which reaction temperature has been reached

after 30 minutes. Meanwhile, FFCA formation started at t=0 and increased up to 30 minutes, then staying constant. When t=0 FFCA is already present in the reaction medium; it can be hypotised that this intermediate derived from DFF conversion since HMFCA is not converted in the first 30 minutes of reaction. Moreover, the presence of a lower amount of DFF at t=0 compared to HMFCA, can probably due to the fact that this molecule undergoes a fast conversion. FDCA formation started after 30 minutes exactly when HMFCA is converted to FFCA; this probably means that FDCA formation can't proceed through to the reaction pathway which involves DFF formation. DFF is converted to FFCA but this intermediate accumulates in the reaction medium. On the contrary, when HMFCA concentration decreases FDCA selectivity increases; FFCA remained constant while increasing the reaction time probably because the reaction rates which involve its formation and its transformation are very similar.

Thus, the obtained data seem to indicate that, using Au-NiO sample, significant changes in product selectivities are observed after 30 minutes reaction. Indeed, in the earliest reaction stage, HMFCA and DFF are produced in parallel with different reaction rate and can be both considered as primary intermediates of HMF oxidation.

On the contrary, FFCA formation increased up to 40% in the early period of the reaction and then its concentration remains constant with time, probably due to a similar rate of formation and conversion to FDCA. It has to be said that this molecule, which is normally found in very low amount in presence of base, due to its fast transformation to FDCA, is present with high quantity with respect to HMFCA.

Finally, the diacid product started to be formed at 30 min and continue to increase its concentration with time.

In order to verify the possibility to increase the catalytic activity by base addition, HMF oxidation was evaluated by adding 2 equivalents of the NaOH in the reaction medium. As already observed for Pd-nNiO, also in the case of gold containing sample the higher pH did not increase the rate of FDCA formation. Indeed, HMF conversion was promoted (68% vs 15% after 30 min of reaction) and the yield in HMFCA was higher (36% vs 7%) but HMF degradation was predominant and carbon loss was found to be very high.

The significant change in the activity of Au-nNiO sample after few minutes reaction in base-free conditions can be due to possible modification occurring to the catalyst and/or the inhibition effect on sample due to reactive intermediates produced during HMF oxidation.

For better understanding the reaction mechanism, some catalytic tests using the intermediates as starting reagents have been carried out (Table 4-3).

Entry	Reactant	Conversion (%)	FFCA Sel. (%)	FDCA Sel. (%)	Unknown compound X	Unknown compound Y
1	**FFCA**	30	-	100	No	No
2	**DFF**	28	32	-	Yes	No
3	**DFF***	17	27	-	Yes	No
4	**DFF (on NiO)**	34	4	-	Traces	Yes
5	**HMFCA**	36	69	31	Traces	No

Table 4-3 Catalytic tests using reaction intermediates (FFCA, DFF and HMFCA) as starting material. Reaction conditions: 90°C, 2h, 10 bar O_2, HMF:metal loading = 100 catalyst Au/nNiO. *Catalytic test performed after 30 minutes reaction with HMF

First, a preliminary experiment was carried out by reacting FFCA with the catalyst, to verify its ability to convert this reaction intermediate. After 2 h reaction time, a 30% conversion of FFCA was shown (Table 4-3 entry 1) with complete transformation of the reagent into FDCA, confirming the activity of the catalyst towards FFCA conversion with low rate but high selectivity.

The use of DFF as the reagent (Table 4-3, entry 2) resulted in 28% conversion with formation of FFCA; however, when DFF was loaded with a catalyst already used for 30 minutes in HMF oxidation (Table 4-3, entry 3) conversion decreased, confirming that something is happening to the system after the first 30 minutes of reaction. The change in activity could be due to:

1) Partial covering of Au nanoparticles by NiO
2) Inhibition of catalyst activity in some of the HMF oxidation step

Thus, in order to verify the first hypothesis, a test using only NiO to oxidise DFF has been carried out (Table 4-3, entry 4). In these conditions, high DFF conversion is obtained (34%) but low FFCA selectivity was observed. nNiO, which is inactive in HMF oxidation, is able to convert DFF. However, the formation of a new product (named as Y) could be detected from HPLC analysis; this means that the reactivity of nNiO is significantly different from that of Au/nNiO and the complete covering of Au with nNiO cannot be hypothesised since using the metal supported catalyst this new product was not formed. It is very important to underline that the product formed with nNiO is different from the one revealed in the other reactions when DFF was used. Moreover, it must be noticed that FDCA is never formed when DFF is used as starting material, meaning that the only available route

for its formation proceeds through HMFCA. Thus, we may conclude that catalyst was inhibited by the presence of DFF, which prevents FFCA transformation to FDCA. The presence of DFF as reagent led also to the formation of an unknown compound whose identification is still undergoing. Therefore, a poisoning effect of DFF can be hypothesised: when it is present in the reaction mixture, it prevents FFCA transformation. This suggestion has been confirmed by two further tests, where DFF and FFCA are used as starting material. FDCA yield at the end of the 2h of reaction was around 2%, both in the case of lower and in the case of higher DFF concentration. The obtained results are definitively far from that reported in Table 4-3, entry 1 where higher amount of FDCA were formed, demonstrating the negative effect played by the presence of DFF in the diacid production.

The oxidation reaction using HMFCA as reagent (Table 4-3, entry 5) produced both FFCA and FDCA, confirming the possibility to produce the diacid through HMFCA reaction pathway.

The more active AuPd-nNiO catalyst displayed a more emphasised catalytic behaviour, leading to the formation of FDCA and FFCA as major products, while DFF and HMFCA were present at any time in low amounts after 30 minutes (Figure 4-5).

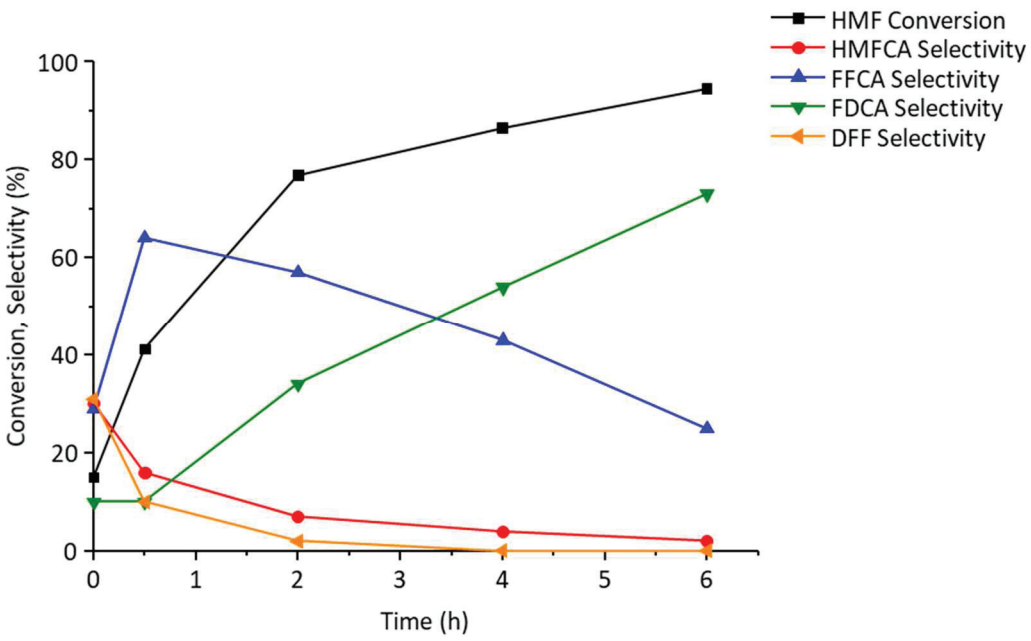

Figure 4-5 HMF Conversion and product selectivity as a function of time using AuPd-nNiO. Reaction conditions: 90°C, 10 bar O2, HMF:metal loading = 100. Legend: ■ HMF, ● HMFCA, ♦ DFF, ▲ FFCA, x FDCA.

In this case, the catalytic system is so active that small amount of FDCA is already present at t=0, together with all the other reaction intermediates. The shape of the curves belonging to FDCA and FFCA clearly shows the typical trend of consecutive products, while the amounts of detectable DFF and HMFCA are very low after the early period of the reaction. These two intermediates are both

formed from HMF over AuPd-nNiO catalyst and their concentration decreases with reaction time with a similar trend and similar reaction rate, despite of what observed for Au supported catalyst. In order to verify the ability of the bimetallic catalyst to convert these two different intermediates, HMFCA and DFF were separately used as reagent (Table 4-4). After 2 h of reaction, a very high conversion of both molecules was obtained, demonstrating that FFCA can be derived from whether DFF or HMFCA conversion. Although, the use of gold promoted FFCA formation from DFF, FDCA was not produced with this catalyst; on the contrary, the use of a bimetallic system favoured also FDCA formation from DFF.

Reactant	Conversion (%)	FFCA Selectivity (%)	FDCA Selectivity (%)
HMFCA	94	41	59
DFF	93	83	17

Table 4-4 Catalytic tests using reaction intermediates DFF and HMFCA as starting material. Reaction conditions: 90°C, 2h, 10 bar O2, Catalyst AuPd-nNiO, HMF:metal loading = 100.

Nevertheless, product selectivity significantly differs on the basis of the used reactant suggesting the presence, in the case of DFF of some inhibition effects on the transformation of FFCA to FDCA.

4.5 Catalysts stability and reusability

Since catalyst stability is one of the most important features that must be taken into account during the development of a new material, reusability tests were carried out on the sample characterised by the highest performance (Figure 4-6).

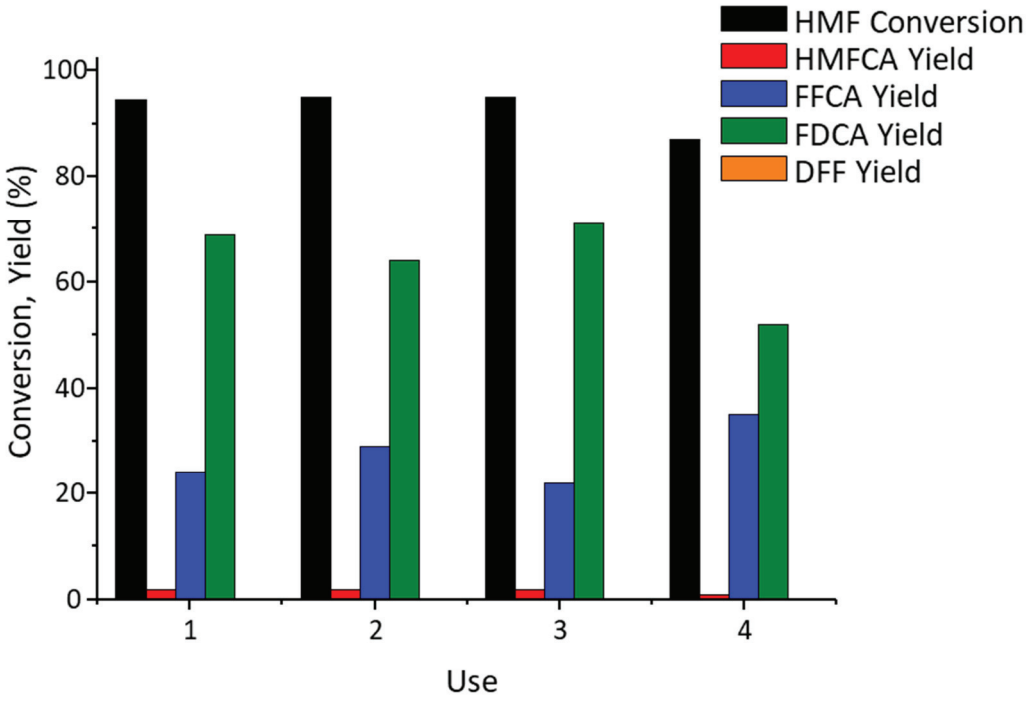

Figure 4-6 Reusability tests for the oxidation of HMF using Au/Pd-nNiO catalyst. Reaction conditions: 90°C, 6h, 10 bar O_2, HMF:metal loading = 100. Legend: ■ HMF, ■ HMFCA, ■ FFCA, ■ FDCA.

The bimetallic catalyst seems to be quite stable since it can be used three times without any loss of activity; nevertheless, the fourth reaction carried out on the used material is characterized by a small decrease in the catalytic performance. XRF analysis of the obtained reaction mixtures did not reveal any metal in the solution, excluding a deactivation phenomenon correlated to a leaching effect.

In the presence of metal supported catalyst, a check for the metal leaching in the reaction medium is always required. XRF analysis were performed on the final reaction solution confirming that the metals (both Au and Pd) do not leach from the support during the reaction. Furthermore, an additional 2 h catalytic test was carried out after removing the catalyst from the reaction mixture to verify the presence of homogeneous catalyst (Figure 4-7). Since neither the conversion nor the product yield changed in the absence of the Au/Pd-nNiO catalyst, we confirmed that our catalyst did not leach any metals.

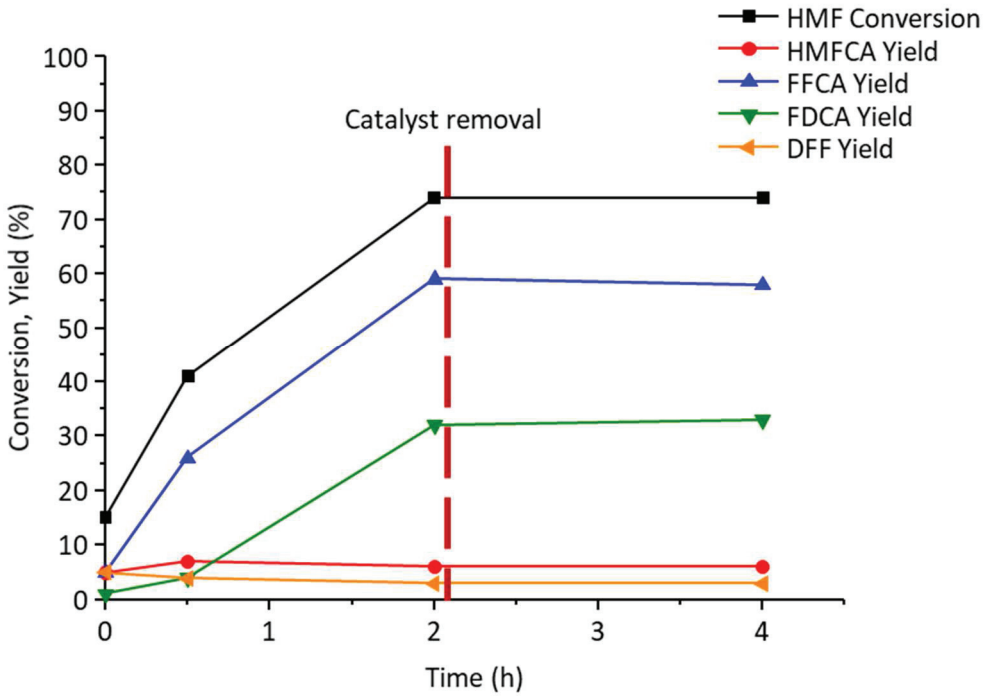

Figure 4-7 Leaching tests for the prepared AuPd-nNiO.: first 2h test with catalysts, then catalyst has been removed for the following 2h. Reaction conditions: 90°C, 10 bar O_2, HMF:metal loading = 100. Legend ■ HMF, ■ HMFCA, ■ FFCA, ■ FDCA, ■ DFF.

4.6 Conclusion

Au-based nanoparticles supported onto nanosized NiO were found to be active in the base-free HMF oxidation in relatively mild conditions (90°C, 10bar O_2). High yield of FDCA was reported for the Au-Pd bimetallic system, indicating that the cooperative effect of the two precious metal takes places also in such base-free conditions. Then, by doping Au nanoparticles with Pd it has been possible to reduce the DFF inhibition behavior. In addition to this, good reusability of the bimetallic system was found.

4.7 Bibliography

1. Casanova, O.; Iborra, S.; Corma, A., Biomass into Chemicals: Aerobic Oxidation of 5-Hydroxymethyl-2-furfural into 2,5-Furandicarboxylic Acid with Gold Nanoparticle Catalysts. *ChemSusChem* **2009,** *2* (12), 1138-1144.

2. Albonetti, S.; Pasini, T.; Lolli, A.; Blosi, M.; Piccinini, M.; Dimitratos, N.; Lopez-Sanchez, J. A.; Morgan, D. J.; Carley, A. F.; Hutchings, G. J.; Cavani, F., Selective oxidation of 5-hydroxymethyl-2-

furfural over TiO2-supported gold–copper catalysts prepared from preformed nanoparticles: Effect of Au/Cu ratio. *Catalysis Today* **2012,** *195* (1), 120-126.

3. Lolli, A.; Albonetti, S.; Utili, L.; Amadori, R.; Ospitali, F.; Lucarelli, C.; Cavani, F., Insights into the reaction mechanism for 5-hydroxymethylfurfural oxidation to FDCA on bimetallic Pd–Au nanoparticles. *Applied Catalysis A: General* **2015,** *504* (Supplement C), 408-419.

4. Albonetti, S.; Lolli, A.; Morandi, V.; Migliori, A.; Lucarelli, C.; Cavani, F., Conversion of 5-hydroxymethylfurfural to 2,5-furandicarboxylic acid over Au-based catalysts: Optimization of active phase and metal–support interaction. *Applied Catalysis B: Environmental* **2015,** *163* (Supplement C), 520-530.

5. Villa, A.; Schiavoni, M.; Campisi, S.; Veith, G. M.; Prati, L., Pd-modified Au on Carbon as an Effective and Durable Catalyst for the Direct Oxidation of HMF to 2,5-Furandicarboxylic Acid. *ChemSusChem* **2013,** *6* (4), 609-612.

6. Gupta, N. K.; Nishimura, S.; Takagaki, A.; Ebitani, K., Hydrotalcite-supported gold-nanoparticle-catalyzed highly efficient base-free aqueous oxidation of 5-hydroxymethylfurfural into 2,5-furandicarboxylic acid under atmospheric oxygen pressure. *Green Chemistry* **2011,** *13* (4), 824-827.

7. Gao, Z.; Xie, R.; Fan, G.; Yang, L.; Li, F., Highly Efficient and Stable Bimetallic AuPd over La-Doped Ca–Mg–Al Layered Double Hydroxide for Base-Free Aerobic Oxidation of 5-Hydroxymethylfurfural in Water. *ACS Sustainable Chemistry & Engineering* **2017,** *5* (7), 5852-5861.

8. Villa, A.; Chan-Thaw, C. E.; Veith, G. M.; More, K. L.; Ferri, D.; Prati, L., Au on Nanosized NiO: A Cooperative Effect between Au and Nanosized NiO in the Base-Free Alcohol Oxidation. *ChemCatChem* **2011,** *3* (10), 1612-1618.

Chapter 5. Catalysts grafted onto electrospun polymeric membranes

5.1 Introduction

Membranes are widely used tools in different industrial fields, and among the others, reactor engineering represents a sector in which the versatility of these means has given a large contribution to the development of advanced technologies and setups. For instance, catalytic membrane reactors (CMR) have been designed, in which the reaction occurs on the membrane network, and, at the same time, separation could occur.[1]

In this frame, catalytically active membranes could be divided into two families: inorganic (mainly metallic and inorganic) and polymeric ones. The previous find application when harsh operative conditions are required, such as methane-steam reforming and water/gas shift to name a few.[2] As far as the polymeric membranes are concerned, obvious thermal limitations hinder their use, suggesting their usage in the field of biotechnology.[3] At the same time, thanks to their lower production cost if compared to the inorganic membrane, it could be conceived their use in bioderived molecules upgrade processes, which generally require mild operative conditions. Another advantage related to the use of polymers as matrix for catalytically active membranes is linked to the possibility to embed both heterogeneous and homogeneous catalysts within the polymeric frame. In this way, catalysts could be immobilised and the resulting membrane can be used in continuous flow setups.

In view of this, it has been designed the use of polymeric membranes obtained via electrospinning technique as matrixes for metal nanoparticles embedding. The resulting materials were tested in aqueous HMF oxidation under batch conditions, with the aim to develop catalytically active membranes which could be further implemented in continuous flow reactor setups specifically designed for this reaction.

The following paragraphs briefly illustrates the electrospinning technique principles and the application of electrospun materials in catalysis.

5.1.1 Electrospinning technique

Electrospinning is one of the most useful technique to produce polymeric fibers. The reason of this success relies on the possibility to obtain nanofibers well defined in size with a simple setup, easy to scale up and relatively cost effective if compared to other techniques.[4]

This technique is based on the electrostatic attraction of charges which are generated by an electrostatic field: a polymer solution is forced to pass through a needle which is charged by an external power supply, the resulting charged polymeric spray (obtained by instantaneous solvent evaporation) is collected over the collector surface, which on its turn, is oppositely charged and placed few centimeters far from the needle tip. As already mentioned, during the processes, solvent is rapidly evaporated, and the polymeric chains tend to align creating electrostatic interchain interactions, which on their turn lead to fiber formation.

This morphological features of the resulting fibers are influenced by several parameters that concur altogether to the definition of the fiber features and can be namely divided into three families: solution parameters, instrumental and ambient ones.[5] Thus, it is evident that a fully knowledge and a fine tuning of the operational parameters is mandatory to obtain fibers having the desired properties.

5.1.2 Electrospun membranes in catalysis

Although electrospun membranes find major application in biomedical application (wound recovery, scaffolds, drug delivery the main fields)[6], catalysis can be considered as one of the emerging applicational fields for these materials.

For instance, electrospun membranes can be used as immobilizing agent for metal nanoparticles (NPs). In a common approach, electrospun membranes can be impregnated with a metal salt precursor solution and then the resulting material can be suitably reduced, leading to the desired NPs,[7-11] or metal salt precursor is dissolved in the polymer solution before electrospinning procedure, and then reduced to obtain the desired NPs.[12-13]

Alternatively, NPs can be suspended in the polymer solution prior electrospinning process[14] or even synthesized in polymer solution. However, it must be noticed that this approach must take into account the compatibility of the solvents required for NPs synthesis and polymer solvent (or even the polymer itself).

On the other hand, inorganic precursor/polymer composite electrospun fibers can be used as precursor for structured catalysts.[15-17]

In this work it has been chosen to electrospin polymer solutions in which the active noble metal is already present as nano-aggregate, i.e. as Au/Pd NPs or as Pt carbonylic cluster.
This approach arose some question about the protocol to set for the synthesis of the materials. In fact, as already mentioned, the biggest issue is related to the relative solubility of polymer and metal NPs in a solvent that could be efficiently used in the electrospinning process. Thus, considering that AuPd NPs are prepared in aqueous solutions and Pt cluster are soluble in DMF, nylon and polyacrylonitrile have been chosen as matrixes for the preparation of the materials, since the previous is water tolerant while the latter is fully soluble in DMF and it is electrospun in the same solvent.
In light of these premises, three different procedures have been designed:

1. Electrospinning of suspensions of PAN and supported AuPd NPs onto TiO_2 in DMF
2. Electrospinning of Pt clusters and PAN solutions in DMF
3. Electrospinning of Nylon and AuPd NPs suspension in formic acid (FA) and dichloromethane (DCM)

The synthesized materials were characterized by means of BET, SEM, TEM, TGA and their catalytic activity was tested in the batch HMF oxidation under aqueous conditions.

5.2 PAN electrospun fibers as matrix for Au-containing supported nanoparticles

In view of their activity,[*] supported Au-containing NPs have been considered as active phase for the synthesis of catalytically active membranes. The optimized synthetic protocol developed in the "Catalytic processes development" research group of the Industrial Chemistry department at Università di Bologna for Au-based NPs synthesis, uses water as solvent, which is highly incompatible with PAN. Thus, it has been designed the introduction of the active phase in the polymeric membrane as TiO_2-supported NPs. The following paragraphs describe the protocol for the preparation of composite AuNPs (or Au_6Pd_1 NPs) TiO_2 membranes, their characterization and their usage as catalyst in HMF oxidation reaction.

[*] The reader is referred to Chapter 4 for a wider overview of Au-based NPs role in HMF oxidation

5.2.1 Experimental

Nanoparticle synthesis and immobilization on TiO_2

Two different sets of NPs have been synthesized: monometallic Au NPs and alloyed bimetallic Au/Pd NPs.

As far as monometallic NPs are concerned, they were synthesized according the procedure optimised by Pasini et al.,[18] while the bimetallic system has been synthesized by modifying the procedure described by Lolli et al..[19]

In detail, the NPs were obtained by glucose-driven reduction of the metal salts precursors ($HAuCl_4$ and $PdCl_2$, or Au and Pd, respectively) dissolved in NaOH water solution. PVP was used as stabilizing agent. Table 5-1 reports the operative conditions and the ratios of the reactant used in these syntheses.

	Au NPs	**Au_6Pd_1 NPs**
Au:Pd ratio	-	6
NaOH:metal ratio	8	8
PVP:metal ratio	3.14	3.14
Glucose:metal ratio	2	3.28
Synthesis temperature	95°C	95°C

Table 5-1 Experimental parameters for the synthesis of Au and Au_6Pd_1 NPs

In both cases, the resulting nanoparticles suspensions were concentrated in order to obtain a suitable volume and then they were impregnated onto TiO_2 (1.5% of total metal in weight) by means of incipient wetness impregnation.

Composite membranes preparation

The suspensions for electrospinning have been prepared by suspending the inorganic powder (i.e. pristine TiO_2, Au/TiO_2 and Au_6Pd_1/TiO_2) in a suitable amount of DMF. After 30 minutes of stirring, a precise amount of PAN (8% in weight respect to the solvent) was added to the suspension, in order to have a definite metal/polymer ratio. The resulting suspensions were placed in a glass syringe and they were electrospun using an apparatus described by Gualandi et al.[20] The operative parameters for electrospinning were set according to the composition and the viscosity of the solutions, as reported in Table 5-2.

Parameter	Range
Voltage	19-23kV
Flow rate	0.6-1.2mL/h
Collector-needle distance	20cm
Temperature	20-22°C
Humidity	35-48%

Table 5-2 Experimental parameters for the preparation of electrospun PAN membranes

Materials characterization

The resulting membranes were characterized by means of BET, TGA, SEM and TEM techniques.

Catalytic tests

Catalytic tests were performed in bench scale autoclave described in Chapter 2.

In a typical experiment, 25mL of a 18mM water solution of HMF are prepared. Then NaOH (2equivalent respect to HMF) and a suitable amount of catalyst (in order to have a metal:HMF molar ratio equal to 1:100) are added to the solution. Composite membranes were introduced in the solution as small squares having average size of 0.25cm^2. The resulting suspension is loaded in the autoclave, purged with O_2 and then pressurized to 10bar with the same gas. Temperature is then set to desired set point and at the end of the catalytic test, reaction is quenched in an ice bath. The reaction mixture is filtered on a buchner funnel in order to collect the used catalyst and the filtrated is then analyzed in HPLC as described in Chapter 2.

5.2.2 Results and discussion

Unsupported and supported nanoparticle characterization

The synthetic protocol for the synthesis of Au and Au/Pd nanoparticles led to the formation of small nanoparticle as revealed by XRD analysis (Table 5-3).

Nanoparticle	Au/Pd ratio	NP dimension
Au	-	4.5
AuPd	6	4

Table 5-3 Nanoparticle composition and dimension

Then, they were supported onto TiO_2 via incipient wetness impregnation which did not lead to any substantial increase of NPs dimension (Table 5-4).

Catalyst	Total metal loading (w/w%)	NP dimension	BET specific area (m^2/g)
Au/TiO_2	1.5	5.5	77
$AuPd/TiO_2$	1.5	6.5	69

Table 5-4 TiO_2 impregnated catalysts

Composite membrane preparation and characterization

Several membranes have been prepared with different active phases and different inorganic loadings. Table 5-5 summarizes the experimental parameters used to synthesize the membranes tested in this study, and in Table 5-6 chemical composition and specific surface area of the samples are reported.

Sample name	Voltage (kV)	Flow rate (mL/h)	Collector-needle distance (cm)	Temperature (°C)	Humidity (%)
PAN	19	1.2	20	20	44
PAN-33TiO_2	20	0.6	20	22	35
PAN-66TiO_2	23	1.2	20	21	48
PAN-33TiO_2-0.6Au	20	0.8	20	21	37
PAN-66TiO_2-1Au	23	0.8	20	21	39
PAN-66TiO_2-1AuPd	23	1.2	20	22	44

Table 5-5 PAN based membranes synthesized in this study and respective electrospinning operative parameters

Sample name	TiO_2 loading (wt%)	Total metal (Au+Pd) loading (wt%)	Au/Pd molar ratio	BET specific surface area (m^2/g)
PAN	-	-	-	11
PAN-33TiO_2	33	-	-	48
PAN-66TiO_2	66	-	-	48
PAN-33TiO_2-0.6Au	33	0.6	-	43
PAN-66TiO_2-1Au	66	1.0	-	46
PAN-66TiO_2-1AuPd	66	1.0	6	46

Table 5-6 TiO_2 and metal loading, Au/Pd molar ratio and specific surface area for the electrospun PAN-based membranes

As could be seen from Table 5-2, operative parameters have to be finely tuned within a narrow range to obtain the desired membrane. A general trend seems to indicate that the higher the inorganic content the higher the voltage to be applied. This could be due to the higher isolating effect of composite membranes. Another feature is related to the higher specific surface area of the composite membranes respect to the PAN membrane, indicating that TiO_2 addition leads to an increase of this parameter (Table 5-6).

SEM analyses performed on the PAN sample, showed that the electrospinning operative conditions can lead to the formation of continuous randomly oriented fibers, and no polymer agglomerates were detected, while the morphology of composite TiO_2/PAN membranes is characterized by the formation of aggregates, independently from the inorganic loading of the membrane

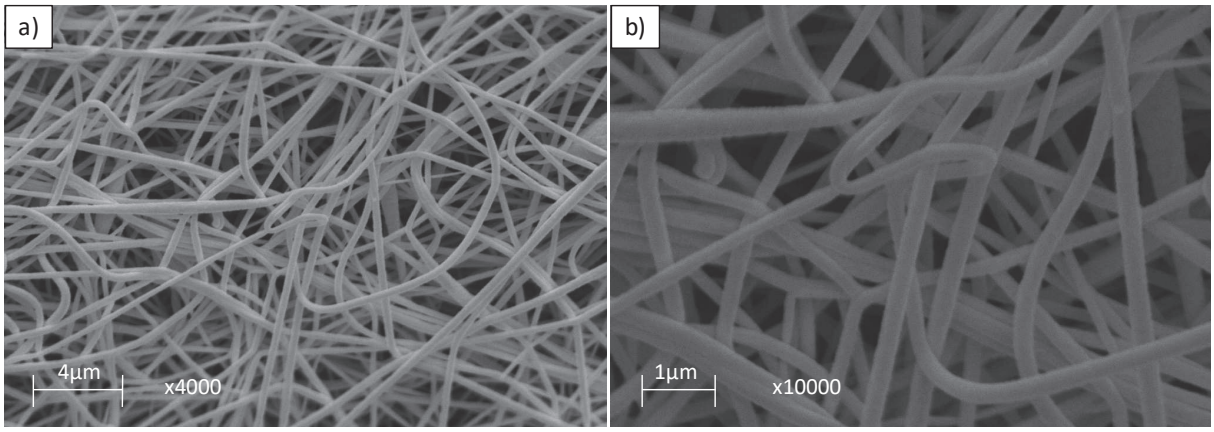

Figure 5-1 SEM analyses of PAN membrane.

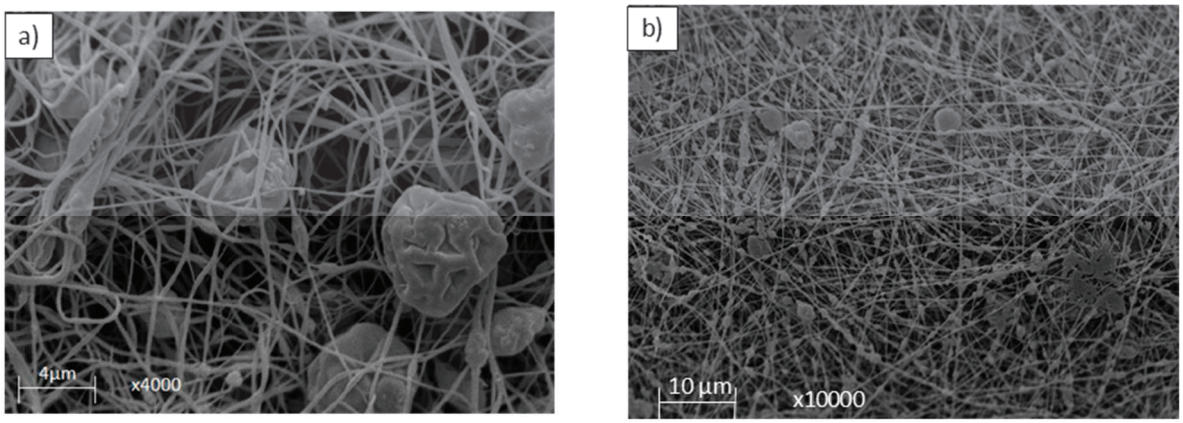

Figure 5-2 SEM analyses of composite TiO_2-PAN membranes: a) PAN-33TiO_2, b) PAN-66TiO_2

Elemental analyses performed on the agglomerates of the composite membranes by EDX technique revealed that they are characterized by an excess of C (54% wt) respect to Ti and O (22 and 24%, respectively). Thus, it is possible to hypothesize that during membrane formation TiO_2 grains are wrapped by polymer fibers.

Similar morphology was also revealed for metal containing composites, i.e. PAN-66TiO_2-1Au, PAN-66TiO_2-1AuPd, indicating that metal NPs do not interfere with polymer electrospinning procedure. A deeper overview of the composite morphology was obtained via TEM analysis which revealed that granules of NP-decorated TiO_2 powder are embedded in the fiber. Thus, it could be hypothesized that only a small percentage of the total active sites will be exposed to the reactants.

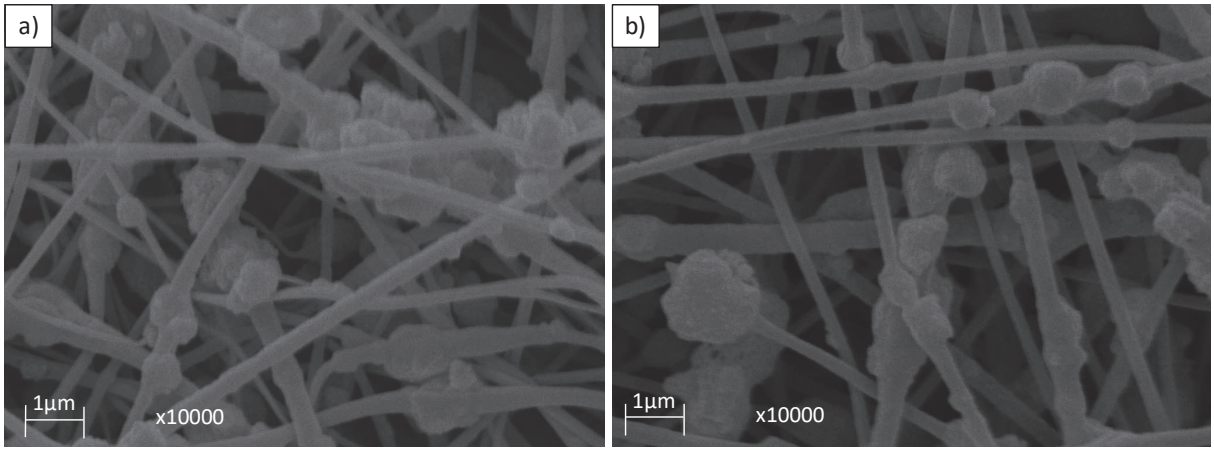

Figure 5-3 SEM analyses of metal loaded PAN composites: a) PAN-66TiO_2-1Au, PAN-66TiO_2-1AuPd

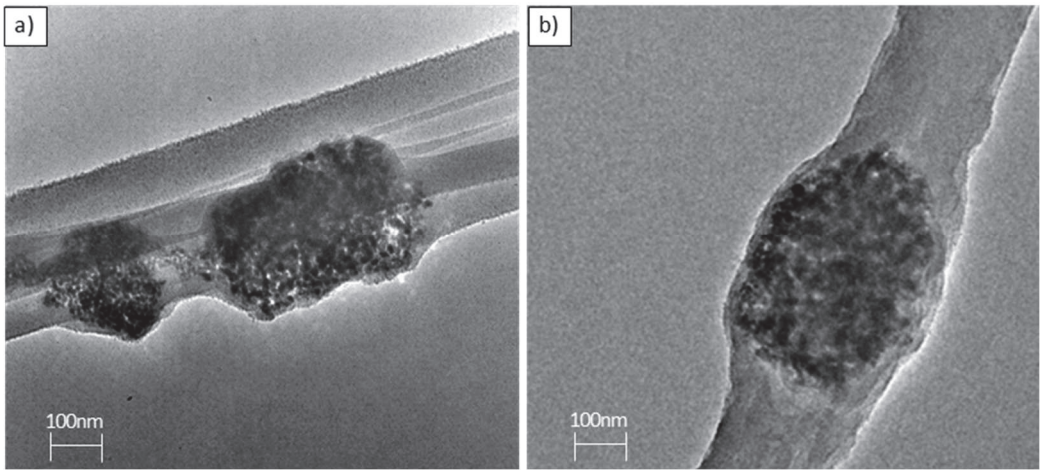

Figure 5-4 TEM images of PAN-66TiO_2-1Au (left) and PAN-66TiO_2-1AuPd (right) samples.

TGA analyses performed on the PAN membrane showed that polymer decomposition occurs in two different steps: the first occurs at around 310°C and accounts for around 40% of the weight loss, while the second happens in a broad range (from 400 to 680°C) and lead to the complete decomposition of the polymer (Figure 5-5).

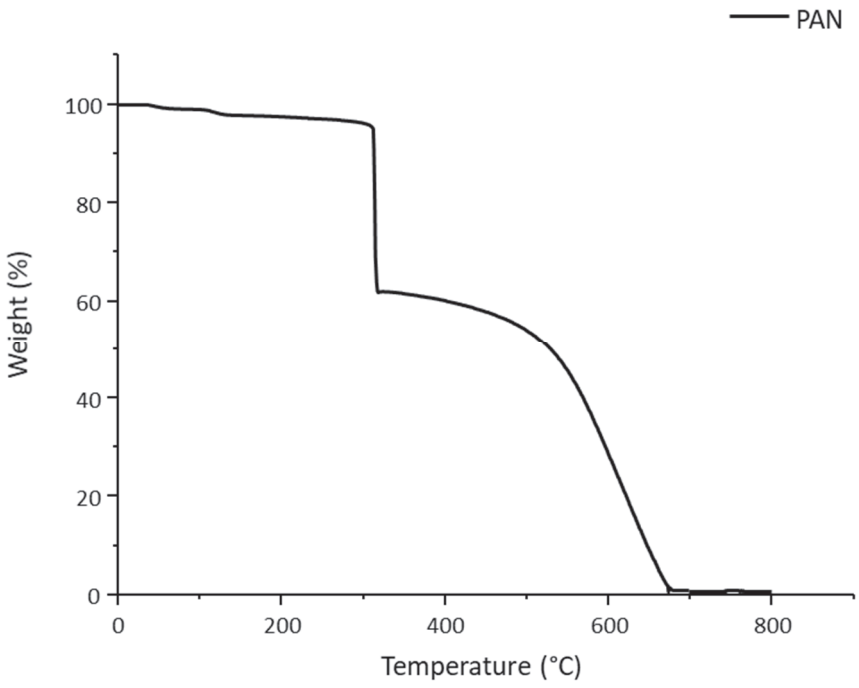

Figure 5-5 TGA in air (flow rate 100ml/min, temperature ramp 10°C/min) of PAN

This decomposition pattern is in well agreement with the ones reported in the literature and the first of the two weight losses could be attributed to the release of nitrogen compounds,while the second is related to the complete degradation of the polymer.[21]

Similar decomposition trend was found for the TiO_2 containing membranes, indicating that the inorganic component does not interfere with the polymer degradation phenomena (Figure 5-6).

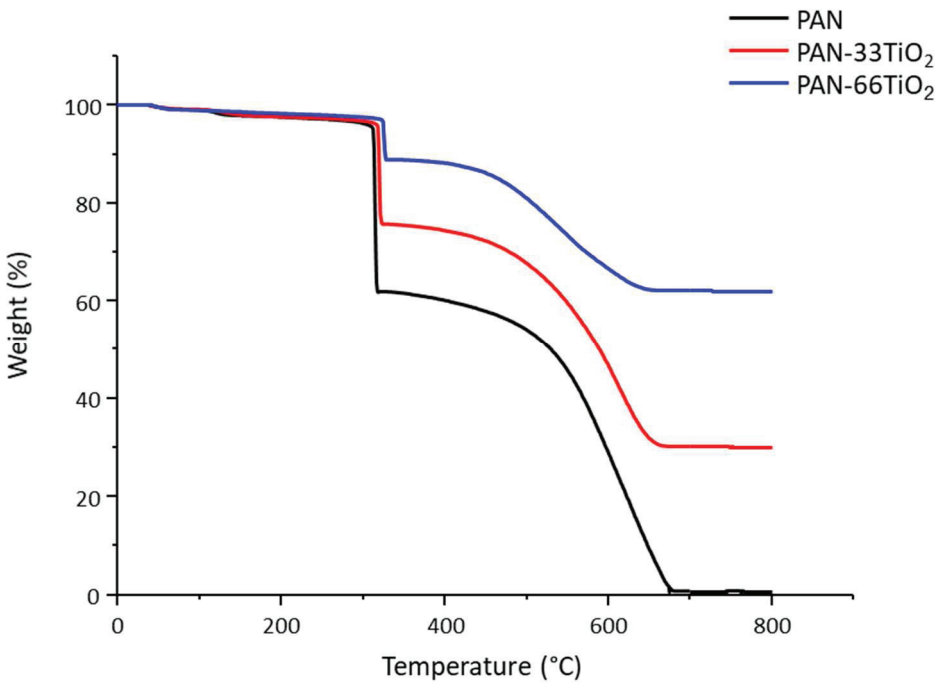

Figure 5-6 Effect of TiO_2 loading on thermal induced decomposition of PAN-containing composite fibers.

Another information that could be obtained from this comparison is that the electrospinning procedure allows a quantitative introduction of the inorganic component within polymer fibers: in fact, the weight percentage of the inorganic residue at the end of the TGA corresponds in good approximation to the TiO_2 percentage in the electrospun suspensions (Table 5-7).

Sample name	Nominal TiO_2 loading (wt%)	TGA residue (wt%)
PAN	-	0
PAN-33TiO₂	33	31
PAN-66TiO₂	66	63

Table 5-7 Comparison between the nominal TiO_2 and the TGA residue for PAN-containing composite membranes

As far as the effect of the metal in the TGA of composite membranes is concerned, it could be noticed that the polymer decomposition occurs at lower temperature when metal NPs are present in the membrane (Figure 5-7 and Table 5-8), indicating that those NPs can catalyze polymer oxidation.

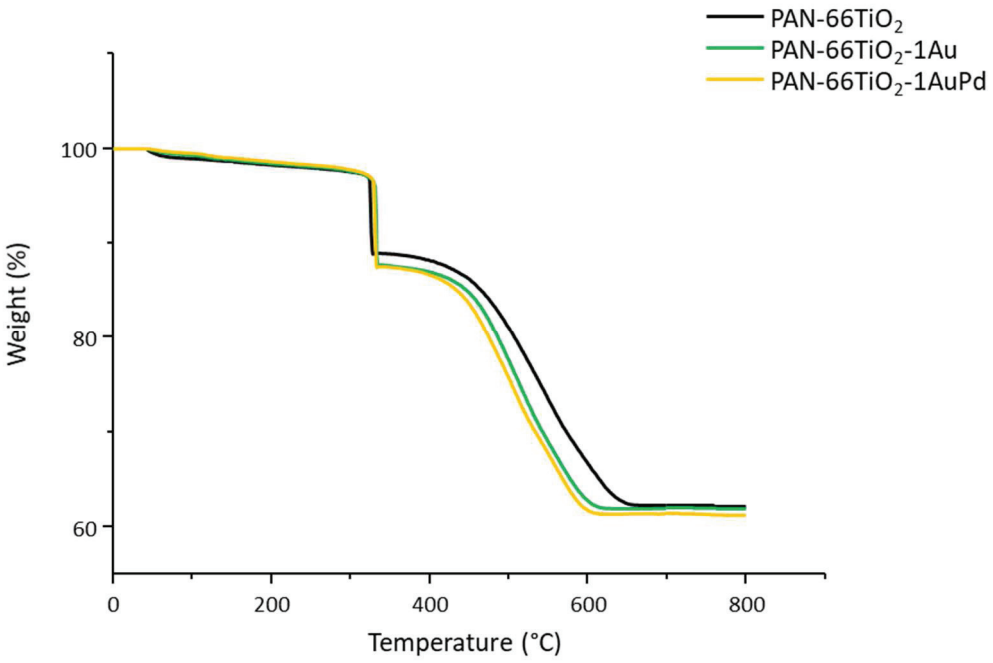

Figure 5-7 Effect of metal NPs on thermal induced decomposition of PAN-66TiO_2 composite membranes

Sample name	TGA residue (wt%)	Minimum weight temperature (°C)
PAN-66TiO_2	63	655
PAN-66TiO_2-1Au	63	615
PAN-66TiO_2-1AuPd	61	610

Table 5-8 Weight residues and temperature at which the minimum weight is reached for TiO_2 containing composite membranes (PAN-66TiO_2, PAN-66TiO_2-1Au and PAN-66TiO_2-1AuPd)

Catalyst screening

Catalytic activity of the membranes without NPs was evaluated in order to verify an eventual activity of the polymeric membrane.

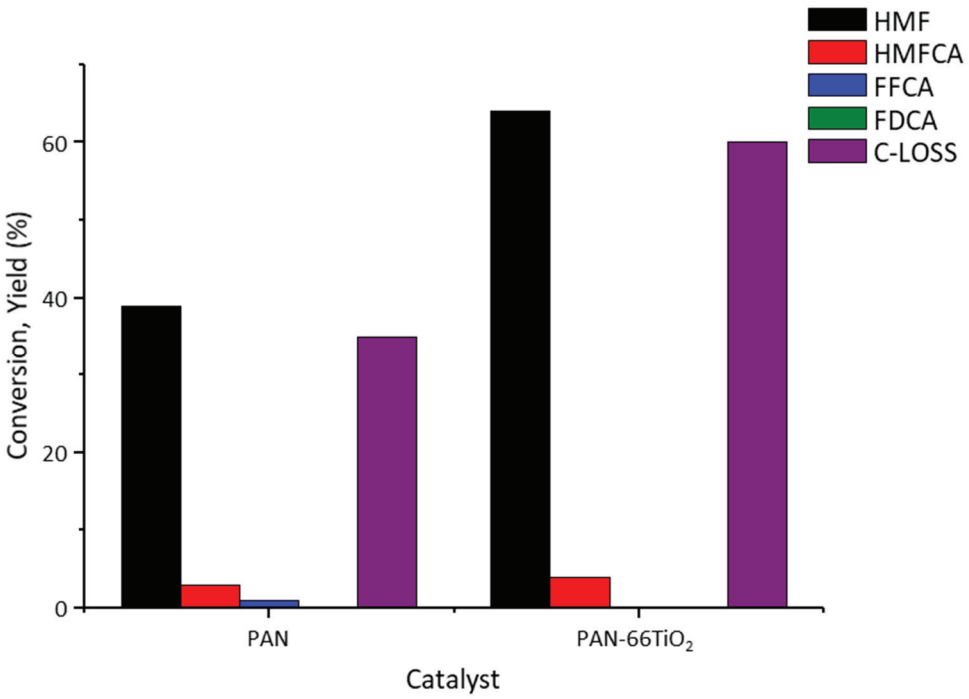

Figure 5-8 Catalytic performances of PAN and PAN-66TiO_2 sample. Operative conditions: temperature 70°C, O_2 pressure 10bar, 25mL water, HMF concentration 18mM, HMF:NaOH molar ratio 1:2

The results showed that neither the PAN membrane and the composite PAN-66TiO_2 possess catalytic activity toward HMF oxidation, since HMF is mostly converted into degradation byproducts, whose formation is favored by the high pH conditions.

On the other hand, when Au-decorated TiO_2 is inserted in the membrane network, the resulting materials possess a certain activity, which seems to be strongly correlated to the concentration of the active phase (i.e. Au NPs) in the membrane itself (Figure 5-9). In fact, HMF conversion increases from 33 to 69% by increasing Au content, and also HMFCA and FFCA yields are higher when composites with higher Au loading are used. However, it must be noticed that composite catalytic activity is far lower if compared to the powder catalyst. This could be attributed to the fewer active sites exposed in the composite membrane respect to the overall active sites of the powder (see TEM analysis in paragraph 5.2.2).

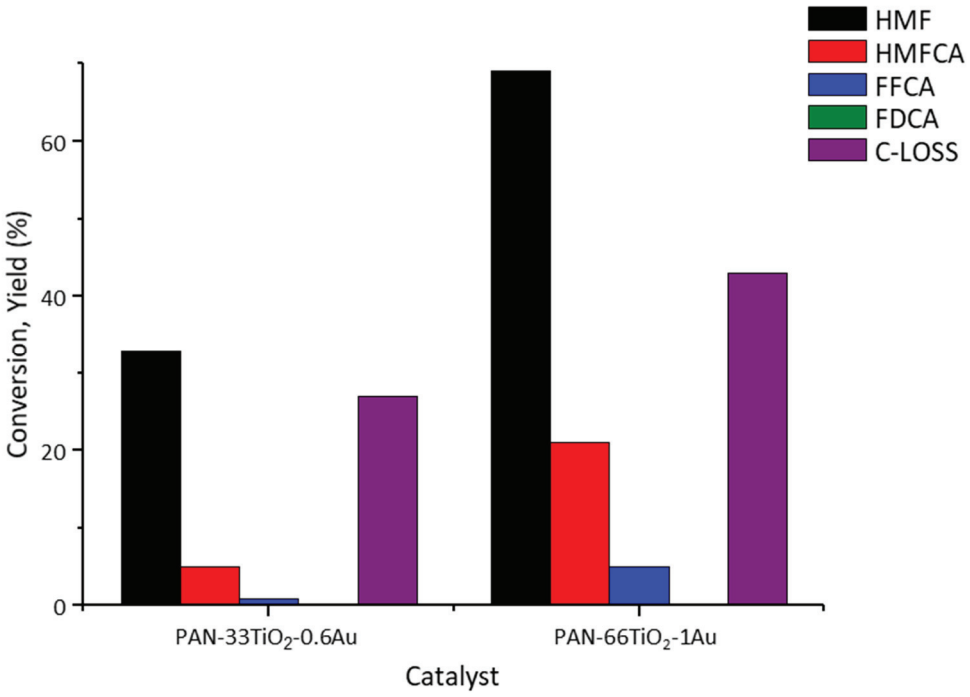

Figure 5-9 Effect of Au loading on the catalytic performances of PAN-TiO_2 composite membranes. Operative conditions: temperature 70°C, O_2 pressure 10bar, 25mL water, HMF concentration 18mM, HMF:NaOH molar ratio 1:2, HMF:Au molar ratio 100:1

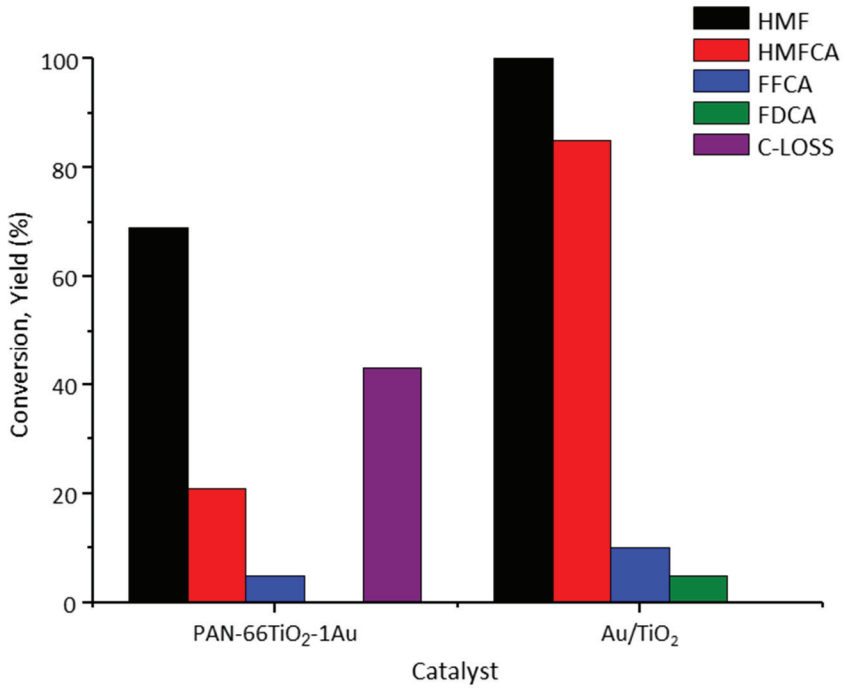

Figure 5-10 Comparison between the catalytic performances of PAN-TiO_2 composite membranes and supported Au/TiO_2 catalyst. Operative conditions: temperature 70°C, O_2 pressure 10bar, 25mL water, HMF concentration 18mM, HMF:NaOH molar ratio 1:2, HMF:Au molar ratio 100:1

The use of the bimetallic systems induced an increase of the catalytic performance of the composite membrane: HMF conversion increased from 69 to 94%, and a small amount of FDCA (2%) was detected when the bimetallic system was used (Figure 5-11).

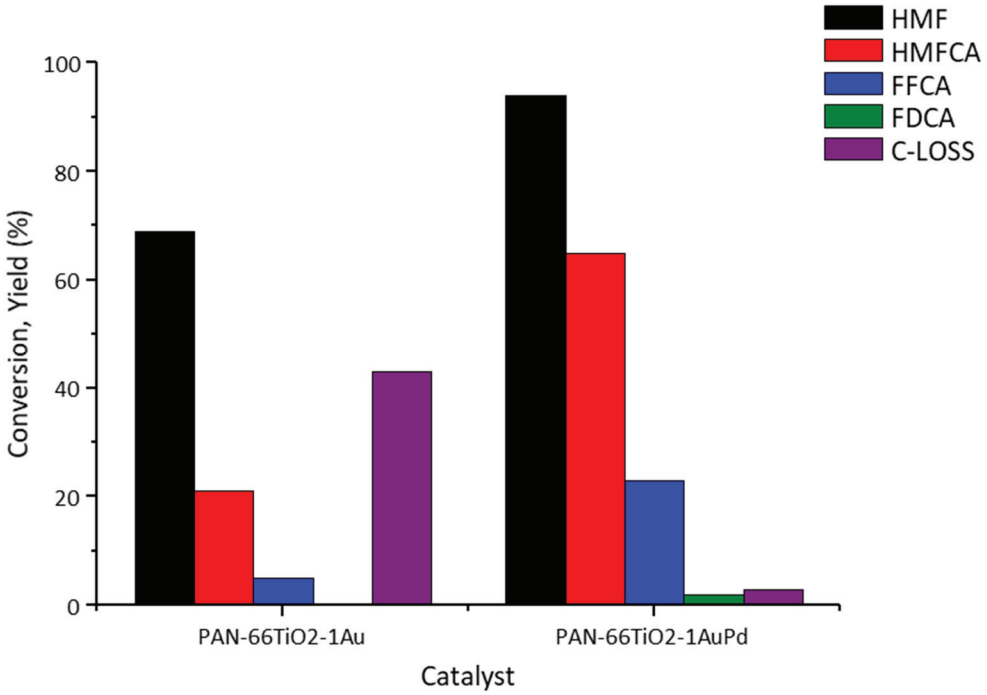

Figure 5-11 Effect of alloyed AuPd NPs on PAN/TiO_2 composite membranes catalytic activity. Operative conditions: temperature 70°C, O_2 pressure 10bar, 25mL water, HMF concentration 18mM, HMF:NaOH molar ratio 1:2, HMF:Au (or Au+Pd) molar ratio 100:1

The improved performances of the bimetallic system respect to the one of the Au monometallic systems is a well known feature for Au-based NPs in HMF oxidation, and it is correlated to the cooperative effect of the two metal in the alloyed system.

However, also in this case the catalytic activity of the AuPd-containing membrane is far lower than the one of the respective powder sample, indicating that also in this case substrate access to the catalyst active sites is hindered by the polymer chain of the fibers.

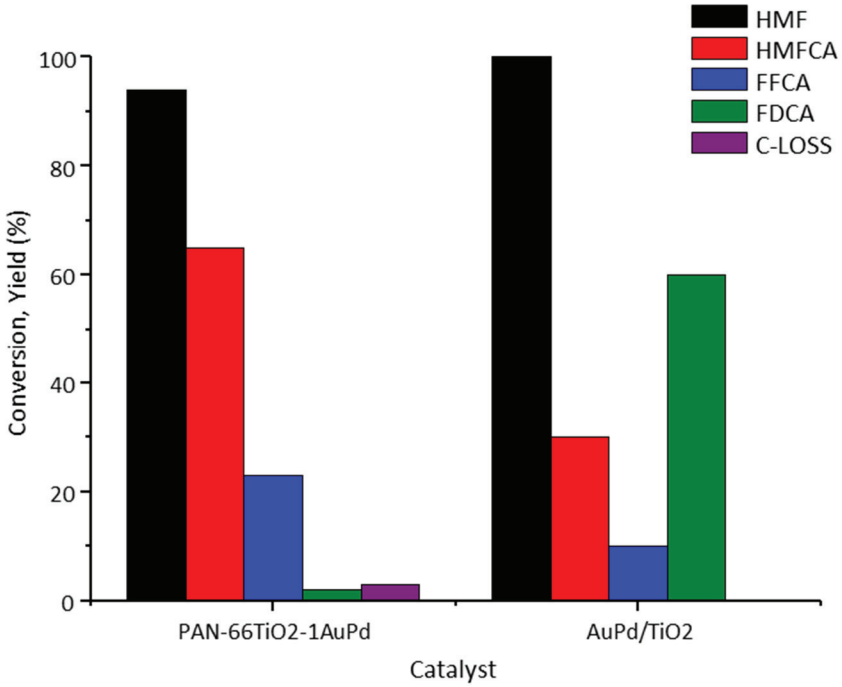

Figure 5-12 Comparison between the catalytic performances of PAN-TiO_2 composite membranes and supported AuPd/TiO_2 catalyst. Operative conditions: temperature 70°C, O_2 pressure 10bar, 25mL water, HMF concentration 18mM, HMF:NaOH molar ratio 1:2, HMF:Au molar ratio 100:1

In order to overcome this problem, it was tried to treat the PAN-66TiO_2-1AuPd composite membrane at temperature higher than the PAN glass transition temperature. This has been done with the aim to induce a movement of the polymer chains which could lead, on its turn, to an improved exposure of the active sites. Alternatively, another batch of untreated composite membrane, has been calcined at 300°C, with the aim to understand if the thermal induced PAN cyclisation has a positive effect on the composite catalytic performances. Thus, two samples have been obtained by treating the PAN-66TiO_2-1AuPd composite to 120°C and 300°C in static air. The catalytic activity of those membranes was tested and compared to the untreated one (Figure 5-13).

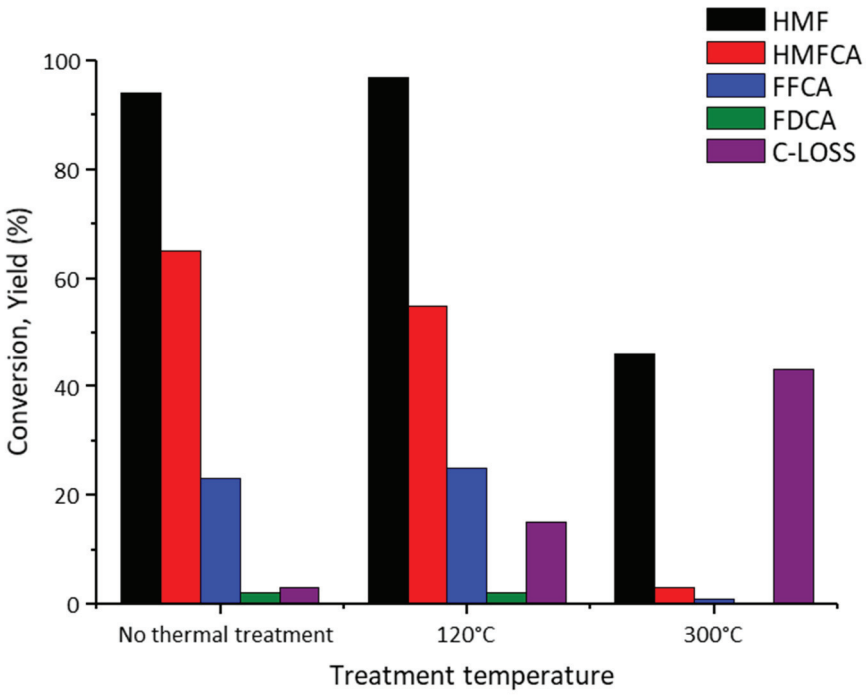

Figure 5-13 Effect of thermal treatments on PAN-66TiO_2-1AuPd composite membranes catalytic activity. Operative conditions: temperature 70°C, O_2 pressure 10bar, 25mL water, HMF concentration 18mM, HMF:NaOH molar ratio 1:2, HMF:(Au+Pd) molar ratio 100:1

The comparison of the catalytic activity of those membranes showed that the thermal treatment has a detrimental effect on the composite activity, indicating that active sites remains still hindered within polymer fibers even after the treatment at 120°C, and, when high temperature are used (i.e. 300°C), catalyst is completely inactive, probably due to the fact that during calcination NPs undergo a size increase which makes them inactive toward HMF oxidation.

5.2.3 Conclusion

This part of the work showed that the preparation of composite membranes made by NPs-decorated TiO_2 and PAN is a viable option for the synthesis of active materials in the HMF oxidation. However, due to the reduced active sites exposure in the membranes, the latter are less active than the powder catalyst as it. Thus, further works could aim to understand how to reduce the tendency of TiO_2 to form aggregates within the polymer fiber, leading then to a higher active membrane.

5.3 Pt inorganic cluster as catalyst precursor for composite PAN-TiO_2 membranes

As shown in Chapter 3, Pt NPs obtained via carbonylic clusters decomposition were found to be active in base free HMF oxidation. In view of this, and considering their solubility in DMF, which is

the solvent for PAN electrospinning, it has been evaluated the possibility to prepare Pt-containing PAN membranes via direct electrospinning of the polymer and Pt cluster solution. Similarly, composites membranes were prepared via electrospinning of DMF suspension containing Pt cluster, PAN and TiO_2. Then, the prepared materials were tested in the HMF oxidation under base-free conditions.

5.3.1 Experimental

Pt-containing composite membrane preparation

The cluster used in this study is the Chini cluster $[PPh_4]_2[Pt_{12}(CO)_{24}]$ (named as Pt_{12}), whose synthesis and characterisation are reported in Paragraph 3.2.1. The so obtained cluster has been solubilized in DMF and, to the resulting solution, an appropriate amount of PAN was added, in order to have concentration of 8% in weight of PAN respect to DMF. This PAN/Pt_{12} solution in DMF was then divided in two different batches: the first was electrspun as it in the already described setup in order to obtain a Pt/PAN composite membrane having a Pt weight loading of 2.5% (named as PAN-2.5Pt), while to the second a suitable amount of TiO_2 was added and the resulting suspension was electrospun, leading to a Pt/TiO_2/PAN membrane (named as PAN-66TiO_2-2.5Pt), whose Pt and TiO_2 nominal weight percentages are 2.5 and 66, respectively.

Sample name	Voltage (kV)	Flow rate (mL/h)	Collector-needle distance (cm)	Temperature (°C)	Humidity (%)
PAN-2.5Pt	23	1.2	20	25	42
PAN-66TiO_2-2.5Pt	20	1.2	20	25	50

Table 5-9 Pt-containing PAN based composite membranes synthesized in this study and respective electrospinning operative parameters

Sample name	TiO_2 loading (wt%)	Pt loading (wt%)	BET specific surface area (m^2/g)
PAN-2.5Pt	-	2.5	11
PAN-66TiO_2-2.5Pt	66	2.5	54

Table 5-10 TiO_2 and Pt loading and specific surface area for the electrospun PAN-based membranes

Catalytic tests

Catalytic tests were performed in bench scale autoclave described in Chapter 2.

In a typical experiment, a water solution of HMF (0.0310g in 25mL) are prepared, and a suitable amount of catalyst (in order to have a metal:HMF molar ratio equal to 1:100) are added to the

solution. Composite membranes were introduced in the solution as small squares having average size of 0.25cm^2. The resulting suspension is loaded in the autoclave, purged with O_2 and then pressurized to 10bar with the same gas. Temperature is then set to 90°C and at the end of the catalytic test, reaction is quenched in an ice bath. The reaction mixture is filtered on a buchner funnel in order to collect the used catalyst and the filtrated is then analyzed in HPLC as described in Chapter 2.

5.3.2 Results and discussion

Composite membrane morphological characterization

The SEM analysis of the PAN-2.5Pt composite membrane showed that randomly oriented fibers are obtained, and spherical agglomerates are present within the fiber network. EDX analyses performed over those agglomerates revealed that they are mainly made of polymer, since a large excess of C was detected (91.5 wt%) respect to the measured Pt concentration, 2.5 wt% which corresponds to the nominal Pt loading, indicating that during the electrospinning procedure there is not any substantial loss of Pt.

A more detailed insight on the Pt distribution in the PAN-2.5Pt composite sample was obtained by means of STEM analysis, which revealed that clusters are homogeneously dispersed within PAN fibers and are oriented toward the fiber direction.

As far as the TiO_2 containing composite is concerned (PAN-66TiO_2-2.5Pt), it was revealed the formation of aggregates having different shape respect the ones shown before, since TiO_2 agglomerates modify the overall fiber morphology. Another modification due to TiO_2 presence is related to Pt distribution: in fact, as revealed by STEM analysis, Pt tends to be present on TiO_2 aggregates rather than within PAN fibers.

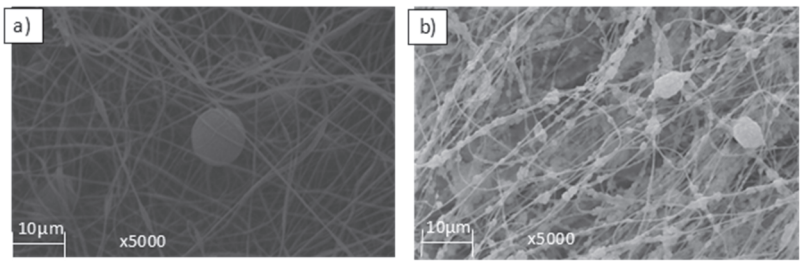

Figure 5-14 SEM characterisation of Pt-containing composite membranes: PAN-2.5Pt and PAN-66TiO_2-2.5Pt, (left and right, respectively)

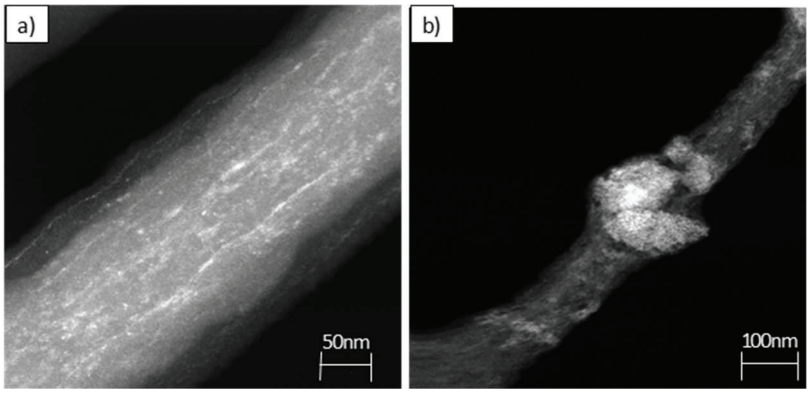

Figure 5-15 STEM characterisation of Pt-containing composite membranes: PAN-2.5Pt and PAN-66TiO_2-2.5Pt, (left and right, respectively)

Effect of inorganic compounds in composite thermal decomposition

TGA analyses were performed with the aim to understand how the inorganic compounds alter the membrane decomposition behavior. Such study, performed over PAN, PAN-2.5Pt and PAN-66TiO_2-2.5Pt samples, revealed that Pt affects the thermal induced decomposition of the PAN membrane. In particular, when both TiO_2 and Pt are present in the membrane (sample PAN-66TiO_2-2.5Pt, red line in Figure 5-16), polymer decomposition occurs in just one step, indicating that Pt strongly promotes polymer degradation. On the other hand, when just Pt is present within fiber network, polymer decomposition occurs in two different steps (PAN-2.5Pt, blue line in Figure 5-16). However, comparing the weight loss during the first decomposition step of the PAN-2.5Pt sample with the PAN one (black line in Figure 5-16), it is evident that the weight drop is more pronounced when Pt is present. This could be due to the fact that Pt catalyses PAN degradation until a certain extent, probably until it is present as reduced species.

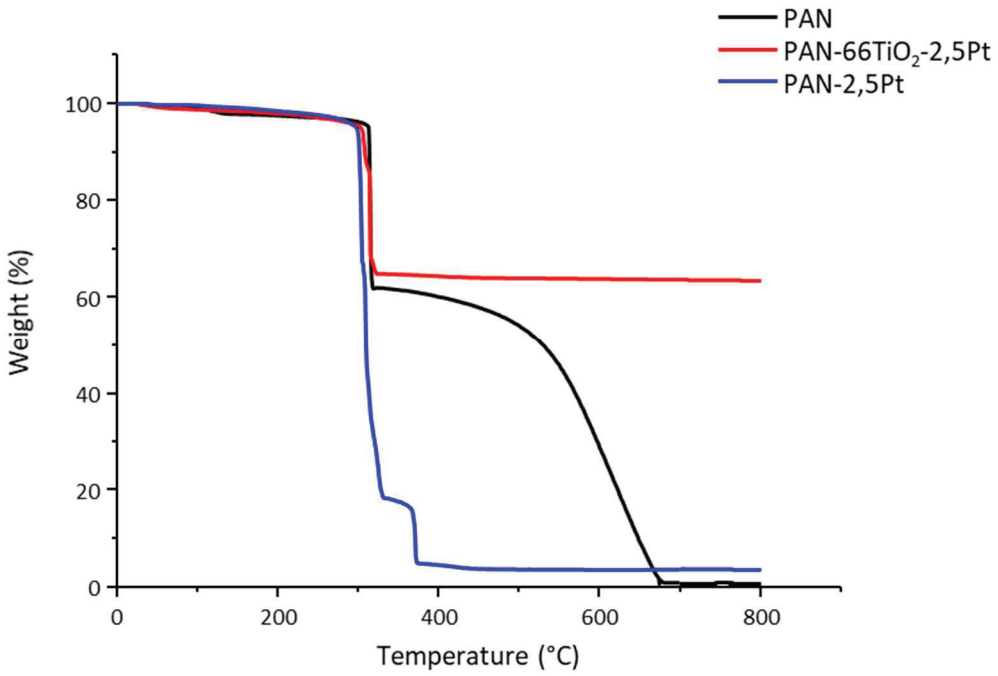

Figure 5-16 Effect of Pt and TiO_2 addition on thermal induced decomposition of PAN based membranes

Sample name	TGA residue (wt%)	Minimum weight temperature (°C)
PAN	0	673
PAN-2.5Pt	3	385
PAN-66TiO_2-2.5Pt	66	320

Table 5-11 Weight residues and temperature at which the minimum weight is reached for PAN based membranes (PAN, PAN-2.5Pt and PAN-66TiO_2-2.5Pt)

Effect on cluster structure during electrospinning protocol

In order to evaluate the evolution on cluster structure during membrane electrospinning, IR technique has been used. In particular, as described in paragraph 3.3, CO stretching bands were used as probe signals for the detection of potential cluster structural changes.

The comparison between the IR spectrum of a PAN membrane and the Pt-containing ones (i.e. PAN-2.5Pt and PAN-66TiO_2-2.5Pt) revealed that the latter, alongside to the characteristic bands of PAN, shows two extra peaks at 1887 and 2056cm^{-1} which were attributed to the terminal and bridged carbonyls of the parent Pt_{12} cluster, respectively. Thus, it is possible to affirm that neither the electrospinning procedure nor the TiO_2 presence affect the chemical structure of the Pt_{12} cluster, hypothesizing that polymer presence prevents cluster decomposition.

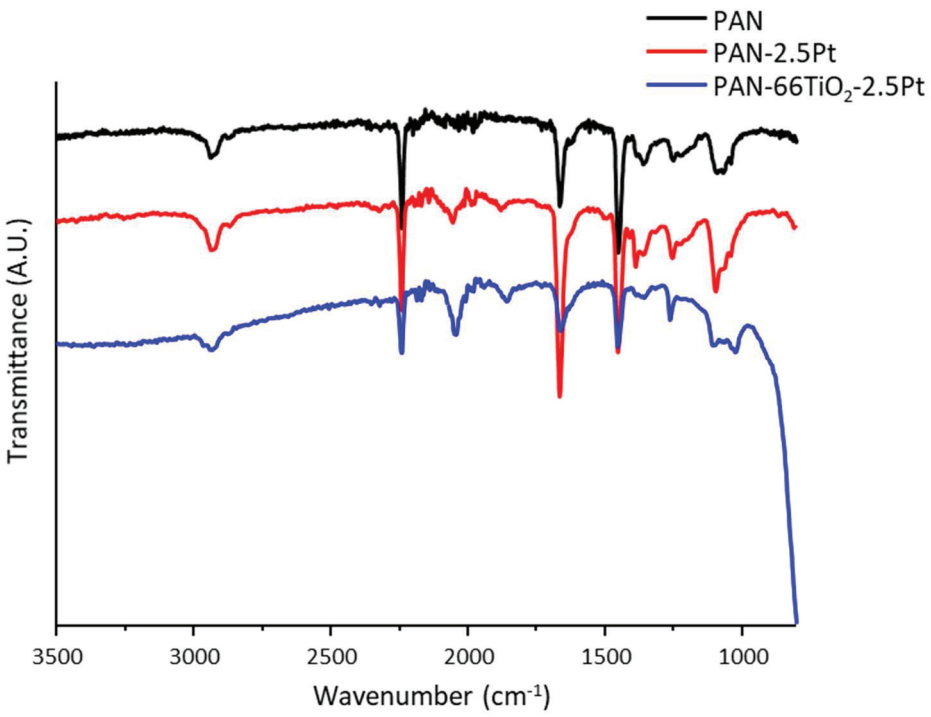

Figure 5-17 FTIR analysis of the PAN composite membranes

Catalytic tests

The prepared composite membranes were tested in the base-free HMF oxidation. The preliminary screening showed that among the two composites, the TiO_2 containing membrane possess higher activity in both terms of HMF conversion and FDCA yield respect to the PAN-2.5Pt one. This difference in catalytic activity could be due to the higher specific surface area of the PAN-66TiO_2-2.5Pt and to the intrinsic improved exposure of active sites in this sample, since, as previously seen, Pt is mainly present on the TiO_2 agglomerates rather than within the fiber matrix.

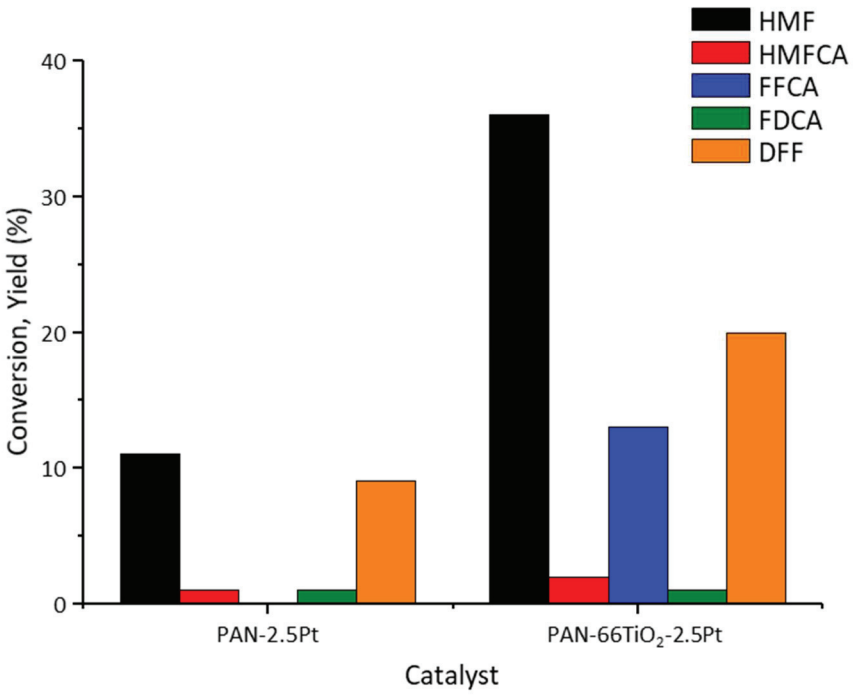

Figure 5-18 Effect of TiO_2 addition on catalytic properties of Pt-containing PAN membranes. Operative conditions: temperature 110°C, O_2 pressure 10bar, 25mL water, HMF 0.0310g, molar ratio HMF/total metal=50.

However, comparing the catalytic activity of the PAN-TiO_2-2.5Pt membrane with the catalyst prepared by cluster impregnation on TiO_2 (2-Pt-c-H[†]) it is evident that the composite catalyst possesses lower activity, which could be attributable to the lower active sites exposure of the latter. On the other hand, composite catalyst has a comparable activity respect to the metal salt impregnated catalyst 2-Pt-s-H.[‡] This could be due to the fact that the lower exposure of active sites in the PAN-TiO_2-2.5Pt catalyst is offset by an intrinsically higher activity of the cluster derived active sites.

[†] See paragraph 3.2.1 for its synthesis
[‡] See paragraph 3.2.2 for its synthesis

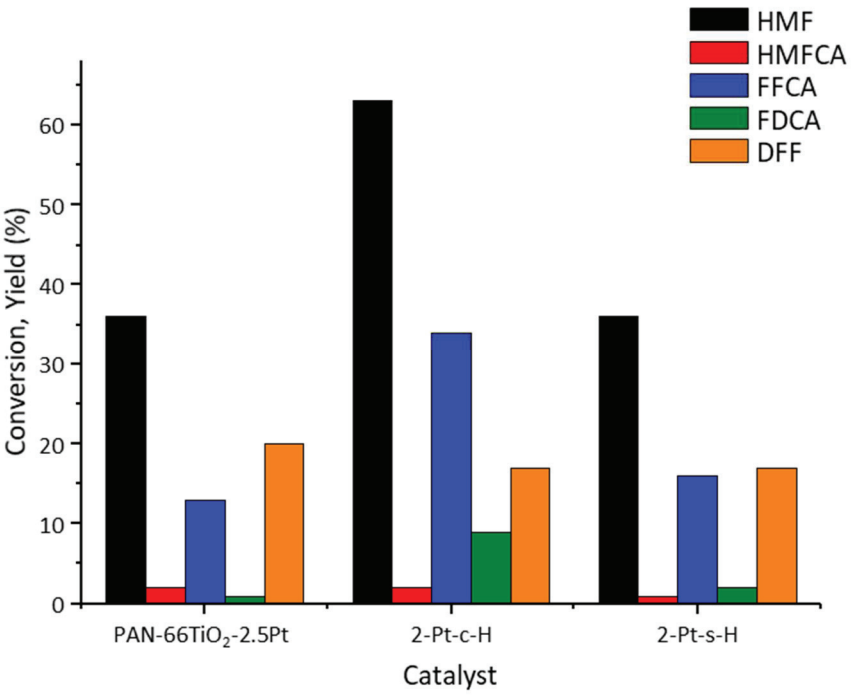

Figure 5-19 Effect synthetic protocol on the catalytic performances of Pt-containing materials: electrospun PAN membranes (PAN-66TiO_2-2.5Pt), Pt clusters impregnated on TiO_2 (2-Pt-c-H_2, see 3.2.1) and metal salt impregnated on TiO_2 (2-Pt-s-H_2, see 3.2.2). Operative conditions: temperature 110°C, O_2 pressure 10bar, 25mL water, HMF 0.0310g, molar ratio HMF/total metal=50

PAN-66TiO_2-2.5Pt reusability test

In order to evaluate PAN-66TiO_2-2.5Pt stability, reusability tests have been carried out (Figure 5-20). The result of this test showed that this composite membrane progressively loses its catalytic activity, since HMF yield drops from 36 to 25% after the first reuse. This drop in catalytic activity could be attributable to the decomposition of Pt cluster, as revealed by the absence of the CO bands in the IR spectrum of the used membrane (Figure 5-21), which could cause on its turn the formation of oxidized Pt NPs, which are less active then the reduced one. Then, this Pt oxidation trend could be the responsible of the further composite activity drop, since in the third use HMF conversion is more than halved respect to same parameter reported after the first use.

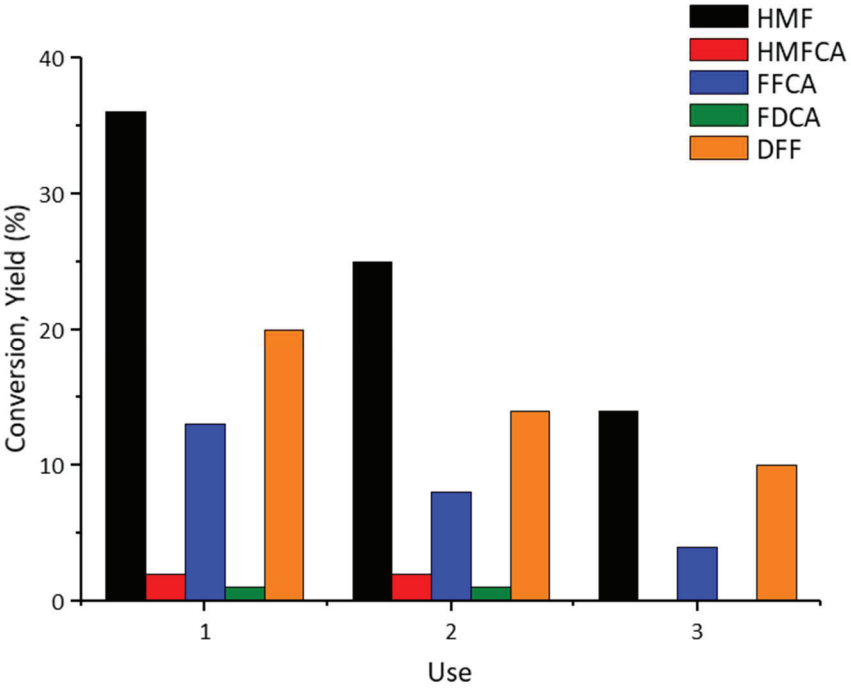

Figure 5-20 Reusability tests performed over PAN-66TiO_2-2.5Pt composite membrane. Operative conditions: temperature 110°C, O_2 pressure 10bar, 25mL water, HMF 0.0310g, molar ratio HMF/total metal=50

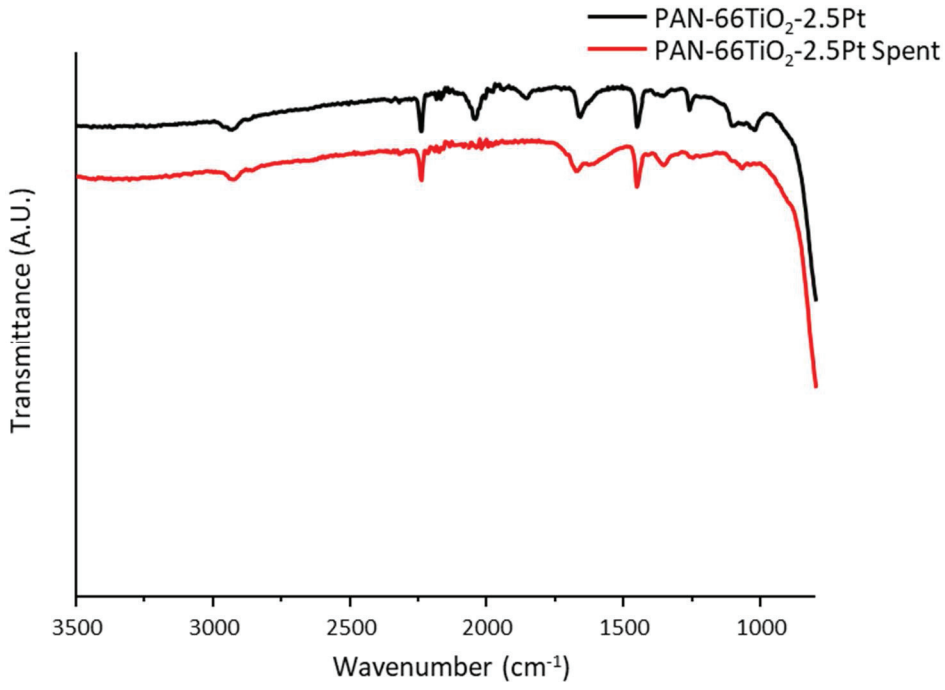

Figure 5-21 FTIR spectra recorded for the PAN-66TiO_2-2.5Pt membrane as electrospun and used

5.3.3 Conclusion

This study revealed that Pt-containing composite PAN membranes can be obtained via direct electrospinning of cluster solutions, whose chemical structure does not undergo any modification during electrospinning procedure, as revealed by IR study. The activity of the electrospun material toward base-free HMF oxidation is strongly correlated to the surface area which can be increased by addition of TiO_2 within the membrane network. The TiO_2/Pt containing composite membrane was proven to suffer from progressive deactivation issue, which could be ascribed to the cluster decomposition after composite use.

5.4 Unsupported Au-nanoparticles embedded in electrospun nylon membrane

5.4.1 Experimental

Nanoparticle synthesis

In view of their higher activity in HMF oxidation respect to monometallic Au NPs, only Au_6Pd_1 NPs were used in this study. Their preparation has been performed as described in paragraph 5.2.1.

Composite membrane preparation

To prepare a solution that would be electrospun, a suitable volume of NPs colloidal suspension was washed with formic acid by centrifugation using 50 kDa Amicon Ultra filters (Millipore) in order to eliminate as much water as possible. The washing process was followed by DLS analysis to check eventual evolution on the hydrodynamic diameter of the NPs, and the final size of the NPs was determined by XRD measurement.

To the resulting NPs suspension was added a suitable amount of FA, and dried TiO_2 was added to this suspension. Once TiO_2 was fully suspended by stirring, Nylon 6,6 was added and dissolved under vigorous stirring. After full dissolution of the polymer, CH_3Cl was added.

The electrospinning apparatus was composed of a high voltage power supply (Spellman, UM 40*30), a syringe pump (New ERA NE-1000), a glass syringe, a stainless-steel needle (inner diameter: 0.84 mm) connected with the power supply electrode and a grounded aluminum plate-type collector (250 × 250 mm). The needle was placed in front of the collecting plate that was in a vertical position.

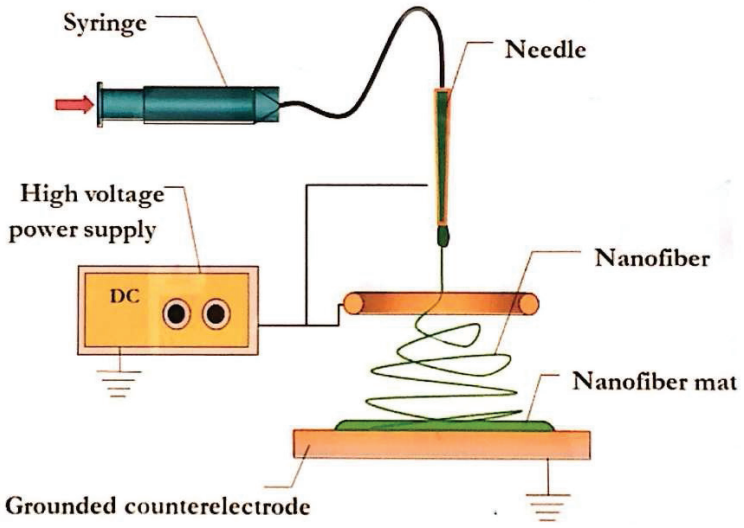

Figure 5-22 Experimental electrospinning apparatus

The experimental conditions of the electrospinning were set according to the composition and the viscosity of the solutions. Typical experimental conditions are reported in Table 5-12.

Parameter	Range
Voltage	18-20kV
Flow rate	0.20-0.25mL/h
Collector-needle distance	15cm
Temperature	20-23°C
Humidity	35-40%

Table 5-12 Experimental parameters for the preparation of electrospun Nylon membranes

The residual solvent in the obtained membranes was evaporated by thermal treatment at 80°C for 3h in static air. The mass loss due to the drying was no bigger than 3% for all the prepared membranes.

Catalytic tests

Catalytic tests were performed in bench scale autoclave described in Chapter 2.

In a typical experiment, 25mL of a 18mM water solution of HMF are prepared. Then NaOH (2equivalent respect to HMF) and a suitable amount of catalyst (in order to have a metal:HMF molar ratio equal to 1:100) are added to the solution. Composite membranes were introduced in the solution as small squares having average size of 0.25cm^2. The resulting suspension is loaded in the autoclave, purged with O_2 and then pressurized to 10bar with the same gas. Temperature is then set to desired set point and at the end of the catalytic test, reaction is quenched in an ice bath. The

reaction mixture is filtered on a buchner funnel in order to collect the used catalyst and the filtrated is then analyzed in HPLC as described in Chapter 2.

5.4.2 Results and discussion

Nanoparticle synthesis

AuPd NPs suspension was characterized by means of DLS in order to evaluate the distribution of the hydrodynamic volume of the NPs after the synthesis. Such analysis revealed that NPs having monomodal distribution were obtained, having average diameter of 32.6nm (Figure 5-23, black line). Such value progressively decreased after the two washing steps indicating that capping agent (i.e. PVP) is gradually removed from the NP surfaces (Figure 5-23, red and blue lines).

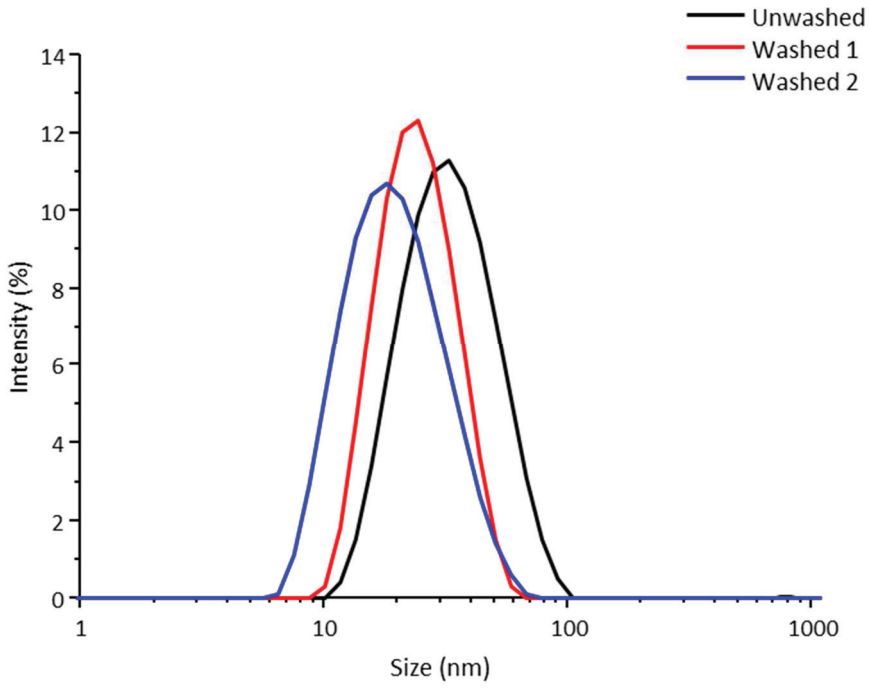

Figure 5-23 DLS analyses of NPs suspensions: as synthesized (black line), after 1 washing step (red line), after 2 washing steps (blue line).

XRD analysis were performed on the dried NPs suspensions as synthesized and after two washing steps (Figure 5-24). Such analysis revealed that crystallite size remains unaffected by washing procedure since it remains constant (4.5nm).

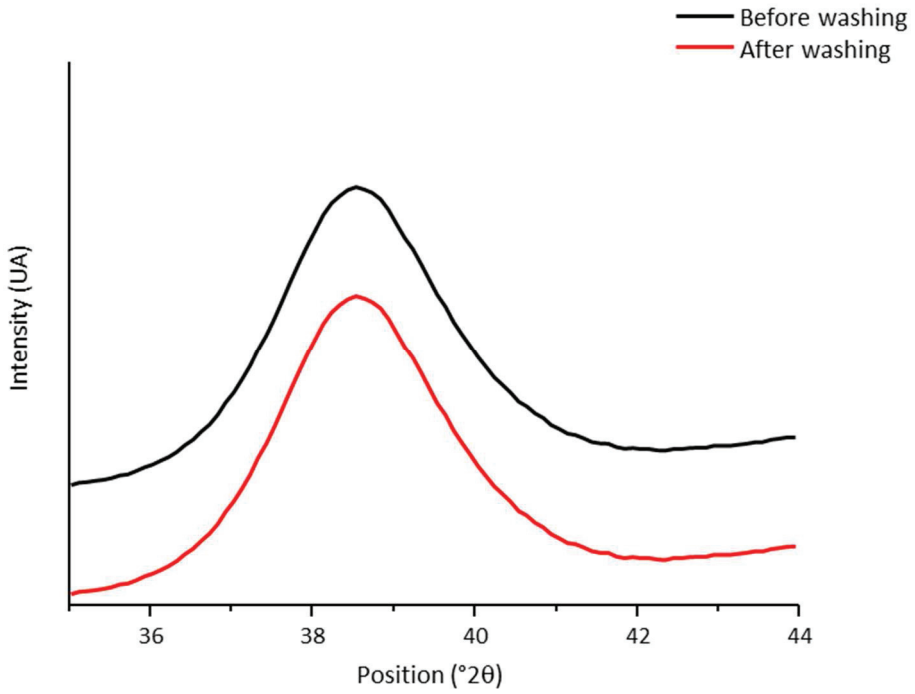

Figure 5-24 XRD analyses of dried NPs suspensions: before and after washing (black and red line, respectively)

Membrane preparation and characterization

Three sets of membranes were electrospun, as reported in table.

Sample name	Voltage (kV)	Flow rate (mL/h)	Collector-needle distance (cm)	Temperature (°C)	Humidity (%)	FA/DCM Volume ratio
Nylon	18	0.20	15	20	35	60/40
Nylon-2AuPd	20	0.20	15	23	38	60/40
Nylon-31.5TiO_2-2AuPd	19	0.25	15	23	40	60/40

Table 5-13 Nylon based composite membranes synthesized in this study and respective electrospinning operative parameters

Sample name	TiO_2 loading (wt%)	Total metal (Au+Pd) loading (wt%)	BET specific surface area (m^2/g)
Nylon	-	-	<10
Nylon-2AuPd	-	2	<10
Nylon-31.5TiO_2-2AuPd	31.5	2	36

Table 5-14 TiO_2 and metal loading and specific surface area for the electrospun Nylon-based membranes

The comparison of the BET specific surface area of the three electrospun materials revealed that the introduction of TiO_2 leads to an increase of this parameter, which could lead on its turn to an increased activity of the composite membrane.

SEM analysis of the Nylon sample revealed that with the reported electrospinning parameters continuous randomly oriented Nylon fibers were obtained, whose average diameter is around 0.4µm. The addition of AuPd NPs does not lead to any modification of the fiber morphology and size. On the other hand, TiO_2 addition to the polymer causes the formation of aggregates, without any substantial modification of the fiber diameter (Figure 5-25).

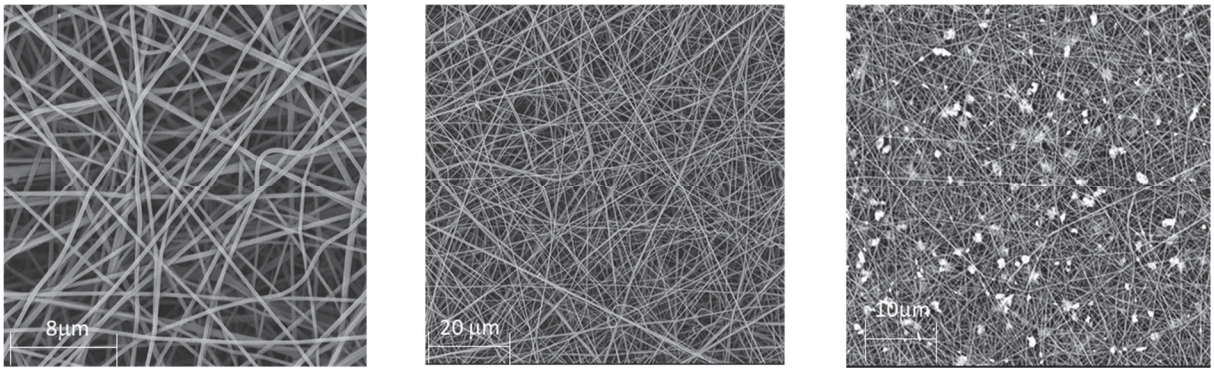

Figure 5-25 SEM analysis for Nylon, Nylon-2AuPd and Nylon-31.5TiO_2-2AuPd (from left to right)

Catalytic tests

The screening of the catalytic performances of the composite membranes revealed that in the reported operative conditions the electrospun nylon membrane does not possess any catalytic activity, since more than 90% of the fed HMF is converted into undefined byproduct. The addition of the AuPd NPs in the composite makes these membranes active, and highest catalytic performances are obtained with the membrane with the highest specific surface area, i.e. the Nylon-31.5TiO_2-2AuPd, since both FDCA yield and carbon balance result maximized with this catalyst. This feature indicates that the availability of the catalytic active sites is enhanced by TiO_2 addition, as seen previously see for PAN-based composite membranes (see paragraph 5.2.2).

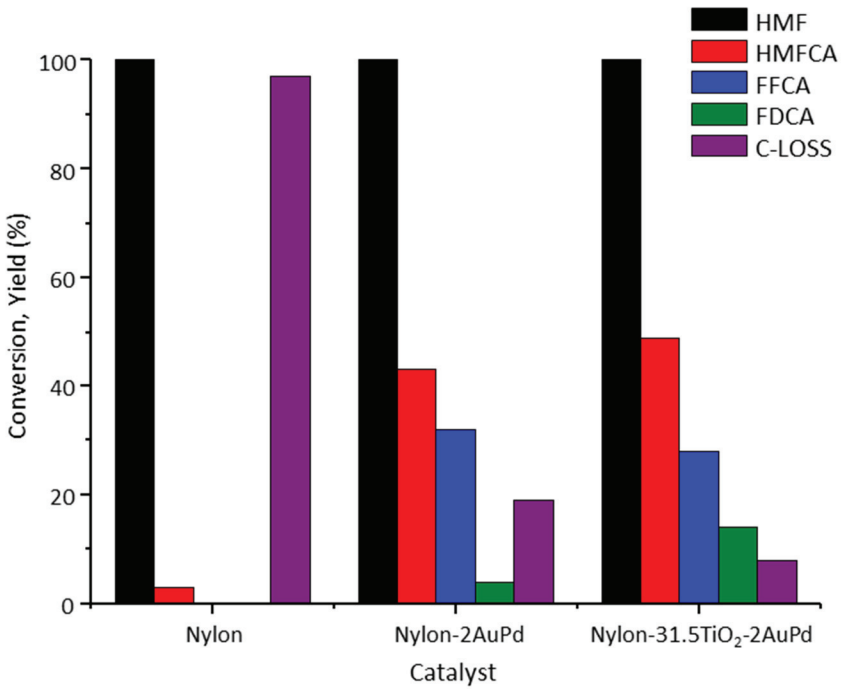

Figure 5-26 Effect of AuPd and TiO_2 addition to composite Nylon membranes catalytic properties. Operative conditions: temperature 70°C, O_2 pressure 10bar, 25mL water, HMF concentration 18mM, HMF:NaOH molar ratio 1:2, HMF:(Au+Pd) molar ratio 100:1

However, it must be noticed that the activity of the composite membrane is slightly lower if compared to the one of the sample prepared by supporting the same AuPd NPs over TiO_2. This could be attributed to the higher availability active sites of the supported catalyst respect to the composite membrane ones.

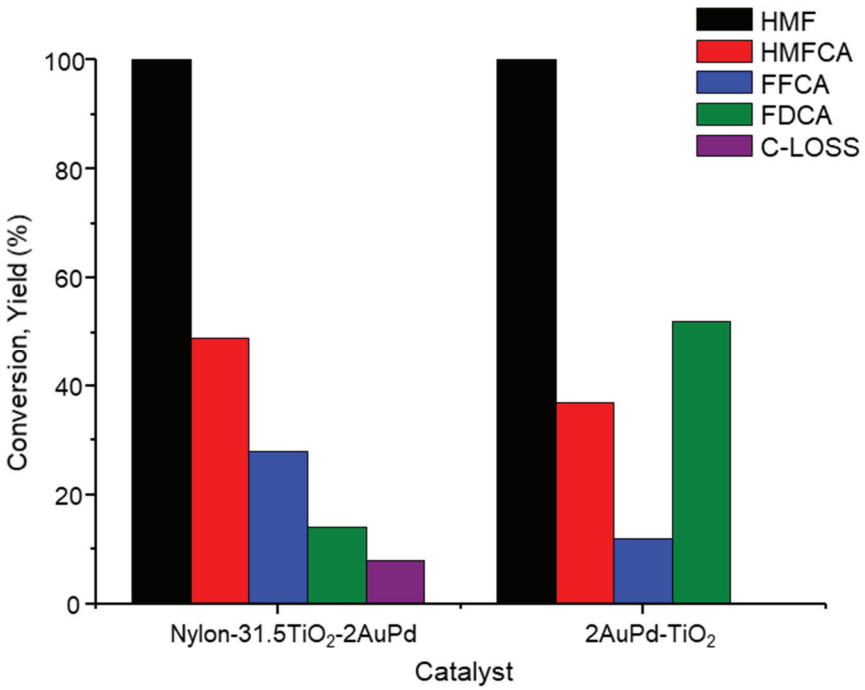

Figure 5-27 Comparison between the catalytic activity of composite memrbane and the TiO_2 supported AuPd NPs. Operative conditions: temperature 70°C, O_2 pressure 10bar, 25mL water, HMF concentration 18mM, HMF:NaOH molar ratio 1:2, HMF:(Au+Pd) molar ratio 100:1

Effect of reaction temperature on catalyst performances

With the aim to enhance FDCA yield, it has been evaluated the behavior of the most performing membrane (i.e. Nylon-31.5TiO_2-2AuPd) at reaction temperature higher than 70°C.

This study showed that temperature has a strong positive effect on FDCA yield, since it raises from 14 to 67% by increasing reaction temperature from 70 to 110°C. On the other hand, also carbon loss shows a similar trend, but its increment is not as significant as reported for FDCA yield. This feature has been related to the smaller increase of the degradation reaction rates respect to the rate increase of the reactions that lead to the desired product.

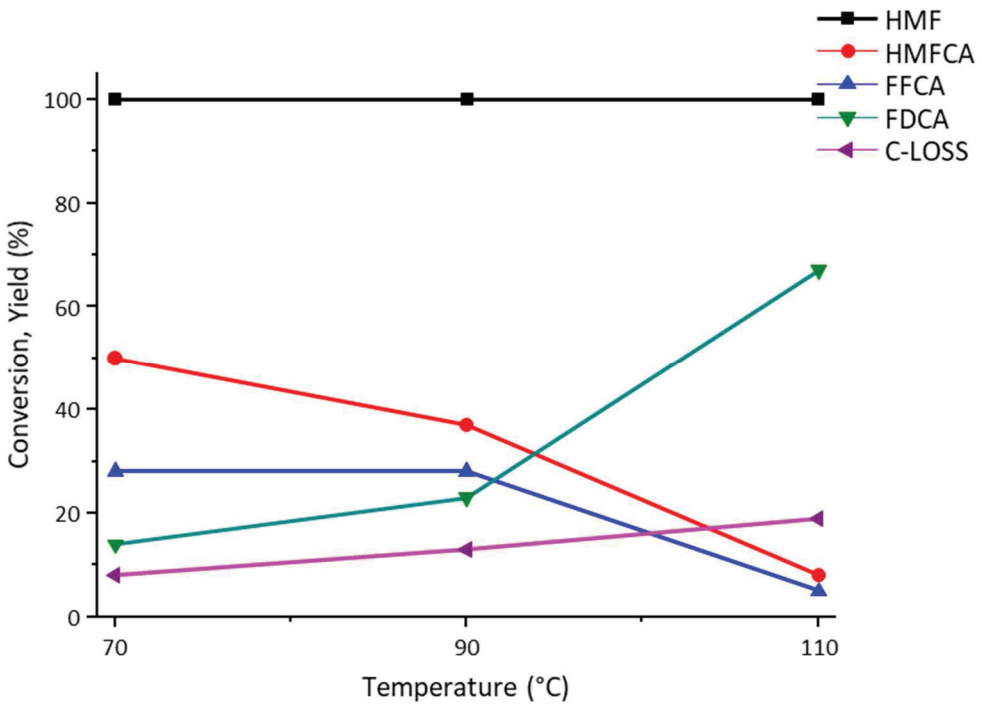

Figure 5-28 Reaction temperature effect on the catalytic performance of Nylon-66TiO_2-2AuPd sample. Operative conditions: O_2 pressure 10bar, 25mL water, HMF concentration 18mM, HMF:NaOH molar ratio 1:2, HMF:(Au+Pd) molar ratio 100:1

Membrane stability: reuse tests

In order to evaluate the Nylon-31.5TiO_2-2AuPd membrane stability, reusability tests have been performed. This study has been carried out at 90°C, since this temperature led to a good compromise between catalyst activity and undesired reactions presence as seen in the previous paragraph.

This test showed that composite catalytic activity is improved after the first use, since carbon loss falls to 2 from 19% and, at the same time, FDCA yield raises to 34 from 19%. To explain this carbon loss reduction, it has been hypothesized that during the membrane first use some intermediates are adsorbed within polymer matrix and the same are released and converted into FDCA during the composite second use. To corroborate this hypothesis, the used composite has been characterized by means of ATR with the aim to look for bands attributable to furanic-based compounds.

This analysis showed that no furanic-compounds are present within the membrane, and no change in its chemical composition occurs during the reaction, as revealed by the comparison between used and as-spun membrane.

A further use of the membrane led to a small drop of catalyst activity, but FDCA yield and overall carbon balance are still higher respect to the first use.

In light of this results, it is possible to hypothesize that catalytic active sites, which are hindered in the original membrane network, are made accessible by the use of the membrane in the reported operative conditions, probably due to thermal induced movement of polymer chains during the reaction which could occur because of the fact that membrane operates in temperature conditions (90°C) higher than its glass transition temperature (50°C).

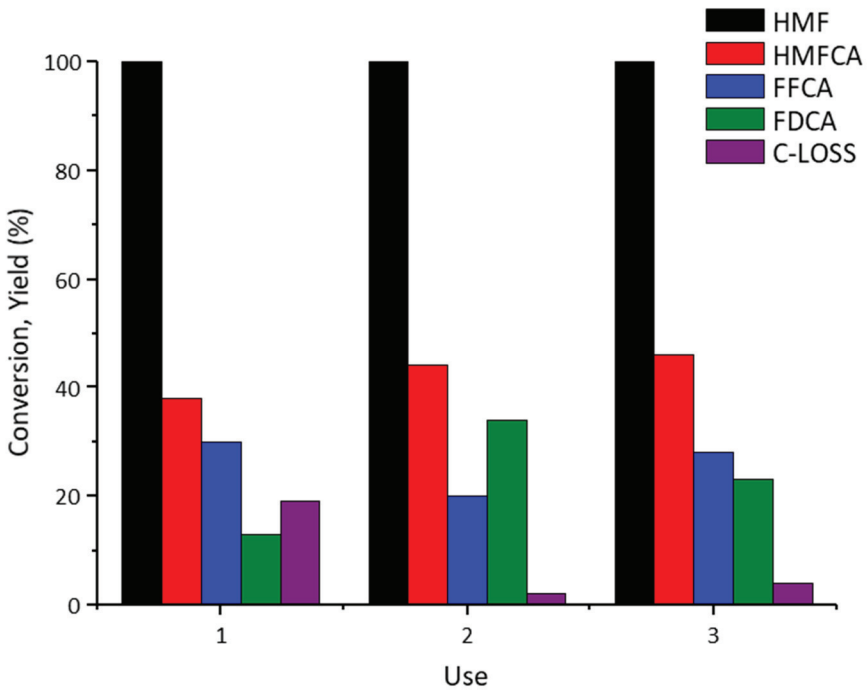

Figure 5-29 Reusability tests performed over PAN-66TiO_2-2AuPd composite membrane. Operative conditions: temperature 70°C, O_2 pressure 10bar, 25mL water, HMF concentration 18mM, HMF:NaOH molar ratio 1:2, HMF:(Au+Pd) molar ratio 100:1

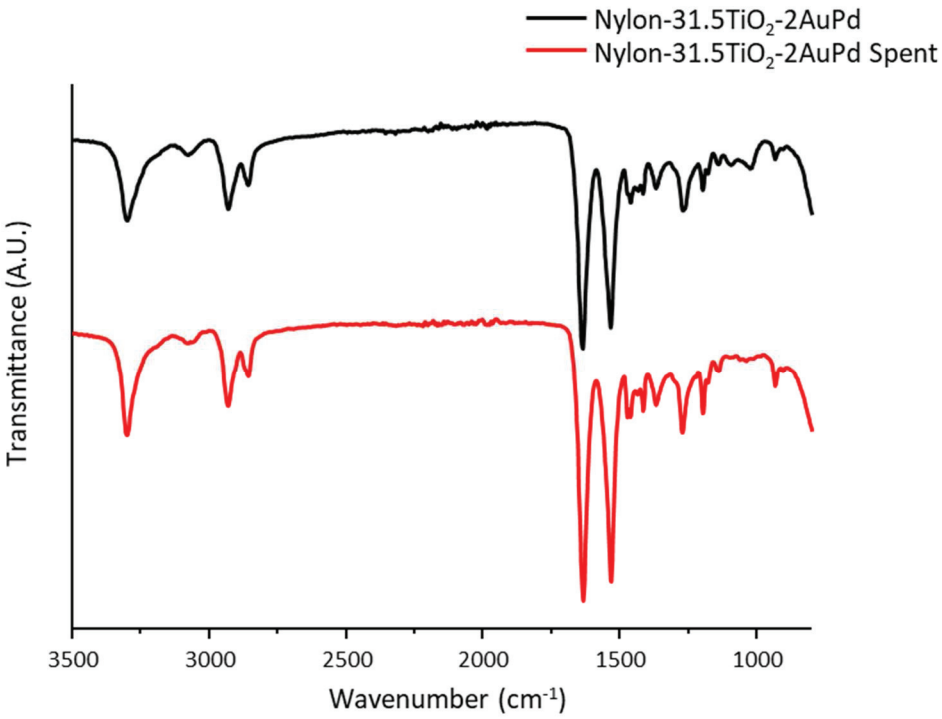

Figure 5-30 FTIR spectra recorded for the PAN-66TiO_2-2AuPd membrane as electrospun and used

5.4.3 Conclusion

AuPd NPs-containing electrospun Nylon membranes were proven to be effective catalyst for the HMF oxidation, being their activity directly correlated to their surface area, as revealed by the comparison between the membranes with and without TiO_2.

The Nylon-31.5TiO_2-2AuPd membrane showed good thermal stability, no chemical modifications in the reaction conditions and good catalytic activity in high temperature conditions. In addition to this, reusability tests showed that membrane activity is improved after the first use, probably due to an increase of active sites exposure, which could be due to the thermal-induced movement of the polymer chains during the reaction.

In light of these observation, Nylon-31.5TiO_2-2AuPd could be considered as good candidate for the development of continuous catalytic setups for the conversion of HMF into FDCA.

5.5 Bibliography

1. Vankelecom, I. F. J., Polymeric Membranes in Catalytic Reactors. *Chemical Reviews* **2002,** *102* (10), 3779-3810.

2. Stankiewicz, A., Reactive separations for process intensification: an industrial perspective. *Chemical Engineering and Processing: Process Intensification* **2003,** *42* (3), 137-144.

3. Giorno, L.; Drioli, E., Biocatalytic membrane reactors: applications and perspectives. *Trends in Biotechnology* **2000,** *18* (8), 339-349.

4. Ramakrishna, S., *An Introduction to Electrospinning and Nanofibers*. World Scientific: 2005.

5. Bhardwaj, N.; Kundu, S. C., Electrospinning: A fascinating fiber fabrication technique. *Biotechnology Advances* **2010,** *28* (3), 325-347.

6. Thenmozhi, S.; Dharmaraj, N.; Kadirvelu, K.; Kim, H. Y., Electrospun nanofibers: New generation materials for advanced applications. *Materials Science and Engineering: B* **2017,** *217*, 36-48.

7. Fang, X.; Ma, H.; Xiao, S.; Shen, M.; Guo, R.; Cao, X.; Shi, X., Facile immobilization of gold nanoparticles into electrospun polyethyleneimine/polyvinyl alcohol nanofibers for catalytic applications. *Journal of Materials Chemistry* **2011,** *21* (12), 4493-4501.

8. Gopiraman, M.; Bang, H.; Yuan, G.; Yin, C.; Song, K.-H.; Lee, J. S.; Chung, I. M.; Karvembu, R.; Kim, I. S., Noble metal/functionalized cellulose nanofiber composites for catalytic applications. *Carbohydrate Polymers* **2015,** *132*, 554-564.

9. Xu, P.; Cen, C.; Chen, N.; Lin, H.; Wang, Q.; Xu, N.; Tang, J.; Teng, Z., Facile fabrication of silver nanoparticles deposited cellulose microfiber nanocomposites for catalytic application. *Journal of Colloid and Interface Science* **2018,** *526*, 194-200.

10. Hu, D.; Xiao, Y.; Liu, H.; Wang, H.; Li, J.; Zhou, B.; Liu, P.; Shen, M.; Shi, X., Loading of Au/Ag bimetallic nanoparticles within electrospun PVA/PEI nanofibers for catalytic applications. *Colloids and Surfaces A: Physicochemical and Engineering Aspects* **2018,** *552*, 9-15.

11. Du, M.; Chen, B.; Hu, Y.; Chen, J.; Nie, J.; Ma, G., Pt-based alloy nanoparticles embedded electrospun porous carbon nanofibers as electrocatalysts for Methanol oxidation reaction. *Journal of Alloys and Compounds* **2018,** *747*, 978-988.

12. Tang, H.; Chen, W.; Wang, J.; Dugger, T.; Cruz, L.; Kisailus, D., Electrocatalytic N-Doped Graphitic Nanofiber – Metal/Metal Oxide Nanoparticle Composites. *Small* **2018,** *14* (11), 1703459.

13. Li, M.; Zhu, Y.; Song, N.; Wang, C.; Lu, X., Fabrication of Pt nanoparticles on nitrogen-doped carbon/Ni nanofibers for improved hydrogen evolution activity. *Journal of Colloid and Interface Science* **2018,** *514*, 199-207.

14. Sekar, A. D.; Muthukumar, H.; Chandrasekaran, N. I.; Matheswaran, M., Photocatalytic degradation of naphthalene using calcined FeZnO/ PVA nanofibers. *Chemosphere* **2018,** *205*, 610-617.

15. Shahini, P.; Ashkarran, A. A., Immobilization of plasmonic Ag-Au NPs on the TiO2 nanofibers as an efficient visible-light photocatalyst. *Colloids and Surfaces A: Physicochemical and Engineering Aspects* **2018,** *537*, 155-162.

16. Möller, M.; Tarabanko, N.; Wessel, C.; Ellinghaus, R.; Over, H.; Smarsly, B. M., Electrospinning of CeO2 nanoparticle dispersions into mesoporous fibers: on the interplay of stability and activity in the HCl oxidation reaction. *RSC Advances* **2018,** *8* (1), 132-144.

17. Dankeaw, A.; Gualandris, F.; Silva, R. H.; Norrman, K.; Gudik-Sørensen, M.; Hansen, K. K.; Ksapabutr, B.; Esposito, V.; Marani, D., Amorphous saturated cerium–tungsten–titanium oxide nanofiber catalysts for NOx selective catalytic reaction. *New Journal of Chemistry* **2018,** *42* (12), 9501-9509.

18. Pasini, T.; Piccinini, M.; Blosi, M.; Bonelli, R.; Albonetti, S.; Dimitratos, N.; Lopez-Sanchez, J. A.; Sankar, M.; He, Q.; Kiely, C. J.; Hutchings, G. J.; Cavani, F., Selective oxidation of 5-hydroxymethyl-2-furfural using supported gold–copper nanoparticles. *Green Chemistry* **2011,** *13* (8), 2091-2099.

19. Lolli, A.; Albonetti, S.; Utili, L.; Amadori, R.; Ospitali, F.; Lucarelli, C.; Cavani, F., Insights into the reaction mechanism for 5-hydroxymethylfurfural oxidation to FDCA on bimetallic Pd–Au nanoparticles. *Applied Catalysis A: General* **2015,** *504*, 408-419.

20. Gualandi, C.; Govoni, M.; Foroni, L.; Valente, S.; Bianchi, M.; Giordano, E.; Pasquinelli, G.; Biscarini, F.; Focarete, M. L., Ethanol disinfection affects physical properties and cell response of electrospun poly(l-lactic acid) scaffolds. *European Polymer Journal* **2012,** *48* (12), 2008-2018.

21. Xue, T. J.; McKinney, M. A.; Wilkie, C. A., The thermal degradation of polyacrylonitrile. *Polymer Degradation and Stability* **1997,** *58* (1), 193-202.

Chapter 6. Conclusion

This work showed how FDCA production could be achieved by HMF selective oxidation using different innovative catalytic systems.

In Chapter 3 (Pt and Pt/Sn clusters as precursors for the synthesis of catalysts), it has been demonstrated that cluster decomposition is a viable option for the preparation of active and small Pt-based nanoparticles whose activity is strongly affected by the atmosphere used in the thermal treatment. Another key parameter is the Pt/Sn molar ratio, since specific ratio leads to the formation of bimetallic phases which possess higher activity and improved stability.

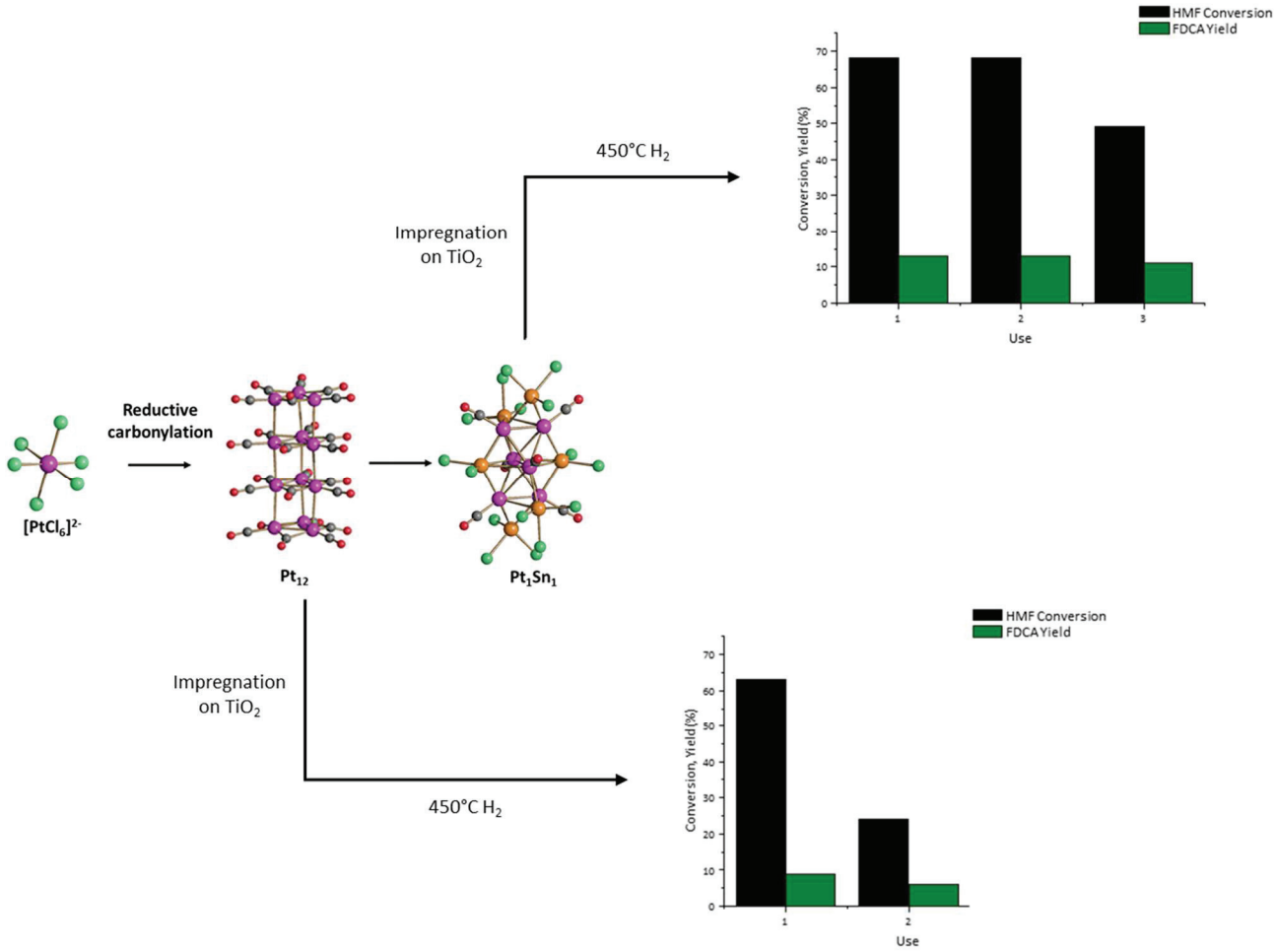

Chapter 4 (Au based nanoparticles supported on nanosized NiO) described the use on nanosized NiO as support for Au-containing nanoparticles. Good FDCA yield have been revealed in relatively mild conditions (10bar O_2, 90°C) for the bimetallic systems Au/Pd (Au/Pd molar ratio 6:4). Then, it has been highlighted that the monometallic Au system suffers from inhibition played by DFF adsorption. Thus, it has been hypothesized that Pd (which is barely active in itself) plays a dual role

when it is alloyed with Au: it enhances catalyst activity and prevents intermediate adsorption on catalyst active sites.

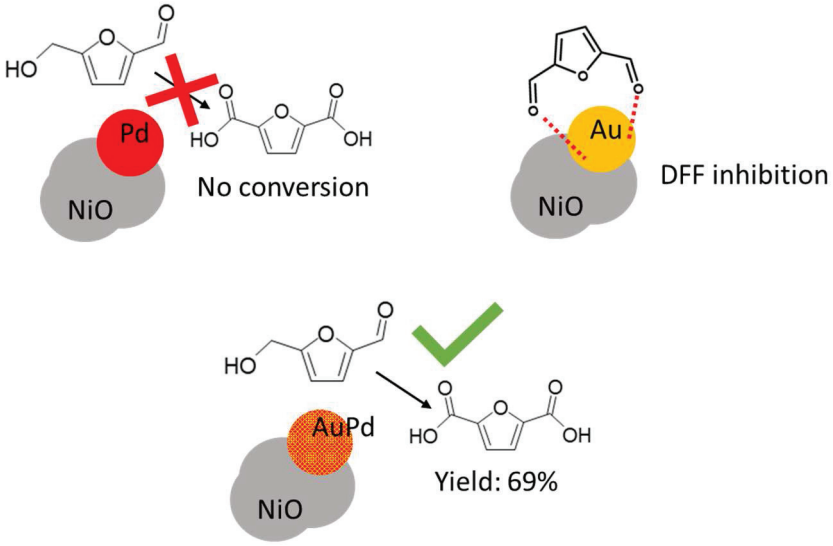

Summing up the results gathered in these two chapters it could be said that in the catalyst design for base-free HMF oxidation both active phase protocol synthesis and support choice must be taken into account since they play a fundamental role in the definition of catalyst activity.

In Chapter 5 (Catalysts grafted onto electrospun polymeric membranes) the use of catalytically polymeric composite membranes has been evaluated. Three different approaches have been tested to embed the active metals in the polymeric framework: (1) as supported nanoparticles on TiO_2 (Paragraph 5.2 PAN electrospun fibers as matrix for Au-containing supported nanoparticles), (2) as carbonylic metal clusters (Paragraph 5.3 Pt inorganic cluster as catalyst precursor for composite PAN-TiO_2 membranes) and (3) as unsupported nanoparticles (Paragraph 5.4 Unsupported Au-nanoparticles embedded in electrospun nylon membrane).

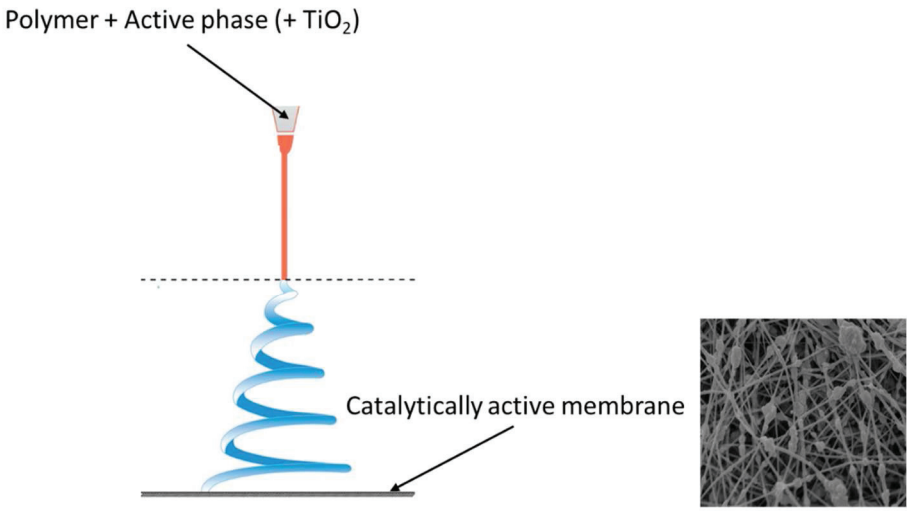

Conclusion

Summing up the results obtained in this study, the role of TiO_2 introduction in the polymeric fiber has been highlighted, since it enhances membrane surface area leading to higher activity. Among all the membranes tested within this study, nylon-based ones afforded the highest activity, suggesting that membranes need to operate at higher temperature than their glass transition temperature.

List of publication

Book chapters

Bonincontro, D.; Quadrelli, E. A., CO_2 Reduction Reactions by Rhodium-Based Catalysts. In *Rhodium Catalysis*, Claver, C., Ed. Springer International Publishing: Cham, 2018; pp 263-282.

Tabanelli, T.; Bonincontro, D.; Albonetti, S.; Cavani, F., Conversion of CO_2 to Valuable Chemicals: Organic Carbonate as Green Candidates for the Replacement of Noxious Reactants. Accepted for *Horizons in Sustainable Industrial Chemistry and Catalysis*, Elsevier

Papers

Grazia, L.; Bonincontro, D.; Lolli, A.; Tabanelli, T.; Lucarelli, C.; Albonetti, S.; Cavani, F., Exploiting H-transfer as a tool for the catalytic reduction of bio-based building blocks: the gas-phase production of 2-methylfurfural using a $FeVO_4$ catalyst. *Green Chemistry* **2017,** *19* (18), 4412-4422.

Lolli, A.; Maslova, V.; Bonincontro, D.; Ortelli, S.; Basile, F.; S. Albonetti, Selective oxidation of HMF by heterogeneous and photocatalytic processes using metal supported catalysts accepted for *Molecules*

Lolli, A; Ortelli, S.; Blosi, M.; Carella, F.; Zanoni, I.; Bonincontro, D.; Costa, A.; Albonetti, S.,

Innovative synthesis of nanostructured composite materials by a spray-freeze drying process: efficient catalysts and photocatalysts preparation accepted for *Catalysis Today*